MULTIBLOCK MODELING OF FLOW IN POROUS MEDIA AND APPLICATIONS

by

Gergina Pencheva

M.S. Mathematics, University of Sofia, Bulgaria, 1992

Submitted to the Graduate Faculty of

the Department of Mathematics in partial fulfillment

of the requirements for the degree of

Doctor of Philosophy

University of Pittsburgh

2007

UNIVERSITY OF PITTSBURGH

MATHEMATICS DEPARTMENT

This dissertation was presented

by

Gergina Pencheva

It was defended on

January 4th 2007

and approved by

Prof. Ivan Yotov, Department of Mathematics, University of Pittsburgh

Prof. William Layton, Department of Mathematics, University of Pittsburgh

Prof. Beatrice Riviere, Department of Mathematics, University of Pittsburgh

Dr. Myron Sussman, Bettis Atomic Power Laboratory and Department of Mathematics, University of Pittsburgh

Dissertation Director: Prof. Ivan Yotov, Department of Mathematics, University of Pittsburgh

MULTIBLOCK MODELING OF FLOW IN POROUS MEDIA AND APPLICATIONS

Gergina Pencheva, PhD

University of Pittsburgh, 2007

We investigate modeling flow in porous media in multiblock domain. Mixed finite element methods are used for subdomain discretizations. Physically meaningful boundary conditions are imposed on the non-matching interfaces via mortar finite element spaces.

We investigate the *pollution* effect of nonmatching grids error on the numerical solution away from interfaces. We prove that most of the error in the velocity occurs along the interfaces, and that high accuracy is preserved in the interior of the subdomains. In case of discontinuous coefficients, the pollution from the singularity affects the accuracy in the whole domain.

We investigate the upscaling error resulting when fine resolution data is approximated on a very coarse scale. Extending work of Wheeler and Yotov, we incorporate this upscaling error in an *a posteriori* error estimator for the pressure, velocity and mortar pressure.

We employ a non-overlapping domain decomposition method reducing the global system to one that is solved iteratively via a preconditioned conjugate gradient method. This approach is suitable for parallel implementation. The balancing domain decomposition method for mixed finite elements following Cowsar, Mandel, and Wheeler is extended to the case of mortar mixed finite elements on non-matching multiblock grids. The algorithm involves solution of a mortar interface problem with one local Dirichlet solve and one local Neumann solve on each iteration. A coarse solve is used to guarantee consistency and to provide global exchange of information. Quasi-optimal condition number bounds independent of the jump in coefficients are derived.

We finally consider multiscale mortar mixed finite element discretizations for single and two phase flows. We show optimal convergence and some superconvergence in the fine scale for the solution and its flux. We also derive efficient and reliable *a posteriori* error estimators suitable for adaptive mesh refinement.

We have incorporated the above methods into a parallel multiblock simulator on unstructured prismatic meshes employing a non-overlapping domain decomposition algorithm and mortar spaces. Numerical experiments are presented confirming all theoretical results.

To my husband Dimitar and my daughter Kalina

Acknowledgments

I would like to express my appreciation and gratitude to my advisor, Professor Ivan Yotov, for his guidance, patience, and generous support these past years, and for introducing me to the fascinating field of flow in porous media. I feel lucky to have been his student.

I am also grateful to Professor William Layton and Professor Beatrice Riviere for their enthusiastic and stimulating lectures which proved invaluable in producing this thesis.

I am especially in debt to Dr. Mike Sussman for his ever-insightful help with software, hardware, and everything in between. This work benefited from his helpful suggestions and comments.

A note of gratitude also goes to my collaborators from ICES, Professor Mary Wheeler, Professor Todd Arbogast, and my colleague Sunil Thomas.

A very special thank you to Stu Pomerantz for countless discussions and patient explanations of the mysteries of C++ programming.

A big thank you to the many friends I have made in the Department of Mathematics at Pitt, in particular to Stephanie Hoogendoorn, Yixin Guo, Carolina and Evandro Manica, Danail Vassilev. Special thanks go to my closest friend Colleen Stu-Pomerantz who has always made time to listen to my frustrations and has offered her moral support and understanding. We had fun together and I will always remember their friendship.

I would also like to thank my parents and brother for their constant love and support from overseas.

Finally, words are not enough to express my gratitude toward my husband Dimitar and my daughter Kalina. Without their understanding for the endless nights and weekends spent working, I could not have ever achieved this. I am eternally thankful to my family for their sacrifices and their love - I owe them everything.

TABLE OF CONTENTS

LIST OF TABLES

LIST OF FIGURES

1.0 INTRODUCTION

Computer modeling of subsurface and surface flow and transport has a major economic impact on environmental and energy industries. It can provide dependable and cost-effective solutions to global problems like contaminant surface water and groundwater remediation and enhanced oil recovery.

Multiblock methodology. Some of the features that make the above problems difficult for numerical simulation are coupling of different physical and mathematical models, irregular geometries, multiscale processes (heterogeneities, energy dissipation), large gradients, and multiple phases. The coupled systems of partial differential equations that govern these processes are transient, highly nonlinear and often advection dominated. The resulting algebraic systems are large and ill-conditioned.

Our approach to the above difficulties is based on a recently developed multiblock domain decomposition methodology. We divide the simulation domain into a series of smaller subdomains (blocks). The governing equations are imposed on each subdomain; on the interfaces we set physically meaningful boundary conditions. We cover each block by a local grid and don't require neighboring grids to match on interfaces between blocks. *Mortar finite element spaces* are employed to impose interface conditions.

The multiblock approach has many advantages. It allows the possibility of *multiphysics* formulations where different physical processes and different mathematical models may be associated with different blocks, e.g., coupling single-phase flow with multiphase flow in reservoir modeling. In addition, *multinumerics* is also possible since we can apply appropriate discretization methods locally, e.g. coupling mixed finite element with discontinuous Galerkin methods. The multiblock approach is very flexible in handling domains with *general geometry* and/or *internal boundaries*. A typical example is modeling large scale geological

structures such as faults and layers for flow in porous media. It also naturally leads to algorithms that are easy to *parallelize*, hence, it can increase the *efficiency* with which a solution is found without sacrifice in the accuracy. This approach is very suitable for *multiscale resolution* since we can couple highly refined regions where fine scale phenomena occur, e.g. high gradients near wells, with more coarsely discretized regions via mortar space. Last, but not least, this approach allows for a *code reuse*. By coupling existing codes developed in academia or industry over the years, one can solve more complex problems with just minimal code modifications.

There are two key factors in the success of the multiblock method. First, on subdomain interfaces one has to impose proper matching conditions in a numerically stable and accurate way. Second, the resulting systems of equations have to be solved in a fast and efficient manner.

In this work we consider mixed finite element (MFE) methods for subdomain discretizations. Mixed methods owe their popularity to their local (element-wise) mass conservation property and the simultaneous and accurate approximation of two variables of physical interest, e.g., pressure and velocity in fluid flow. The mortar mixed method can be viewed as an extension to non-matching grids of the partially hybridized form of the mixed method where Lagrange multiplier pressures are introduced on the inter-block boundaries.

The four main topics of this thesis are:

• **Interior error estimates.** Although using computational grids that might not match across interfaces has its many advantages, there is also price to be paid - a numerical error is introduced. We want to investigate if this error pollutes the numerical solution away from interfaces.

• **A posteriori error estimates.** An important part of any successful computational method is the development of such estimators and adaptive mesh refinement strategies that help reduce the computational cost while achieving good overall accuracy.

• **Balancing domain decomposition.** The multiblock approach leads to a big, ill-conditioned system of equations. The feasibility of the domain decomposition solver depends critically on the rate of convergence of the interface iteration and ultimately on the conditioning of the interface operator. Our goal is to develop and implement an efficient

preconditioner that will speed up the domain decomposition solver.

• **Multiscale mortar mixed finite element method:** Flow in porous media computations could be especially difficult when the permeability field is highly heterogeneous and varies on a very fine scale. A direct approach to discretization would require full fine scale grid and will lead to a big, highly coupled system of equations. We explore a new multiscale approach based on domain decomposition and mortar finite elements.

1.1 INTERIOR AND SUPERCONVERGENCE ESTIMATES

Interior estimates were first introduced by Nitsche and Schatz in 1974 for primal finite element methods for second order elliptic equations. They show in [58] that the error in an interior domain Ω can be estimated with sum of two terms. The first term has best order of accuracy that is possible locally for the subspaces used. The second term is the error in a weaker norm over a slightly larger domain and it measures the effects from outside the domain Ω. Schatz and Wahlbin [62, 63] derive similar estimates in maximum norm and considered the effect of a perturbation term. In 1985 Douglas and Milner [37] applied the Nitsche-Schatz approach to the mixed finite element methods for second order linear and quasi-linear elliptic equations. J. Wheeler, M. Wheeler, and Yotov [66] derive interior velocity estimates for the enhanced velocity mixed finite element methods on multiblock domains.

Convergence rates of the finite element solution (or its gradient) at certain points (or regions) may exceed the optimal global convergent rate of the approximation, with or without postprocessing. This phenomenon is called superconvergence. There are many papers dealing with the superconvergence phenomenon for mixed methods. In [14] Arnold and Brezzi show for the lowest order Raviart-Thomas (RT_0) spaces for triangular elements that if Lagrange multipliers are used, a new, more accurate approximation of the pressure can be constructed (for RT_0, take the linear non-conforming interpolant of Lagrange multiplier). For rectangular RT spaces Duran [38] proves velocity superconvergence and obtains a higher order approximation of the vector variable via local postprocessing of the numerical solution. Nakata, Weiser and Wheeler [56] show superconvergence for the RT approximations at the

Gauss points while Ewing, Lazarov and Wang [39] derive superconvergence for velocity along the Gaussian lines. Ewing, Liu and Wang [40] consider h^2- uniform grid for quadrilaterals and show superconvergence for velocity. By incorporating certain quadrature rules, Arbogast, Wheeler and Yotov [12] write mixed method with tensor coefficients as a cell centered finite difference method. Superconvergence for the scalar unknown and its gradient and flux for certain discrete norms is proven.

Using techniques from both interior and superconvergence error estimate analyses, we prove that in the case of non-matching grids and smooth solutions, the vector variable is superconvergent in an interior domain. In addition, for the non-mortar mixed finite element method of Arbogast and Yotov [13], we prove superconvergence for the scalar variable. Numerical experiments confirming the theory are presented.

1.2 *A POSTERIORI* ESTIMATES

In order to efficiently capture the fine scale details in flow and transport problems, a local adaptivity based either on mesh refinement, polynomial enrichment, or both, should be incorporated in the approximation process. While there are many papers on *a posteriori* error estimation for conforming grids (Babuska and Rheinboldt [15], Bank and Weiser [17], Ainsworth and Oden [6], Verfürth [65] to name a few), few papers treat the case of mortar finite element methods. In the case of Galerkin finite elements, error estimators have been developed by Wohlmuth [71], [72]. For MFE methods Braess and Verfürth in [19] use mesh-dependent norms to obtain optimal residual-based estimators. Estimators based on superconvergence error estimates are developed by Brandts [21] and Hoppe and Wohlmuth [45]. Carstensen [27] and Wohlmuth and Hoppe [73] use Helmholtz decomposition to derive optimal residual-based estimators in the natural pressure and velocity norms. Hierarchical estimates and implicit estimates based on solving local problems are also investigated in [73]. For the mortar mixed finite element method even less is known. Wheeler and Yotov in [70] derive several *a posteriori* error estimates: an efficient and reliable residual-based estimator for the pressure error which includes also flux-jump and mortar pressure terms; an efficient and reliable estimator for the velocity and mortar pressure based on solving local (element)

problems in a higher-order space.

We investigate the upscaling error resulting when fine resolution data is approximated on a very coarse scale. Extending previous work of Wheeler and Yotov [70], we incorporate this upscaling error into the *a posteriori* error estimator. We prove explicit upper bounds for the pressure, velocity and mortar pressure errors. Numerical experiments confirming the theory are presented.

1.3 BALANCING DOMAIN DECOMPOSITION

A non-overlapping domain decomposition algorithm was developed for matching grids by Glowinski and Wheeler [43, 34] and was later extended to non-matching grids by Wheeler and Yotov [74, 69]. The method reduces the global system to an interface problem which is symmetric and positive definite in the case of elliptic equations and can be solved iteratively via a preconditioned conjugate gradient method. This approach is very suitable for parallel implementation since the dominant cost is solving subdomain problems.

The balancing domain decomposition was introduced by Mandel [54] for Galerkin finite elements and later analyzed by Mandel and Brezina [55]. Cowsar, Mandel, and Wheeler [33] developed the balancing preconditioner for mixed finite elements. The algorithm is based on the Neumann-Neumann preconditioner developed by Bourgat, Glowinski, Le Tallec, Vidrascu, and De Roeck [18, 36, 52] and involves an iterative solution of the interface problem with one local Dirichlet solve (action of the operator) and one local Neumann solve (action of the preconditioner) per subdomain on each iteration. A coarse problem is added to guarantee that the Neumann problems are consistent, which also provides global exchange of information across subdomains. We extend the balancing preconditioner for mixed finite elements developed by Cowsar, Mandel, and Wheeler [33] to the case of non-matching multiblock grids in [59]. Our theoretical results for the mortar balancing preconditioner provide, as in the case of matching grids, a quasi-optimal condition number bound $O((1+\log(\tilde{H}/h))^2)$ which is independent of the jump in coefficients between subdomains. Here h is the discretization parameter and $\tilde{H}$ is the characteristic size of the subdomains. This bound also indicates very weak dependence on the number of subdomains which is confirmed experimentally.

1.4 MULTISCALE MORTAR MIXED FINITE ELEMENT METHOD

It is difficult to solve problem (2.1)–(2.3) (defined in Chapter 2) when the computational domain is large and the permeability coefficient is highly heterogeneous and varying on a fine scale. Discretization on a fine scale would result in a large, highly coupled system of equations which often is computationally unfeasible to solve.

To overcome this difficulty, the variational multiscale method by Hughes, Feijóo, Mazzei, Quincy, and Brezzi [48, 49, 22] and multiscale finite elements by Hou, Wu, and Cai [46, 47] were developed for the problem (2.1)–(2.3) written as a single second order partial differential equation. Arbogast, Minkoff, Keenan, Aarnes, Boyd, Krogstad, and Lie [10, 7, 3, 8, 4], treat the mixed system of two first order equations in a variational multiscale context, while Chen and Hou [30] study it in a multiscale finite element method context. Arbogast and Boyd show that these two approaches are equivalent up to relatively minor differences.

In both methods, the problem (2.1)–(2.3) is decomposed into a series of small subdomains (coarse elements). These local problems are paired with appropriate boundary conditions and solved on the fine scale (to resolve variations in permeability field) to get the coarse scale multiscale finite element basis. This coarse basis is then used to approximate the solution globally. Since the localized problems are small, they are solved more efficiently than the full system. The coarse scale coupling involves just a few degrees of freedom per element face (or edge), so the coarse problem is small and easier to solve.

We develop a new but similar multiscale approach based on domain decomposition theory and mortar finite elements. We partition the computational domain into a series of subdomains (or coarse elements), over which we pose the original problem. The continuity of flux is imposed via a mortar finite element space on the coarse grid scale, while the equations in the coarse elements (or subdomains) are discretized on a fine grid scale. The polynomial degree of the mortar and subdomain approximation spaces may differ; in fact, the mortar space achieves approximation comparable to the fine scale on its coarse grid by using higher order polynomials. Our formulation is related to, but more flexible than, existing multiscale finite element and variational multiscale methods, because it is easy to improve global accuracy by simply refining the local mortar grid where needed. That is, we can easily exploit

adaptive meshing strategies to improve where necessary the strength of the global coupling.

We derive *a priori* error estimates and show, with appropriate choice of the mortar space, optimal order convergence and some superconvergence on the fine scale for both the solution and its flux. We also derive efficient and reliable *a posteriori* error estimators, which are used in an adaptive mesh refinement algorithm to obtain appropriate subdomain and mortar grids. Numerical experiments are presented in confirmation of the theory.

The rest of the thesis is organized as follows. In Chapter 2 the single-phase and two-phase flow problems are formulated. Two mathematical formulations of mixed finite element methods on non-matching grids are given for the single-phase flow problem. Chapter 3 is devoted to interior estimates. The *a posteriori* error estimates are described in Chapter 4 followed by a exposition of balancing domain decomposition for mortar mixed finite elements on non-matching grids in Chapter 5. In Chapter 6 we develop the multiscale mortar mixed method. In the last chapter we present some notes on the implementation of the methods in our parallel multiblock unstructured simulator.

2.0 PROBLEM FORMULATION

2.1 SINGLE-PHASE FLOW IN POROUS MEDIA

The system that models single-phase flow in porous media as well as many other applications is

$$\mathbf{u} = -K\nabla p \quad \text{in } \Omega, \tag{2.1}$$

$$\nabla \cdot \mathbf{u} = f \quad \text{in } \Omega, \tag{2.2}$$

$$p = g \quad \text{on } \partial\Omega, \tag{2.3}$$

where $\Omega \subset \mathbf{R}^d$, $d = 2$ or 3, and K is a symmetric, uniformly positive definite tensor with $L^\infty(\Omega)$ components satisfying, for some $0 < k_0 \leq k_1 < \infty$,

$$k_0 \xi^T \xi \leq \xi^T K(x) \xi \leq k_1 \xi^T \xi, \quad \forall \mathbf{x} \in \mathbf{R}^d, \ \forall x \in \Omega. \tag{2.4}$$

Here p is the pressure, $\mathbf{u}$ is the Darcy velocity, and K represents the permeability divided by the viscosity. Equation (2.1) is known as Darcy's Law, while (2.2) is conservation of mass. The Dirichlet boundary conditions are considered merely for simplicity. Neumann boundary condition $\mathbf{u} \cdot \nu = g^N$ and Robin boundary condition can also be considered. We assume that the problem (2.1)–(2.3) is at least $H^{3/2+\varepsilon}$-regular, for some $\varepsilon > 0$. In some cases we assume H^2-regularity, i.e., there exists a positive constant C depending only on K and Ω such that

$$\|p\|_2 \leq C(\|f\| + \|g\|_{3/2,\partial\Omega}). \tag{2.5}$$

We have H^2-regularity, for example, if $f \in L^2(\Omega)$, $g \in H^{3/2}(\partial\Omega)$, the components of $K \in C^{0,1}(\bar{\Omega})$, and Ω is convex or $\partial\Omega$ is smooth enough (see [44, 53, 42]).

We will make use of the following standard notation. For a bounded subdomain $G \subset \mathbf{R}^d$, the $L^2(G)$ inner product (or duality pairing) and norm are denoted by $(\cdot,\cdot)_G$ and $\|\cdot\|_G$, respectively, for scalar and vector valued functions. We may omit G in the subscript if $G = \Omega$. For a section of a subdomain boundary $S \subset \cup_{i=1}^n \partial\Omega_i$ we write $\langle\cdot,\cdot\rangle_S$ and $\|\cdot\|_S$ for the $L^2(S)$ inner product (or duality pairing) and norm, respectively.

We will use the Sobolev space $H^m(G)$ of m-times differentiable functions in $L^2(G)$ with a norm

$$\|u\|_{m,G} = \left(\sum_{|\alpha|\le m} \int_G |D^\alpha u|^2 \, dx \right)^{1/2}.$$

For a non-integer $r = m + s, 0 < s < 1, H^r(G)$ is defined by interpolation of $H^m(G)$ and $H^{m+1}(G)$ (see [53]) with a norm

$$\|u\|_{r,G} = \left\{ \|u\|_{m,G}^2 + \sum_{|\alpha|=m} \int_G \int_G \frac{|D^\alpha u(x) - D^\alpha u(y)|^2}{|x-y|^{d+2s}} \, dx \, dy \right\}^{1/2}.$$

The Sobolev spaces on ∂G are defined in a similar fashion.

Throughout the thesis the constants c and C will denote generic constants independent of mesh size or domain size.

The velocity and pressure functional spaces for the mixed weak formulation of (2.1)–(2.3) are defined as usual [26] to be

$$\mathbf{V} = H(\mathrm{div};\Omega) = \{\mathbf{v} \in (L^2(\Omega))^d : \nabla\cdot\mathbf{v} \in L^2(\Omega)\}, \quad W = L^2(\Omega),$$

with norms

$$\|\mathbf{v}\|_{\mathbf{V}} = (\|\mathbf{v}\|^2 + \|\nabla\cdot\mathbf{v}\|^2)^{1/2}, \quad \|w\|_W = \|w\|.$$

A weak solution of (2.1)–(2.3) is a pair $\mathbf{u} \in \mathbf{V}$, $p \in W$ such that

$$(K^{-1}\mathbf{u}, \mathbf{v}) = (p, \nabla\cdot\mathbf{v}) - \langle g, \mathbf{v}\cdot\nu\rangle_{\partial\Omega}, \ \ \mathbf{v} \in H(\mathrm{div};\Omega), \tag{2.6}$$

$$(\nabla\cdot\mathbf{u}, w) = (f, w), \ \ w \in L^2(\Omega), \tag{2.7}$$

where ν is the outward unit normal vector on $\partial\Omega$. It is well known (see, e.g., [26, 61]) that (2.6)–(2.7) has a unique solution.

We also consider an alternative domain decomposition formulation. Let Ω be decomposed into non-overlapping and shape-regular subdomain blocks Ω_i with diameters $O(\tilde{H})$, i.e., there exists a reference domain $\hat{\Omega}$ with a diameter $O(1)$ and bijective mappings F_i such that

$$\Omega_i = F_i(\hat{\Omega}), \quad \|DF_i\| \leq C\tilde{H}, \quad \|DF_i^{-1}\| \leq C\tilde{H}^{-1},$$

so that $\overline{\Omega} = \cup_{i=1}^n \overline{\Omega}_i$ and $\Omega_i \cap \Omega_j = \emptyset$ for $i \neq j$. The blocks need not share complete faces, i.e., they need not form a conforming partition. Let $\Gamma_{i,j} = \partial\Omega_i \cap \partial\Omega_j$, $\Gamma = \cup_{1\leq i<j\leq n}\Gamma_{i,j}$, and $\Gamma_i = \partial\Omega_i \cap \Gamma = \partial\Omega_i \backslash \partial\Omega$ denote interior block interfaces. Denote by

$$\mathbf{V}_i = H(\mathrm{div}; \Omega_i), \quad W_i = L^2(\Omega_i)$$

the subdomain functional spaces. To cast the problem (2.1)–(2.3) in a multiblock form, we write on each block Ω_i:

$$\mathbf{u} = -K\nabla p \qquad \text{in } \Omega_i, \tag{2.8}$$

$$\nabla \cdot \mathbf{u} = f \qquad \text{in } \Omega_i, \tag{2.9}$$

$$p = g \qquad \text{on } \partial\Omega_i \cap \partial\Omega \tag{2.10}$$

and on each interface $\Gamma_{i,j}$:

$$p_i = p_j, \qquad \mathbf{u}_i \cdot \nu_i + \mathbf{u}_j \cdot \nu_j = 0,$$

i.e., both the pressure and the flux are continuous across $\Gamma_{i,j}$. Here, for any f defined on Ω, we denote both $f|_{\Omega_k}$ and its trace $f|_{\Gamma_k}$ by f_k.

We will use the notion of a shape-regular, quasi-uniform triangulation (partition) of domain G. We will call a triangulation $\mathcal{T}_h$ of G *shape-regular* or *non-degenerate* if there exists a constant σ such that

$$\frac{h_E}{\rho_E} \leq \sigma, \quad \forall E \in \mathcal{T}_h.$$

We will call it *quasi-uniform* if there exists a constant γ such that

$$\frac{h}{h_E} \leq \gamma, \quad \forall E \in \mathcal{T}_h.$$

Here ρ_E is the diameter of the largest ball contained in E, h_E is the diameter of E and $h = \max_{E\in\mathcal{T}_h} h_E$ (see [32]). It is well known that if a triangulation is quasi-uniform, then inverse inequality holds

$$\forall E \in \mathcal{T}_h, \quad |\mathbf{v}_h|_{1,E} \leq C h_E^{-1} \|\mathbf{v}\|_E, \quad \mathbf{v}_h \in \mathbf{V}_h. \tag{2.11}$$

Here, $\mathbf{V}_h$ is a finite element space, e.g., any of these defined below.

Let $\mathcal{T}_{h,i}$ be a conforming, shape-regular, quasi-uniform affine finite element partition of Ω_i, $1 \leq i \leq n$, of maximal element diameter h_i. To simplify the analysis, we let $h = \max_{1\leq i\leq n} h_i$ and analyze the methods in terms of this single value h. Note that we allow for the possibility that the subdomain partitions $\mathcal{T}_{h,i}$ and $\mathcal{T}_{h,j}$ need not align on $\Gamma_{i,j}$. Define $\mathcal{T}_h = \cup_{i=1}^n \mathcal{T}_{h,i}$ and let $\mathcal{E}_h$ be the union of all interior edges (or faces in three dimensions) not including the subdomain interfaces and the outer boundary. Let

$$\mathbf{V}_{h,i} \times W_{h,i} \subset \mathbf{V}_i \times W_i$$

be any of the usual mixed finite element spaces defined on $\mathcal{T}_{h,i}$ (see [26], Section III.3), the Raviart-Thomas (RT) spaces [60, 57], the Brezzi-Douglas-Marini (BDM) spaces [25], the Brezzi-Douglas-Fortin-Marini (BDFM) spaces [24], the Brezzi-Douglas-Duràn-Fortin (BDDF) spaces [23], or the Chen-Douglas (CD) spaces [29]. The order of the spaces is assumed to be the same on every subdomain. Let $\mathbf{V}_{h,i}$ contain the polynomials of degree k and $W_{h,i}$ contain the polynomials of degree l. For these spaces we have $l = k$ or $l = k-1$. The most commonly used mixed spaces are the Raviart-Thomas spaces of order k, RT_k [64, 60, 57] for which $l = k$. On each element $E \in \mathcal{T}_h$, if E is a triangle

$$\mathbf{V}_h^k(E) = (P_k(E))^d \oplus \underline{x} P_k(E) = \left\{ f : f(x) = p(x) + xq(x), p \in (P_k(E))^d, q \in P_k(E) \right\},$$
$$W_h^k(E) = P_k(E),$$

and if E is a rectangle,

$$\mathbf{V}_h^k(E) = \begin{cases} P_{k+1,k}(E) \times P_{k,k+1}(E), & d = 2 \\ P_{k+1,k,k}(E) \times P_{k,k+1,k}(E) \times P_{k,k,k+1}(E), & d = 3 \end{cases}, \qquad W_h^k(E) = Q_k(E).$$

Here, $P_k(E)$ is the space of polynomials of (total) degree $\leq k$ on E, $P_{k,l}(E)$ is the space of polynomials in $2d$ of degree $\leq k$ in x and $\leq l$ in y with the obvious definition in $3d$,

and $Q_k(E) = P_{k,k}(E)(P_{k,k,k}(E)$, if $d = 3$). Then, the Raviart-Thomas spaces of order k are defined as

$$\mathbf{V}_h^k(\mathcal{T}_h) = \left\{\mathbf{v} \in H(\mathrm{div};\Omega) : \mathbf{v}|_E \in \mathbf{V}_h^k(E), \quad \forall E \in \mathcal{T}_h\right\}$$
$$W_h^k(\mathcal{T}_h) = \left\{w \in L^2(\Omega) : w|_E \in W_h^k(E), \quad \forall E \in \mathcal{T}_h\right\}.$$

The velocity and pressure mixed finite element spaces on Ω are defined as follows:

$$\mathbf{V}_h = \bigoplus_{i=1}^{n} \mathbf{V}_{h,i}, \qquad W_h = \bigoplus_{i=1}^{n} W_{h,i}.$$

Note that the normal components of vectors in $\mathbf{V}_h$ are continuous between elements within each block Ω_i, but not across Γ.

We introduce some projection operators needed in the analysis. For any $\varphi \in L^2(\Omega)$, let $\hat{\varphi} \in W_h$ be its $L^2(\Omega)$-projection satisfying

$$(\varphi - \hat{\varphi}, w) = 0, \quad w \in W_h. \tag{2.12}$$

Let also $\mathcal{Q}_{h,i} : L^2(\Gamma_i) \to \mathbf{V}_{h,i} \cdot \nu_i|_{\Gamma_i}$ be the L^2-orthogonal projection satisfying for any $\phi \in L^2(\Gamma_i)$

$$\langle \phi - \mathcal{Q}_{h,i}\phi, \mathbf{v} \cdot \nu_i \rangle_{\Gamma_i} = 0, \quad \forall \mathbf{v} \in \mathbf{V}_{h,i}. \tag{2.13}$$

We recall that, for any of the standard mixed spaces,

$$\nabla \cdot \mathbf{V}_{h,i} = W_{h,i},$$

and there exists a projection Π_i of $(H^\varepsilon(\Omega_i))^d \cap \mathbf{V}_i$ onto $\mathbf{V}_{h,i}$ (for any $\varepsilon > 0$), satisfying that for any $\mathbf{q} \in (H^\varepsilon(\Omega_i))^d \cap \mathbf{V}_i$,

$$\nabla \cdot \Pi_i \mathbf{q} = \widehat{\nabla \cdot \mathbf{q}}, \tag{2.14}$$
$$(\Pi_i \mathbf{q}) \cdot \nu_i = \mathcal{Q}_{h,i}(\mathbf{q} \cdot \nu_i). \tag{2.15}$$

Define $\Pi : \bigoplus_{i=1}^n \mathbf{V}_i \to \mathbf{V}_h$ such that $\Pi|_{\Omega_i} = \Pi_i$.

Our projection operators have the following approximation properties:

$$\|\varphi - \hat{\varphi}\| \leq C\|\varphi\|_t h^t, \qquad 0 \leq t \leq l+1, \tag{2.16}$$

$$\|\nabla \cdot (\mathbf{q} - \Pi_i \mathbf{q})\|_{\Omega_i} \leq C\|\nabla \cdot \mathbf{q}\|_{t,\Omega_i} h^t, \quad 0 \leq t \leq l+1, \tag{2.17}$$

$$\|\mathbf{q} - \Pi_i \mathbf{q}\|_{\Omega_i} \leq C\|\mathbf{q}\|_{r,\Omega_i} h^r, \qquad 1 \leq r \leq k+1, \tag{2.18}$$

$$\|\psi - \mathcal{Q}_{h,i}\psi\|_{\Gamma_{i,j}} \leq C\|\psi\|_{r,\Gamma_{i,j}} h^r, \qquad 0 \leq r \leq k+1, \tag{2.19}$$

$$\|(\mathbf{q} - \Pi_i \mathbf{q}) \cdot \nu_i\|_{\Gamma_{i,j}} \leq C\|\mathbf{q}\|_{r,\Gamma_{i,j}} h^r, \qquad 0 \leq r \leq k+1. \tag{2.20}$$

Bounds (2.16)–(2.17) and (2.19)–(2.20) are standard L^2-projection approximation results [32]; bound (2.18) can be found in [26, 61].

In the analysis, we will also use the trace theorem

$$\|q\|_{r,\Gamma_{i,j}} \leq C\|q\|_{r+1/2,\Omega_i}, \quad r > 0, \tag{2.21}$$

(see [44, Theorem 1.5.2.1]).

For theoretical purposes it is convenient to define the space of weakly continuous velocities, which is the space

$$\mathbf{V}_h^0 = \left\{ \mathbf{v} \in \mathbf{V}_h : \sum_{i=1}^{n} \langle \mathbf{v}|_{\Omega_i} \cdot \nu_i, \mu \rangle_{\Gamma_i} = 0, \quad \forall \mu \in M_h \right\}.$$

2.1.1 Mortar mixed finite element method

If the solution $(\mathbf{u}, p)$ of (2.6)–(2.7) belongs to $H^1(\Omega) \times L^2(\Omega)$, it is easy to see that it satisfies, for $1 \leq i \leq n$,

$$(K^{-1}\mathbf{u}, \mathbf{v})_{\Omega_i} = (p, \nabla \cdot \mathbf{v})_{\Omega_i} - \langle p, \mathbf{v} \cdot \nu_i \rangle_{\Gamma_i} - \langle g, \mathbf{v} \cdot \nu_i \rangle_{\partial\Omega_i \setminus \Gamma_i}, \ \mathbf{v} \in \mathbf{V}_i, \tag{2.22}$$

$$(\nabla \cdot \mathbf{u}, w)_{\Omega_i} = (f, w)_{\Omega_i}, \ w \in W_i, \tag{2.23}$$

$$\sum_{i=1}^{n} \langle \mathbf{u} \cdot \nu_i, \mu \rangle_{\Gamma_i} = 0, \ \mu \in L^2(\Gamma), \tag{2.24}$$

where ν_i is the outer unit normal to $\partial\Omega_i$. Equation (2.22) is obtained by integrating by parts (2.8) locally on Ω_i, and equation (2.24) implies that $\mathbf{u} \cdot \nu$ is continuous across Γ.

Let $\mathcal{T}_{h,i,j}$ be a non-degenerate, quasi-uniform finite element partition of $\Gamma_{i,j}$ and let $\mathcal{T}^{\Gamma,h} = \cup_{1 \leq i < j \leq n} \mathcal{T}_{h,i,j}$. Recall that k is associated with the degree of the polynomials in $\mathbf{V}_h \cdot \nu$.

Denote by $M_{h,i,j} \subset L^2(\Gamma_{i,j})$ the mortar finite element space on $\Gamma_{i,j}$ containing at least either the continuous or discontinuous piecewise polynomials of degree $k+1$ on $\mathcal{T}_{h,i,j}$. For example, in the case of RT_0, $k=0$, and $M_{h,i,j}$ is the space of piecewise linear (bilinear, if $d=3$ and the grids are hexahedral) polynomials on $\mathcal{T}_{h,i,j}$. Let

$$M_h = \bigoplus_{1\le i<j\le n} M_{h,i,j}$$

be the mortar finite element space on Γ. In the mortar mixed finite element approximation of (2.22)–(2.24) we seek $\mathbf{u}_h \in \mathbf{V}_h$, $p_h \in W_h$, and $\lambda_h \in M_h$ such that, for $1 \le i \le n$,

$$(K^{-1}\mathbf{u}_h, \mathbf{v})_{\Omega_i} = (p_h, \nabla\cdot\mathbf{v})_{\Omega_i} - \langle \lambda_h, \mathbf{v}\cdot\nu_i\rangle_{\Gamma_i} - \langle g, \mathbf{v}\cdot\nu_i\rangle_{\partial\Omega_i\setminus\Gamma_i}, \ \ \mathbf{v}\in\mathbf{V}_{h,i}, \tag{2.25}$$

$$(\nabla\cdot\mathbf{u}_h, w)_{\Omega_i} = (f,w)_{\Omega_i}, \ \ w\in W_{h,i}, \tag{2.26}$$

$$\sum_{i=1}^{n}\langle \mathbf{u}_h\cdot\nu_i, \mu\rangle_{\Gamma_i} = 0, \ \ \mu\in M_h. \tag{2.27}$$

Strictly within each block Ω_i, we have a standard mixed finite element method, and (2.26) enforces local conservation over each grid cell. It is clear from (2.22) and (2.25) that $\lambda_h \in M_h$ is an approximation to the pressure p on Γ. Equation (2.27) enforces weak (with respect to the mortar space M_h) continuity of flux across the block interfaces.

We note that we can eliminate λ_h from the mixed method (2.25)–(2.27) by restricting $\mathbf{V}_h$ to $\mathbf{V}_h^0$; that is, the problem is equivalent to finding $\mathbf{u}_h \in \mathbf{V}_h^0$ and $p_h \in W_h$ such that

$$(K^{-1}\mathbf{u}_h, \mathbf{v}) = \sum_{i=1}^{n}(p_h, \nabla\cdot\mathbf{v})_{\Omega_i} - \langle g, \mathbf{v}\cdot\nu\rangle_{\partial\Omega}, \quad \mathbf{v}\in\mathbf{V}_{h,0}, \tag{2.28}$$

$$\sum_{i=1}^{n}(\nabla\cdot\mathbf{u}_h, w)_{\Omega_i} = (f,w), \qquad\qquad w\in W_h. \tag{2.29}$$

Existence and uniqueness of a solution to (2.25)–(2.27) are shown in [74, 9] along with optimal convergence and superconvergence for both pressure and velocity under the following condition.

Assumption 2.1. *Assume that there exists a constant C independent of h such that*

$$\|\mu\|_{\Gamma_{i,j}} \le C(\|\mathcal{Q}_{h,i}\mu\|_{\Gamma_{i,j}} + \|\mathcal{Q}_{h,j}\mu\|_{\Gamma_{i,j}}), \quad \mu\in M_h, \ \ 1\le i<j\le n. \tag{2.30}$$

Remark 2.1. *The condition (2.30) imposes a limit on the number of mortar degrees of freedom and is easily satisfied in practice [74]. In the case of RT_0 spaces, (2.30) holds under the assumption on the grids in Lemma 5.5, as it can be seen from its proof.*

2.1.2 Non-mortar mixed finite element method

There is another way to impose the boundary conditions on the subdomain interfaces without the use of mortar space (see [13]). On each subdomain, partially hybridized mixed method is employed. Lagrange multiplier pressures are introduced on the faces (or edges) of the elements lying on the subdomain interfaces Γ as in [26, 43]. Since the grids are different on the two sides of Γ, these Lagrange multiplier pressures are doubly valued. Robin type conditions are imposed on Γ to couple the subdomain problems. The method has an advantage in the case where adaptive local refinement techniques will be used, in that there is no mortar grid to refine. Such refinement could be difficult to implement, especially in parallel, since accuracy depends subtly on the relations between the mortar grid and the traces of the grids of the subdomain blocks [9].

To put the problem (2.6)–(2.7) in a multiblock form, choose a parameter $\alpha > 0$ and write on each interface $\Gamma_{i,j}$:

$$\alpha p_i - \mathbf{u}_i \cdot \nu_i = \alpha p_j + \mathbf{u}_j \cdot \nu_j. \tag{2.31}$$

The Robin type interface condition (2.31) is imposed twice on each $\Gamma_{i,j}$ and implies

$$p_i = p_j \qquad \mathbf{u}_i \cdot \nu_i + \mathbf{u}_j \cdot \nu_j = 0,$$

i.e., both the pressure and the flux are continuous across $\Gamma_{i,j}$.

The alternative multiblock variational form is: find $(\mathbf{u}, p) \in \mathbf{V} \times W$ such that for $1 \leq i \leq n$

$$(K^{-1}\mathbf{u}, \mathbf{v})_{\Omega_i} = (p, \nabla \cdot \mathbf{v})_{\Omega_i} - \langle p_i, \mathbf{v} \cdot \nu_i \rangle_{\Gamma_i} - \langle g, \mathbf{v} \cdot \nu_i \rangle_{\partial\Omega_i \setminus \Gamma}, \ \mathbf{v} \in \mathbf{V}_i, \tag{2.32}$$

$$(\nabla \cdot \mathbf{u}, w)_{\Omega_i} = (f, w)_{\Omega_i}, \ w \in W_i, \tag{2.33}$$

$$\langle \alpha p_i - \mathbf{u}_i \cdot \nu_i, \mu_i \rangle_{\Gamma_i} = \sum_{j=1}^{n} \langle \alpha p_j + \mathbf{u}_j \cdot \nu_j, \mu_i \rangle_{\Gamma_{i,j}}, \ \mu_i \in L^2(\Gamma_i) \tag{2.34}$$

Choose $\Lambda_{h,i}$ to be the hybrid MFE Lagrange multiplier space on Γ_i, i.e., $\Lambda_{h,i} = \mathbf{V}_{h,i} \cdot \nu_i$. In the non-mortar mixed finite element approximation of (2.32)–(2.34) we seek $(\mathbf{u}_h, p_h) \in \mathbf{V}_h \times W_h$,

and, for each $i, \lambda_{h,i} \in \Lambda_{h,i}$ such that for $1 \le i \le n$,

$$(K^{-1}\mathbf{u}_h, \mathbf{v})_{\Omega_i} = (p_h, \nabla \cdot \mathbf{v})_{\Omega_i} - \langle \lambda_{h,i}, \mathbf{v} \cdot \nu_i \rangle_{\Gamma_i} - \langle g, \mathbf{v} \cdot \nu_i \rangle_{\partial\Omega_i \setminus \Gamma}, \ \mathbf{v} \in \mathbf{V}_{h,i}, \tag{2.35}$$

$$(\nabla \cdot \mathbf{u}_h, w)_{\Omega_i} = (f, w)_{\Omega_i}, \ w \in W_{h,i}, \tag{2.36}$$

$$\langle \alpha\lambda_{h,i} - \mathbf{u}_{h,i} \cdot \nu_i, \mu_i \rangle_{\Gamma_i} = \sum_{j=1}^{n} \langle \alpha\lambda_{h,j} + \mathbf{u}_{h,j} \cdot \nu_j, \mu_i \rangle_{\Gamma_{i,j}}, \ \mu_i \in \Lambda_{h,i}. \tag{2.37}$$

We can replace (2.37) by the condition that for each $i, 1 \le i \le n$

$$\sum_{j=1}^{n} \langle \alpha(\lambda_{h,i} - \lambda_{h,j}), \mu_i \rangle_{\Gamma_{i,j}} = \sum_{j=1}^{n} \langle \mathbf{u}_{h,i} \cdot \nu_i + \mathbf{u}_{h,j} \cdot \nu_j, \mu_i \rangle_{\Gamma_{i,j}}, \ \mu_i \in \Lambda_{h,i} \tag{2.38}$$

Existence and uniqueness of a solution to (2.35)–(2.37) are shown in [13] along with optimal convergence for both pressure and velocity:

$$\|p - p_h\| + \|\mathbf{u} - \mathbf{u}_h\| + \left(\alpha \sum_{i,j} \|\lambda_{h,i} - \lambda_{h,j}\|^2_{\Gamma_{i,j}} \right)^{1/2} + \left(\frac{1}{\alpha} \sum_{i,j} \|\mathbf{u}_{h,i} \cdot \nu_i + \mathbf{u}_{h,j} \cdot \nu_j\|^2_{\Gamma_{i,j}} \right)^{1/2} \le Ch^r, \tag{2.39}$$

$$1 \le r \le \min(k+1, l+1),$$

$$\left\{ \sum_{i=1}^{n} \|\nabla \cdot (\mathbf{u} - \mathbf{u}_{h,i})\|^2_{\Omega_i} \right\}^{1/2} \le Ch^r, \quad 1 \le r \le l+1. \tag{2.40}$$

2.2 TWO-PHASE FLOW IN POROUS MEDIA

We next consider two-phase immiscible flow in porous media. The governing mass conservation equations [28] are imposed on each subdomain Ω_i:

$$\frac{\partial(\phi\rho_\alpha S_\alpha)}{\partial t} + \nabla \cdot \mathbf{U}_\alpha = q_\alpha, \quad \text{in } \Omega_i \times (0,T], \tag{2.41}$$

where $\alpha = w$ (wetting), n (non-wetting) denotes the phase, S_α is the phase saturation, $\rho_\alpha = \rho_\alpha(P_\alpha)$ is the phase density, ϕ is the porosity, q_α is the source term, and

$$\mathbf{U}_\alpha = -\frac{k_\alpha(S_\alpha)K}{\mu_\alpha}\rho_\alpha(\nabla P_\alpha - \rho_\alpha g \nabla D), \quad \text{in } \Omega_i \times (0,T] \tag{2.42}$$

is the Darcy velocity. Here P_α is the phase pressure, $k_\alpha(S_\alpha)$ is the phase relative permeability, μ_α is the phase viscosity, K is the rock permeability tensor, g is the gravitational constant, and D is the depth. On each interface $\Gamma_{i,j}$ the following physically meaningful continuity conditions are imposed:

$$P_\alpha|_{\Omega_i} = P_\alpha|_{\Omega_j}, \tag{2.43}$$

$$[\mathbf{U}_\alpha \cdot \nu]_{i,j} \equiv \mathbf{U}_\alpha|_{\Omega_i} \cdot \nu_i + \mathbf{U}_\alpha|_{\Omega_j} \cdot \nu_j = 0. \tag{2.44}$$

The above equations are coupled via the volume balance equation and the capillary pressure relation

$$S_w + S_n = 1, \quad p_c(S_w) = P_n - P_w, \tag{2.45}$$

which are imposed on each Ω_i and $\Gamma_{i,j}$. We assume that no flow $\mathbf{U}_\alpha \cdot \nu = 0$ is imposed on $\partial\Omega$, although more general types of boundary conditions can also be treated.

Note that two of the unknowns in (2.41)-(2.42) can be eliminated using relations (2.45). A common practice is to choose as primary variables one pressure and one saturation which we denote by P and S.

Using the expanded mixed finite element formulation [12], let, for $\alpha = w$, n,

$$\tilde{\mathbf{U}}_\alpha = -\nabla P_\alpha.$$

Then

$$\mathbf{U}_\alpha = \frac{k_\alpha(S_\alpha)K}{\mu_\alpha}\rho_\alpha(\tilde{\mathbf{U}}_\alpha + \rho_\alpha g \nabla D).$$

The motivation for introducing the new variable $\tilde{\mathbf{U}}_\alpha$ is to avoid inverting $k_\alpha(S_\alpha)$, which can be zero if phase α is immobile. The gradient $\tilde{\mathbf{U}}_\alpha$ is discretized in the space $\tilde{\mathbf{V}}_{h,i}$, which is the space $\mathbf{V}_{h,i}$ without imposing the no-flow boundary condition. This choice, combined with appropriate quadrature rules for the mass matrices, allows for local elimination of both $\tilde{\mathbf{U}}_\alpha$ and $\mathbf{U}_\alpha$, reducing the method to cell-centered finite differences for the subdomain primary variables P_h and S_h, coupled with the mortar primary variables P_h^M and S_h^M, see [12] for details.

3.0 INTERIOR ERROR ESTIMATES

While using computational grids that do not match across interfaces has its many advantages, there is also price to be paid. Since the local mass conservation is imposed only weakly, this results in some loss of accuracy, especially when using coarser mortar space. In this chapter we study if the numerical error due to the non-matching grids propagates into the interior. The standard error analysis for finite element methods requires regularity conditions of the solution. However, such smoothness will generally not hold if the domain is not smoothly bounded or if the boundary or forcing term is not smooth. In such a case even though the solution will not be globally smooth, it might be and often is smooth in large subdomains away from the boundary and/or singularities in the data. It is therefore important to ask whether the optimal convergence holds in such subdomains, or the singularities deteriorate the convergence globally.

In this chapter we only consider the case of diagonal tensor K and RTN spaces [60, 57] on rectangular grids. Note that here $l = k$.

Let $\Omega_i^{'}$ be compactly contained in $\Omega_i, i = 1, \cdots, n$ and let $\Omega^{'} = \cup_{i=1}^{n} \Omega_i^{'}$.

3.1 INTERIOR ESTIMATES FOR THE MORTAR MIXED FINITE ELEMENT METHODS

Subtracting equations (2.25)–(2.27) from (2.22)–(2.24) gives the error equations for mortar mixed finite element methods:

$$(K^{-1}(\mathbf{u}-\mathbf{u}_h),\mathbf{v}) = \sum_{i=1}^{n}((p-p_h,\nabla\cdot\mathbf{v})_{\Omega_i} - \langle p,\mathbf{v}\cdot\nu_i\rangle_{\Gamma_i}), \qquad \mathbf{v}\in\mathbf{V}_h^0 \tag{3.1}$$

$$\sum_{i=1}^{n}(\nabla\cdot(\mathbf{u}-\mathbf{u}_h),w)_{\Omega_i} = 0, \qquad w\in W_h. \tag{3.2}$$

We will need the following lemma.

Lemma 3.1. *If $\phi\in H^1(\Omega)$ and $\mathbf{v}\in\mathbf{V}_h$, then there exists a constant C independent of h such that*

$$\|(I-\Pi)(\phi\mathbf{v})\| \le C\|\mathbf{v}\|\|\phi\|_1\, h.$$

Proof. For any $\mathbf{v}\in\mathbf{V}_h$, consider the functional

$$l_{\mathbf{v}}(\phi) = \phi\mathbf{v} - \Pi(\phi\mathbf{v}).$$

Since $l_{\mathbf{v}}(\phi) = 0$ for all constant functions ϕ, the statement of the lemma follows from an application of the Bramble-Hilbert lemma [32]. □

We prove the following interior velocity error estimates for mortar mixed finite element methods.

Theorem 3.1. *Assume (2.5). Then, for any $\varepsilon>0$, there exist a constant C_ε independent of h such that*

$$\|\Pi\mathbf{u}-\mathbf{u}_h\|_{\Omega'} \le C_\varepsilon\sum_{i=1}^{n}(\|p\|_{k+2,\Omega_i} + \|\mathbf{u}\|_{k+2,\Omega_i} + \|\nabla\cdot\mathbf{u}\|_{k+1,\Omega_i})h^{k+2-\varepsilon}.$$

Proof. Key ingredients in the proof of the theorem are:

- velocity error estimate (Theorem 4.2 in [9])

$$\|\Pi\mathbf{u}-\mathbf{u}_h\| \le C\sum_{i=1}^{n}(\|p\|_{k+2,\Omega_i} + \|\mathbf{u}\|_{k+1,\Omega_i})h^{k+1}, \tag{3.3}$$

- Durán's type argument (see [38], Theorem 3.1)

$$(K^{-1}(\Pi_i \mathbf{u} - \mathbf{u}), \mathbf{v})_{\Omega_i} \leq C\|\mathbf{u}\|_{k+2,\Omega_i} h^{k+2} \|\mathbf{v}\|_{\Omega_i}, \quad \mathbf{v} \in \mathbf{V}_h, \tag{3.4}$$

- superconvergence for pressure (Theorem 5.1 in [9]), assuming H^2-regularity

$$\|\hat{p} - p_h\| \leq C \sum_{i=1}^{n} (\|p\|_{k+2,\Omega_i} + \|\mathbf{u}\|_{k+1,\Omega_i} + \|\nabla \cdot \mathbf{u}\|_{k+1,\Omega_i}) h^{k+2}. \tag{3.5}$$

For $i = 1, \cdots, n$, consider subdomain sequences $\Omega_i^j, j = 1, 2, \cdots$ such that

$$\Omega_i' \subset\subset \Omega_i^{j+1} \subset\subset \Omega_i^j \subset\subset \Omega_i.$$

Let $\Omega^j = \cup_{i=1}^n \Omega_i^j$. Use cutoff function $0 \leq \phi_{j+1} \in C_0^\infty(\Omega^j)$ with $\phi_{j+1} \equiv 1$ on Ω^{j+1} and $\phi_{j+1} \leq 1$ on Ω^j. The constants that appear below may depend on $\|\phi_{j+1}\|_{1,\infty,\Omega^j}$. Note that, since $\phi_j \equiv 1$ on Ω^j,

$$\|\mathbf{v}\|_{\Omega^j} = \|\phi_j^{1/2}\mathbf{v}\|_{\Omega^j} \leq \|\phi_j^{1/2}\mathbf{v}\|_{\Omega^{j-1}},$$

which will be used repeatedly in our argument.

We have, using (3.1) with $\mathbf{v} = \Pi(\phi_{j+1}(\Pi\mathbf{u} - \mathbf{u}_h))$,

$$\begin{aligned}
&c\|\phi_{j+1}^{1/2}(\Pi\mathbf{u} - \mathbf{u}_h)\|_{\Omega^j}^2 \leq (K^{-1}(\Pi\mathbf{u} - \mathbf{u}_h), \phi_{j+1}(\Pi\mathbf{u} - \mathbf{u}_h))_{\Omega^j} \\
&= (K^{-1}(\Pi\mathbf{u} - \mathbf{u}_h), (I - \Pi)(\phi_{j+1}(\Pi\mathbf{u} - \mathbf{u}_h)))_{\Omega^j} + (K^{-1}(\Pi\mathbf{u} - \mathbf{u}_h), \Pi\phi_{j+1}(\Pi\mathbf{u} - \mathbf{u}_h))_{\Omega^j} \\
&= (K^{-1}(\Pi\mathbf{u} - \mathbf{u}_h), (I - \Pi)(\phi_{j+1}(\Pi\mathbf{u} - \mathbf{u}_h)))_{\Omega^j} + (K^{-1}(\Pi\mathbf{u} - \mathbf{u}), \Pi\phi_{j+1}(\Pi\mathbf{u} - \mathbf{u}_h))_{\Omega^j} \\
&\quad + \sum_{i=1}^{n} (p - p_h, \nabla \cdot (\Pi\phi_{j+1}(\Pi\mathbf{u} - \mathbf{u}_h)))_{\Omega_i^j} \\
&\leq C\|\Pi\mathbf{u} - \mathbf{u}_h\|_{\Omega^j} \|(I - \Pi)(\phi_{j+1}(\Pi\mathbf{u} - \mathbf{u}_h))\|_{\Omega^j} + C \sum_{i=1}^{n} \|\mathbf{u}\|_{k+2,\Omega_i} h^{k+2} \|\Pi\phi_{j+1}(\Pi\mathbf{u} - \mathbf{u}_h)\|_{\Omega^j} \\
&\quad + \sum_{i=1}^{n} (p - p_h, \nabla \cdot \Pi(\phi_{j+1}(\Pi\mathbf{u} - \mathbf{u}_h)))_{\Omega_i^j},
\end{aligned} \tag{3.6}$$

where we have used (3.4) in the last inequality. Using (3.3) and Lemma 3.1, the first term on the right can be easily estimated as

$$\begin{aligned}\|\Pi\mathbf{u}-\mathbf{u}_h\|_{\Omega^j}&\|(I-\Pi)(\phi_{j+1}(\Pi\mathbf{u}-\mathbf{u}_h))\|_{\Omega^j}\\ &\le C\sum_{i=1}^{n}(\|p\|_{k+2,\Omega_i}+\|\mathbf{u}\|_{k+1,\Omega_i})h^{k+1}\|\Pi\mathbf{u}-\mathbf{u}_h\|_{\Omega^j}\|\phi_{j+1}\|_{1,\Omega^j}\,h\\ &\le C\sum_{i=1}^{n}(\|p\|_{k+2,\Omega_i}+\|\mathbf{u}\|_{k+1,\Omega_i})h^{k+2}\|\phi_j^{1/2}(\Pi\mathbf{u}-\mathbf{u}_h)\|_{\Omega^{j-1}}.\end{aligned} \tag{3.7}$$

For the second term on the right in (3.6) we have

$$\begin{aligned}\|\Pi\phi_{j+1}(\Pi\mathbf{u}-\mathbf{u}_h)\|_{\Omega^j}&\le\|(I-\Pi)\phi_{j+1}(\Pi\mathbf{u}-\mathbf{u}_h)\|_{\Omega^j}+\|\phi_{j+1}(\Pi\mathbf{u}-\mathbf{u}_h)\|_{\Omega^j}\\ &\le Ch\|\Pi\mathbf{u}-\mathbf{u}_h\|_{\Omega^j}+\|\phi_{j+1}\|_{\infty,\Omega^j}\|\Pi\mathbf{u}-\mathbf{u}_h\|_{\Omega^j}\\ &\le C\|\phi_j^{1/2}(\Pi\mathbf{u}-\mathbf{u}_h)\|_{\Omega^{j-1}},\end{aligned} \tag{3.8}$$

using Lemma 3.1 for the second inequality. The last term on the right in (3.6) can be bounded as

$$\begin{aligned}(p-p_h,\nabla\cdot\Pi(\phi_{j+1}(\Pi\mathbf{u}-\mathbf{u}_h)))_{\Omega_i^j}&=(\hat{p}-p_h,\nabla\cdot\Pi(\phi_{j+1}(\Pi\mathbf{u}-\mathbf{u}_h)))_{\Omega_i^j}\\ &=(\hat{p}-p_h,\nabla\phi_{j+1}\cdot(\Pi\mathbf{u}-\mathbf{u}_h)))_{\Omega_i^j}\\ &\le C\|\hat{p}-p_h\|_{\Omega_i^j}\|\phi_j^{1/2}(\Pi\mathbf{u}-\mathbf{u}_h)\|_{\Omega_i^{j-1}}\end{aligned} \tag{3.9}$$

using (2.12), (2.14), and (3.2). Summation over the blocks in (3.9) and an application of (3.5) lead to

$$\begin{aligned}\sum_{i=1}^{n}(p-p_h,\nabla\cdot\Pi(\phi_{j+1}(\Pi\mathbf{u}-\mathbf{u}_h)))_{\Omega_i^j}&\le C\|\hat{p}-p_h\|_{\Omega^j}\|\phi_j^{1/2}(\Pi\mathbf{u}-\mathbf{u}_h)\|_{\Omega^{j-1}}\\ &\le C\sum_{i=1}^{n}(\|p\|_{k+2,\Omega_i}+\|\mathbf{u}\|_{k+1,\Omega_i}+\|\nabla\cdot\mathbf{u}\|_{k+1,\Omega_i})h^{k+2}\|\phi_j^{1/2}(\Pi\mathbf{u}-\mathbf{u}_h)\|_{\Omega^{j-1}}.\end{aligned} \tag{3.10}$$

Combining (3.6), (3.7), (3.8), and (3.10), we get

$$\begin{aligned}
&\|\phi_{j+1}^{1/2}(\Pi\mathbf{u}-\mathbf{u}_h)\|_{\Omega^j} \\
&\qquad \le Ch^{\frac{k+2}{2}}\|\phi_j^{1/2}(\Pi\mathbf{u}-\mathbf{u}_h)\|_{\Omega^{j-1}}^{1/2}\left(\sum_{i=1}^{n}(\|p\|_{k+2,\Omega_i}+\|\mathbf{u}\|_{k+2,\Omega_i}+\|\nabla\cdot\mathbf{u}\|_{k+1,\Omega_i})\right)^{1/2} \\
&\qquad \equiv Ch^{\frac{k+2}{2}}\|\phi_j^{1/2}(\Pi\mathbf{u}-\mathbf{u}_h)\|_{\Omega^{j-1}}^{1/2}A^{1/2}.
\end{aligned} \tag{3.11}$$

Replacing $j+1$ with j in (3.11), we obtain

$$\|\phi_j^{1/2}(\Pi\mathbf{u}-\mathbf{u}_h)\|_{\Omega^{j-1}}^{1/2} \le Ch^{\frac{k+2}{4}}\|\phi_{j-1}^{1/2}(\Pi\mathbf{u}-\mathbf{u}_h)\|_{\Omega^{j-2}}^{1/4}A^{1/4}. \tag{3.12}$$

Multiplying (3.11) and (3.12) recurrently leads to

$$\|\phi_{j+1}^{1/2}(\Pi\mathbf{u}-\mathbf{u}_h)\|_{\Omega^j} \le Ch^{(k+2)(\frac{1}{2}+\frac{1}{4}+\cdots)}A^{\frac{1}{2}+\frac{1}{4}+\cdots} \le Ch^{k+2-\varepsilon}A,$$

where we take enough terms so that $\frac{1}{2}+\frac{1}{4}+\cdots \ge 1-\frac{\varepsilon}{k+2}$. □

3.2 INTERIOR ESTIMATES FOR THE NON-MORTAR MIXED FINITE ELEMENT METHOD

Similarly to the case of mortar mixed finite element method, subtracting equations (2.35)–(2.37) from (2.32)–(2.34) and using properties of the projections, we get the error equations for the non-mortar mixed finite element method:

$$(K^{-1}(\mathbf{u}-\mathbf{u}_h),\mathbf{v})_{\Omega_i} = (\hat{p}-p_h,\nabla\cdot\mathbf{v})_{\Omega_i} - \langle p_i-\lambda_{h,i},\mathbf{v}\cdot\nu_i\rangle_{\Gamma_i}, \qquad \mathbf{v}\in\mathbf{V}_{h,i}, \tag{3.13}$$

$$(\nabla\cdot(\mathbf{u}-\mathbf{u}_h),w)_{\Omega_i} = 0, \qquad w\in W_{h,i}, \tag{3.14}$$

$$\sum_{j=1}^{n}\langle\alpha(\lambda_{h,i}-\lambda_{h,j}),\mu_i\rangle_{\Gamma_{i,j}} = \sum_{j=1}^{n}\langle\mathbf{u}_{h,i}\cdot\nu_i+\mathbf{u}_{h,j}\cdot\nu_j,\mu_i\rangle_{\Gamma_{i,j}}, \qquad \mu_i\in\Lambda_{h,i}. \tag{3.15}$$

In addition to the projection operators defined in Chapter 2, we define the L^2-orthogonal projection of a function $f\in L^2(\Gamma_i)$ by $\bar{f}_i\in\Lambda_{h,i}$ satisfying

$$\langle f-\bar{f}_i,\mu_i\rangle = 0, \quad \forall\mu_i\in\Lambda_{h,i}=\mathbf{V}_{h,i}\cdot\nu_i, \tag{3.16}$$

that has the approximation property

$$\|f - \bar{f}_i\|_{\Gamma_{i,j}} \leq C\|f\|_{r,\Gamma_{i,j}} h^r, \quad 0 \leq r \leq k+1. \tag{3.17}$$

One of the key ingredients in the proof of Theorem 3.1, namely superconvergence for pressure, was missing in the analysis of [13]. Using duality, we prove the following pressure superconvergence theorem.

Theorem 3.2. *Assume (2.5). For the pressure p_h of the mixed method (2.35)–(2.37), there exists a positive constant C, independent of h, such that*

$$\|\hat{p} - p_h\| \leq Ch^{r+1/2}, \quad 1 \leq r \leq \min(k+1, l+1). \tag{3.18}$$

Proof. Let $\xi \in H^2(\Omega)$ be the solution of the auxiliary problem

$$\begin{aligned} -\nabla \cdot K\nabla\xi &= \hat{p} - p_h \qquad \text{in } \Omega, \\ \xi &= 0 \qquad\qquad \text{on } \partial\Omega, \end{aligned}$$

and note that by elliptic regularity,

$$\|\xi\|_2 \leq C\|\hat{p} - p_h\|. \tag{3.19}$$

Let $\boldsymbol{\zeta} = -K\nabla\xi$. Taking $\mathbf{v} = \Pi_i\boldsymbol{\zeta} \in \mathbf{V}_{h,i}$ in (3.13) and using (2.14),

$$\|\hat{p}-p_h\|_{\Omega_i}^2 = (\hat{p}-p_h, \nabla\cdot\boldsymbol{\zeta})_{\Omega_i} = (K^{-1}(\mathbf{u}-\mathbf{u}_h), \Pi_i\boldsymbol{\zeta}-\boldsymbol{\zeta})_{\Omega_i} - (\mathbf{u}-\mathbf{u}_h, \nabla\xi)_{\Omega_i} + \langle p_i - \lambda_{h,i}, \Pi_i\boldsymbol{\zeta}\cdot\nu_i\rangle_{\Gamma_i}.$$

Sum over i and use (3.16) and (2.15) to get

$$\begin{aligned} \|\hat{p} - p_h\|^2 &= \sum_{i=1}^n (K^{-1}(\mathbf{u}-\mathbf{u}_h), \Pi_i\boldsymbol{\zeta} - \boldsymbol{\zeta})_{\Omega_i} - \sum_{i=1}^n (\mathbf{u}-\mathbf{u}_h, \nabla\xi)_{\Omega_i} + \sum_{i=1}^n \langle \overline{p_i} - \lambda_{h,i}, \Pi_i\boldsymbol{\zeta}\cdot\nu_i\rangle_{\Gamma_i} \\ &\leq C\|\mathbf{u}-\mathbf{u}_h\| \sum_{i=1}^n \|\Pi_i\boldsymbol{\zeta} - \boldsymbol{\zeta}\|_{\Omega_i} + \sum_{i=1}^n (\nabla\cdot(\mathbf{u}-\mathbf{u}_h), \xi - \hat{\xi})_{\Omega_i} \\ &\quad - \sum_{i=1}^n \langle(\mathbf{u}-\mathbf{u}_{h,i})\cdot\nu_i, \xi\rangle_{\Gamma_i} + \sum_{i=1}^n \langle \overline{p_i} - \lambda_{h,i}, \boldsymbol{\zeta}_i\cdot\nu_i\rangle_{\Gamma_i}, \end{aligned} \tag{3.20}$$

where we integrated by parts the second term and used (3.14). The first two terms in (3.20) are easy to handle. Using (2.39), (2.40) and the approximation properties (2.18) and (2.16), we get

$$\begin{aligned}
&\|\mathbf{u}-\mathbf{u}_h\|\,\|\Pi_i\boldsymbol{\zeta}-\boldsymbol{\zeta}\|_{\Omega_i} \le Ch^r\,h\|\boldsymbol{\zeta}\|_{1,\Omega_i} \le Ch^{r+1}\|\hat{p}-p_h\|, \quad 1\le r\le \min(k+1,l+1),\\
&(\nabla\cdot(\mathbf{u}-\mathbf{u}_h),\xi-\hat{\xi})_{\Omega_i} \le \|\nabla\cdot(\mathbf{u}-\mathbf{u}_h)\|_{\Omega_i}\|\xi-\hat{\xi}\|_{\Omega_i} \le Ch^r h\|\xi\|_{1,\Omega_i}\\
&\qquad\qquad \le Ch^{r+1}\|\hat{p}-p_h\|, \quad 1\le r\le l+1.
\end{aligned} \tag{3.21}$$

Using the continuity of ξ and $\mathbf{u}$, rearrange the third term in (3.20)

$$\begin{aligned}
-\sum_{i=1}^{n}\langle(\mathbf{u}-\mathbf{u}_{h,i})\cdot\nu_i,\xi\rangle_{\Gamma_i} &= -\frac{1}{2}\sum_{i,j}\langle(\mathbf{u}-\mathbf{u}_{h,i})\cdot\nu_i+(\mathbf{u}-\mathbf{u}_{h,j})\cdot\nu_j,\xi\rangle_{\Gamma_{i,j}}\\
&= \frac{1}{2}\sum_{i,j}\langle\mathbf{u}_{h,i}\cdot\nu_i+\mathbf{u}_{h,j}\cdot\nu_j,\overline{\xi_i}\rangle_{\Gamma_{i,j}}+\frac{1}{2}\sum_{i,j}\langle\mathbf{u}_{h,i}\cdot\nu_i+\mathbf{u}_{h,j}\cdot\nu_j,\xi-\overline{\xi_i}\rangle_{\Gamma_{i,j}}.
\end{aligned} \tag{3.22}$$

Bounding the second term on the right in (3.22) is straightforward: (2.39), (3.17) and (2.21) give

$$\begin{aligned}
&\sum_{i,j}\langle\mathbf{u}_{h,i}\cdot\nu_i+\mathbf{u}_{h,j}\cdot\nu_j,\xi-\overline{\xi_i}\rangle_{\Gamma_{i,j}}\\
&\qquad\le \left(\sum_{i,j}\|\mathbf{u}_{h,i}\cdot\nu_i+\mathbf{u}_{h,j}\cdot\nu_j\|^2_{\Gamma_{i,j}}\right)^{1/2}\left(\sum_{i,j}\|\xi-\overline{\xi_i}\|^2_{\Gamma_{i,j}}\right)^{1/2}\\
&\qquad\le Ch^r\left(\sum_{i,j}h^2\|\xi\|^2_{1,\Gamma_{i,j}}\right)^{1/2} \le Ch^{r+1}\left(\sum_{i,j}\|\xi\|^2_{3/2,\Omega_i}\right)^{1/2}\\
&\qquad\le Ch^{r+1}\|\hat{p}-p_h\|, \quad 1\le r\le\min(k+1,l+1).
\end{aligned} \tag{3.23}$$

To handle the first term on the right in (3.22), take $\mu_i = \frac{1}{2}\overline{\xi_i}$ in (3.15), sum over i and rearrange to get

$$\begin{aligned}
\frac{1}{2}\sum_{i,j}\langle \mathbf{u}_{h,i}\cdot\nu_i + \mathbf{u}_{h,j}\cdot\nu_j, \overline{\xi_i}\rangle_{\Gamma_{i,j}} &= \frac{1}{2}\sum_{i,j}\langle \alpha(\lambda_{h,i}-\lambda_{h,j}), \overline{\xi_i}\rangle_{\Gamma_{i,j}} \\
&= \frac{1}{2}\sum_{i<j}\langle \alpha(\lambda_{h,i}-\lambda_{h,j}), \overline{\xi_i}-\overline{\xi_j}\rangle_{\Gamma_{i,j}} \\
&= \frac{1}{2}\sum_{i<j}\langle \alpha(\lambda_{h,i}-\lambda_{h,j}), (\overline{\xi_i}-\xi)+(\xi-\overline{\xi_j})\rangle_{\Gamma_{i,j}} \\
&\le \frac{1}{2}\sum_{i<j}\alpha\|\lambda_{h,i}-\lambda_{h,j}\|_{\Gamma_{i,j}}(\|\xi_i-\overline{\xi_i}\|_{\Gamma_{i,j}} + \|\xi_j-\overline{\xi_j}\|_{\Gamma_{i,j}}) \\
&\le Ch^r h\sum_{i<j}(\|\xi\|_{3/2,\Omega_i} + \|\xi\|_{3/2,\Omega_j}) \\
&\le Ch^{r+1}\|\hat{p}-p_h\|, \quad 1\le r\le \min(k+1,l+1),
\end{aligned} \tag{3.24}$$

where we used (2.39), (3.17), and (2.21) in the last inequality. Using the continuity of $\boldsymbol{\zeta}\cdot\nu$ and p, and rearranging the last term in (3.20), we obtain

$$\begin{aligned}
\sum_{i=1}^{n}\langle \overline{p_i}-\lambda_{h,i}, \boldsymbol{\zeta}_i\cdot\nu_i\rangle_{\Gamma_i} &= \frac{1}{2}\sum_{i,j}\langle \overline{p_i}-\lambda_{h,i}-\overline{p_j}+\lambda_{h,j}, \boldsymbol{\zeta}_i\cdot\nu_i\rangle_{\Gamma_{i,j}} \\
&= \frac{1}{2}\sum_{i,j}\langle \overline{p_i}-\overline{p_j}-\lambda_{h,i}+\lambda_{h,j}, (\boldsymbol{\zeta}_i-\Pi_i\boldsymbol{\zeta}_i)\cdot\nu_i\rangle_{\Gamma_{i,j}} \\
&\quad -\frac{1}{2}\sum_{i,j}\langle \lambda_{h,i}-\lambda_{h,j}, \Pi_i\boldsymbol{\zeta}_i\cdot\nu_i\rangle_{\Gamma_{i,j}} + \frac{1}{2}\sum_{i,j}\langle \overline{p_i}-\overline{p_j}, \Pi_i\boldsymbol{\zeta}_i\cdot\nu_i\rangle_{\Gamma_{i,j}}.
\end{aligned} \tag{3.25}$$

The first term in (3.25) is easy to bound using (2.39), (2.20), (3.17) and (2.21),

$$\begin{aligned}
&\langle \overline{p_i}-\overline{p_j}-\lambda_{h,i}+\lambda_{h,j}, (\boldsymbol{\zeta}_i-\Pi_i\boldsymbol{\zeta}_i)\cdot\nu_i\rangle_{\Gamma_{i,j}} \\
&\qquad \le \left(\|p_i-\overline{p_i}\|_{\Gamma_{i,j}} + \|p_j-\overline{p_j}\|_{\Gamma_{i,j}} + \|\lambda_{h,i}-\lambda_{h,j}\|_{\Gamma_{i,j}}\right)\|(\boldsymbol{\zeta}_i-\Pi_i\boldsymbol{\zeta}_i)\cdot\nu_i\|_{\Gamma_{i,j}} \\
&\qquad \le C\left(h^s\|p_i\|_{s+1/2,\Omega_i} + h^s\|p_j\|_{s+1/2,\Omega_j} + h^r\right)h^{1/2}\|\boldsymbol{\zeta}\|_{1,\Omega_i} \\
&\qquad \le Ch^{r+1/2}\|\hat{p}-p_h\|, \quad 1\le r\le\min(k+1,l+1), \quad 1\le s\le k+1.
\end{aligned} \tag{3.26}$$

To handle the second term in (3.25), take $\mu_i = \frac{1}{2\alpha}\Pi_i\boldsymbol{\zeta}_i \cdot \nu_i$ in (3.15), sum over i, combine the two terms on $\Gamma_{i,j}$ and use the continuity of $\boldsymbol{\zeta} \cdot \nu$ to obtain

$$\begin{aligned}
-\frac{1}{2}\sum_{i,j}\langle \lambda_{h,i} - \lambda_{h,j}, \Pi_i\boldsymbol{\zeta}_i \cdot \nu_i\rangle_{\Gamma_{i,j}} &= -\frac{1}{2\alpha}\sum_{i,j}\langle \mathbf{u}_{h,i}\cdot\nu_i + \mathbf{u}_{h,j}\cdot\nu_j, \Pi_i\boldsymbol{\zeta}_i\cdot\nu_i\rangle_{\Gamma_{i,j}} \\
&= -\frac{1}{2\alpha}\sum_{i<j}\langle \mathbf{u}_{h,i}\cdot\nu_i + \mathbf{u}_{h,j}\cdot\nu_j, \Pi_i\boldsymbol{\zeta}_i\cdot\nu_i + \Pi_j\boldsymbol{\zeta}_j\cdot\nu_j\rangle_{\Gamma_{i,j}} \\
&= \frac{1}{2\alpha}\sum_{i<j}\langle (\mathbf{u}_{h,i}\cdot\nu_i + \mathbf{u}_{h,j}\cdot\nu_j), (\boldsymbol{\zeta}_i - \Pi_i\boldsymbol{\zeta}_i)\cdot\nu_i + (\boldsymbol{\zeta}_j - \Pi_j\boldsymbol{\zeta}_j)\cdot\nu_j\rangle_{\Gamma_{i,j}} \\
&\le \frac{1}{2\alpha}\sum_{i<j}\|\mathbf{u}_{h,i}\cdot\nu_i + \mathbf{u}_{h,j}\cdot\nu_j\|_{\Gamma_{i,j}}(\|(\boldsymbol{\zeta}_i - \Pi_i\boldsymbol{\zeta}_i)\cdot\nu_i\|_{\Gamma_{i,j}} + \|(\boldsymbol{\zeta}_j - \Pi_j\boldsymbol{\zeta}_j)\cdot\nu_j\|_{\Gamma_{i,j}}) \\
&\le C\sum_{i<j} h^r h^{1/2}\|\hat{p} - p_h\|, \quad 1 \le r \le \min(k+1, l+1),
\end{aligned} \tag{3.27}$$

where we used (2.39), (2.20), and (2.21) for the last inequality. Finally, for the last term in (3.25), applying (3.16) and using the continuity of p and $\boldsymbol{\zeta}\cdot\nu$ we get

$$\begin{aligned}
\frac{1}{2}\sum_{i,j}\langle \overline{p_i} - \overline{p_j}, \Pi_i\boldsymbol{\zeta}_i\cdot\nu_i\rangle_{\Gamma_{i,j}} &= \frac{1}{2}\sum_{i,j}\langle p_i - \overline{p_j}, \Pi_i\boldsymbol{\zeta}_i\cdot\nu_i\rangle_{\Gamma_{i,j}} \\
&= \frac{1}{2}\sum_{i,j}\langle p_j - \overline{p_j}, \Pi_i\boldsymbol{\zeta}_i\cdot\nu_i \ + \Pi_j\boldsymbol{\zeta}_j\cdot\nu_j\rangle_{\Gamma_{i,j}} \\
&= \frac{1}{2}\sum_{i,j}\langle p_j - \overline{p_j}, (\Pi_i\boldsymbol{\zeta}_i - \boldsymbol{\zeta}_i)\cdot\nu_i + (\Pi_j\boldsymbol{\zeta}_j - \boldsymbol{\zeta}_j)\cdot\nu_j\rangle_{\Gamma_{i,j}} \\
&\le \frac{1}{2}\sum_{i,j}\|p_j - \overline{p_j}\|_{\Gamma_{i,j}}\left(\|(\boldsymbol{\zeta}_i - \Pi_i\boldsymbol{\zeta}_i)\cdot\nu_i\|_{\Gamma_{i,j}} + \|(\boldsymbol{\zeta}_j - \Pi_j\boldsymbol{\zeta}_j)\cdot\nu_j\|_{\Gamma_{i,j}}\right) \\
&\le C\sum_{i,j} h^r\|p\|_{k+3/2,\Omega_j}h^{1/2}\|\hat{p} - p_h\|, \quad 1 \le r \le k+1,
\end{aligned} \tag{3.28}$$

where we used (3.16), (2.20), and (2.21) at the end. Combining (3.20)–(3.28) finishes the proof of Theorem 3.2. □

Now we are ready to prove the following interior velocity error estimate for the non-mortar mixed finite element method:

Theorem 3.3. *Assume (2.5). Then, for any $\varepsilon > 0$, there exist a constant C_ε independent of h such that*

$$\|\Pi\mathbf{u} - \mathbf{u}_h\|_{\Omega'} \le C_\varepsilon h^{k+3/2-\varepsilon}.$$

Proof. Following the proof of Theorem 3.1, for $i = 1, \cdots, n$, consider subdomain sequences $\Omega_i^m, m = 1, 2, \cdots$ such that

$$\Omega_i^{'} \subset\subset \Omega_i^{m+1} \subset\subset \Omega_i^m \subset\subset \Omega_i.$$

Let

$$\Omega^m = \cup_{i=1}^n \Omega_i^m.$$

Let $0 \leq \phi_{m+1} \in C_0^\infty(\Omega^m)$ with $\phi_{m+1} \equiv 1$ on Ω^{m+1} and $\phi_{j+1} \leq 1$ on Ω^j. Using (3.13) with $\mathbf{v} = \Pi_i(\phi_{m+1}(\Pi_i\mathbf{u} - \mathbf{u}_h))$, we get,

$$\begin{aligned}
c\|\phi_{m+1}^{1/2}(\Pi_i\mathbf{u} - \mathbf{u}_h)\|_{\Omega_i^m}^2 &\leq (K^{-1}(\Pi_i\mathbf{u} - \mathbf{u}_h), \phi_{m+1}(\Pi_i\mathbf{u} - \mathbf{u}_h))_{\Omega_i^m} \\
&= (K^{-1}(\Pi_i\mathbf{u} - \mathbf{u}_h), (I - \Pi_i)(\phi_{m+1}(\Pi_i\mathbf{u} - \mathbf{u}_h)))_{\Omega_i^m} \\
&\quad + (K^{-1}(\Pi_i\mathbf{u} - \mathbf{u}_h), \Pi_i\phi_{m+1}(\Pi_i\mathbf{u} - \mathbf{u}_h))_{\Omega_i^m} \\
&= (K^{-1}(\Pi_i\mathbf{u} - \mathbf{u}_h), (I - \Pi_i)(\phi_{m+1}(\Pi_i\mathbf{u} - \mathbf{u}_h)))_{\Omega_i^m} \\
&\quad + (K^{-1}(\Pi_i\mathbf{u} - \mathbf{u}), \Pi_i\phi_{m+1}(\Pi_i\mathbf{u} - \mathbf{u}_h))_{\Omega_i^m} \\
&\quad + (\hat{p} - p_h, \nabla \cdot (\phi_{m+1}(\Pi_i\mathbf{u} - \mathbf{u}_h)))_{\Omega_i^m},
\end{aligned} \tag{3.29}$$

where we used (2.14) in the last equality. Note that if we take in (3.14)

$$w = \nabla \cdot (\Pi_i\mathbf{u} - \mathbf{u}_h) \in W_{h,i}$$

and use (2.14), we get $\nabla \cdot (\Pi_i\mathbf{u} - \mathbf{u}_h) = 0$ so the last term in (3.29) simplifies to $(\hat{p} - p_h, \nabla\phi_{m+1} \cdot (\Pi_i\mathbf{u} - \mathbf{u}_h))_{\Omega_i^m}$. Summing over the blocks in (3.29), we obtain

$$\begin{aligned}
c\|\phi_{m+1}^{1/2}(\Pi\mathbf{u} - \mathbf{u}_h)\|_{\Omega^m}^2 &\leq C\|\Pi\mathbf{u} - \mathbf{u}_h\|_{\Omega^m}\|(I - \Pi)(\phi_{m+1}(\Pi\mathbf{u} - \mathbf{u}_h))\|_{\Omega^m} \\
&\quad + (K^{-1}(\Pi\mathbf{u} - \mathbf{u}), \Pi\phi_{m+1}(\Pi\mathbf{u} - \mathbf{u}_h))_{\Omega^m} \\
&\quad + \|\hat{p} - p_h\|_{\Omega^m}\|\nabla\phi_{m+1} \cdot (\Pi\mathbf{u} - \mathbf{u}_h)\|_{\Omega^m} \\
&\leq Ch^{k+1}\|\Pi\mathbf{u} - \mathbf{u}_h\|_{\Omega^m}\|\phi_{m+1}\|_{1,\Omega^m} h \\
&\quad + C\sum_{i=1}^n \|\mathbf{u}\|_{k+2,\Omega_i} h^{k+2}\|\Pi\phi_{m+1}(\Pi\mathbf{u} - \mathbf{u}_h)\|_{\Omega^m} \\
&\quad + Ch^{k+3/2}\|\phi_m^{1/2}(\Pi\mathbf{u} - \mathbf{u}_h)\|_{\Omega^{m-1}},
\end{aligned} \tag{3.30}$$

where for the last step we used (2.39), Lemma 3.1, (3.4), and Theorem 3.2. Using again Lemma 3.1 for the second term on the right in (3.30), we get

$$\begin{aligned} \|\Pi\phi_{m+1}(\Pi\mathbf{u}-\mathbf{u}_h)\|_{\Omega^m} &\leq Ch\|\Pi\mathbf{u}-\mathbf{u}_h\|_{\Omega^m} + \|\phi_m^{1/2}(\Pi\mathbf{u}-\mathbf{u}_h)\|_{\Omega^{m-1}} \\ &\leq C\|\phi_m^{1/2}(\Pi\mathbf{u}-\mathbf{u}_h)\|_{\Omega^{m-1}}. \end{aligned} \tag{3.31}$$

Combining (3.30) and (3.31) and taking square root leads to

$$\|\phi_{m+1}^{1/2}(\Pi\mathbf{u}-\mathbf{u}_h)\|_{\Omega^m} \leq Ch^{\frac{1}{2}(k+3/2)}\|\phi_m^{1/2}(\Pi\mathbf{u}-\mathbf{u}_h)\|_{\Omega^{m-1}}^{1/2},$$

which, when applied recurrently, completes the proof. □

3.3 NUMERICAL SIMULATIONS

We present three numerical tests confirming the theoretical results of Section 3.1. All examples are on the unit square. The domain is divided into four subdomains with interfaces along the $x = 1/2$ and $y = 1/2$ lines. We tested four types of methods on non-matching interfaces: 1 (continuous piecewise linear mortars), 2 (discontinuous piecewise linear mortars), 3 (Robin type interface conditions - non-mortar mixed finite element method), and 4 (piecewise constant mortars). For the third example we tested also matching grids (denoted by mortar 0). In the numerical experiments we report the rates of convergence of the numerical solution (pressure and velocity) to the true solution. The convergence rates are established by running each test case on five (four for Example 3.3) levels of grid refinement and computing a least squares fit to the error. The initial mesh on each block is uniform (shown on Figure 3.1) and the initial mortar grids on all interfaces are given in Table 3.1. The interior subdomains $\Omega_i^{'}$ were chosen on the initial mesh to have a one-element border and were kept fixed during the mesh refinement. The boundary conditions are Dirichlet on the left and right edge and Neumann on the rest of the boundary. In first two tests we solve problems with known analytical solutions.

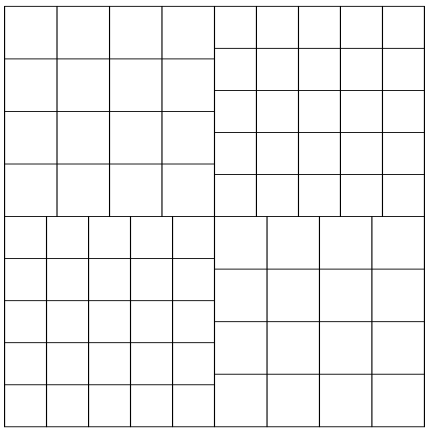

Figure 3.1: Initial grid for Examples 3.1, 3.2, and 3.3

Example 3.1.

We choose permeability

$$K = \begin{cases} I & , 0 \leq x < 1/2 \\ 10 * I & , 1/2 < x \leq 1 \end{cases}$$

and the solution

$$p(x,y) = \begin{cases} x^2y^3 + \cos(xy) & , 0 \leq x < 1/2 \\ \left(\frac{2x+9}{20}\right)^2 y^3 + \cos(\frac{2x+9}{20}y) & , 1/2 < x \leq 1 \end{cases}$$

is chosen to be continuous and to have continuous normal flux at $x = 1/2$. Plots of the computed solution and the numerical error for Example 3.1 are shown in Figure 3.2. As shown in Table 3.2, the interior velocity error is superconvergent of order $\mathcal{O}(h^2)$ and most of the error occurs near the interfaces, as it can be seen from the flux error. Recall that optimal convergence for the solution to (2.25)–(2.27) was shown ([9]) under the assumption that M_h contains at least piecewise polynomials of degree $k+1$. In the case of mortar 4, M_h contains only piecewise constant functions, and the interface error is predicted by the theory to be of order $\mathcal{O}(1)$. Still, even for that case we observe superconvergence of order $\mathcal{O}(h^2)$ for the interior velocity error.

Table 3.1: Initial number of elements in mortar grids for Examples 3.1, 3.2, and 3.3

mortar	1	2	3	4
elements	3	3	1	5

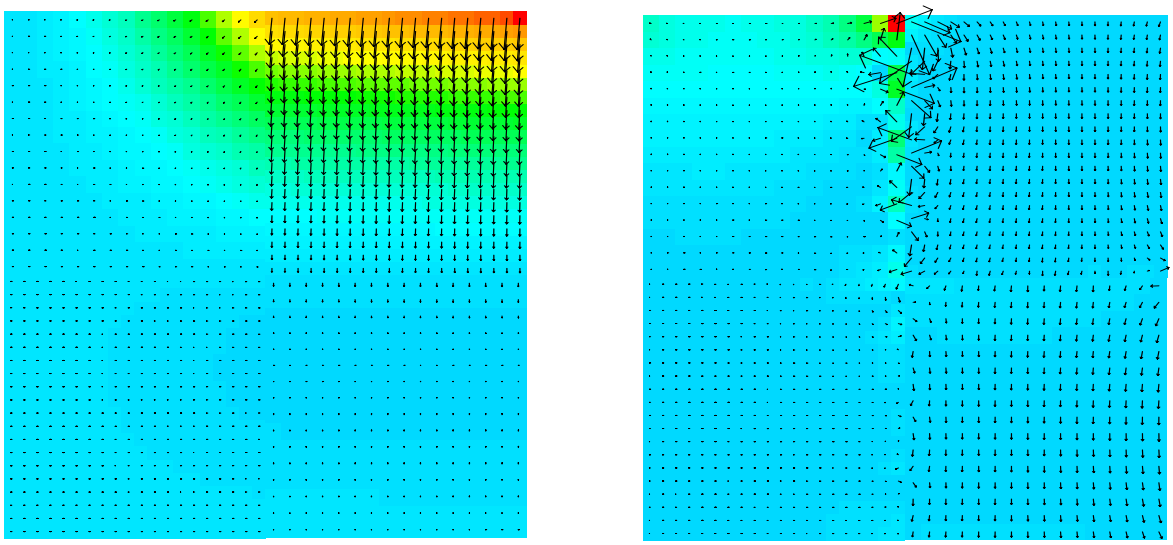

A. Computed pressure and velocity

B. Pressure and velocity error

Figure 3.2: Solution and error (magnified) for Example 3.1

Table 3.2: Convergence rates for Example 3.1

mor	*flux*	*press*	*velocity* L^2		*velocity* L^∞	
tar	*err*	*err*	Ω	*Int.*	Ω	*Int.*
1	1.00	2.01	1.79	1.99	0.87	1.97
2	1.01	1.96	1.97	2.00	1.25	1.97
3	0.22	1.98	1.66	1.97	0.75	1.96
4	0.11	1.78	1.18	1.98	0.20	1.97

Example 3.2.

We choose a discontinuous full tensor

$$K = \begin{cases} \begin{pmatrix} 2 & 1 \\ 1 & 2 \end{pmatrix} & , 0 \le x < 1/2 \\ I & , 1/2 < x \le 1 \end{cases}$$

and solution

$$p(x,y) = \begin{cases} xy & , 0 \le x \le 1/2 \\ xy + (x - 1/2)(y + 1/2) & , 1/2 \le x \le 1. \end{cases}$$

The results for Example 3.2 are in Figure 3.3 and Table 3.3. Even though the proof we gave is not valid for the case of full tensor, the numerical results show that the error in the case of non-matching grids and smooth solutions occurs mainly along the interfaces and high accuracy is preserved in the interior.

Table 3.3: Convergence rates for Example 3.2

mor	*flux*	*pres*	*velocity* L^2		*velocity* L^∞	
tar	*err*	*err*	Ω	*Int.*	Ω	*Int.*
1	1.30	2.00	1.46	1.98	0.96	1.89
2	1.19	2.00	1.46	1.98	0.97	1.87
3	0.05	1.94	0.75	2.03	0.25	1.99
4	-0.02	1.79	0.58	2.04	0.06	1.83

Example 3.3.

In this test we did not have any analytical solution. Instead, the solution from the initial run for the finest grid was saved and was used to calculate the errors for all coarser grids. The finest grid in the case of matching grids was chosen to be 128×128. The finest non-matching and mortar grids are shown in Table 3.4B and C. The permeability tensor is $K = a(x,y)I$, where

$$a(x,y) = \begin{cases} 100 & , \text{if } x < 1/2, y < 1/2 \text{ or } x > 1/2, y > 1/2 \\ 1 & , \text{otherwise} \end{cases}$$

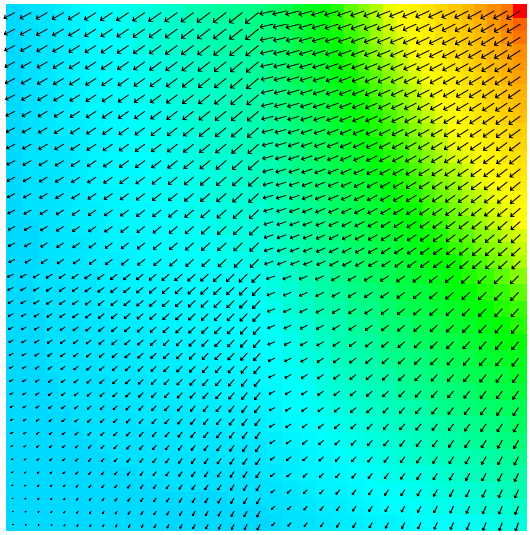

A. Computed pressure and velocity

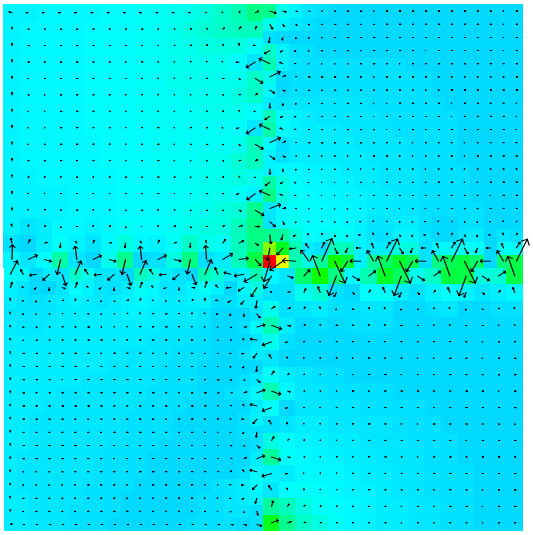

B. Pressure and velocity error

Figure 3.3: Solution and error (magnified) for Example 3.2

L^∞ errors are not reported since the true velocity is not in $L^\infty(\Omega)$. As the results show (Figure 3.4, Table 3.4A), because of the strong singularity at the cross-point $(1/2, 1/2)$, there is no superconvergence even in the interior. The rate of convergence for the interior velocity error is of order $\mathcal{O}(h^{3/4})$. Therefore to control the error we need some local refinement near this cross-point. This issue is addressed in the next chapter.

Table 3.4: Finest grids and convergence rates for Example 3.3

mor	*flux*	*press*	*velocity* L^2	
tar	*err*	*err*	Ω	*Int.*
0	0.09	0.67	0.60	0.74
1	0.09	0.68	0.61	0.74
2	0.07	0.68	0.60	0.74
3	0.09	0.70	0.64	0.77
4	0.09	0.68	0.61	0.74

A. Convergence rates

64×64	80×80
80×80	64×64

B. Finest grids for non-matching grids

mortar	1	2	3	4
elements	48	48	16	80

C. Mortar grids

Summarizing the test results in Section 3.3, we may conclude that in smooth cases

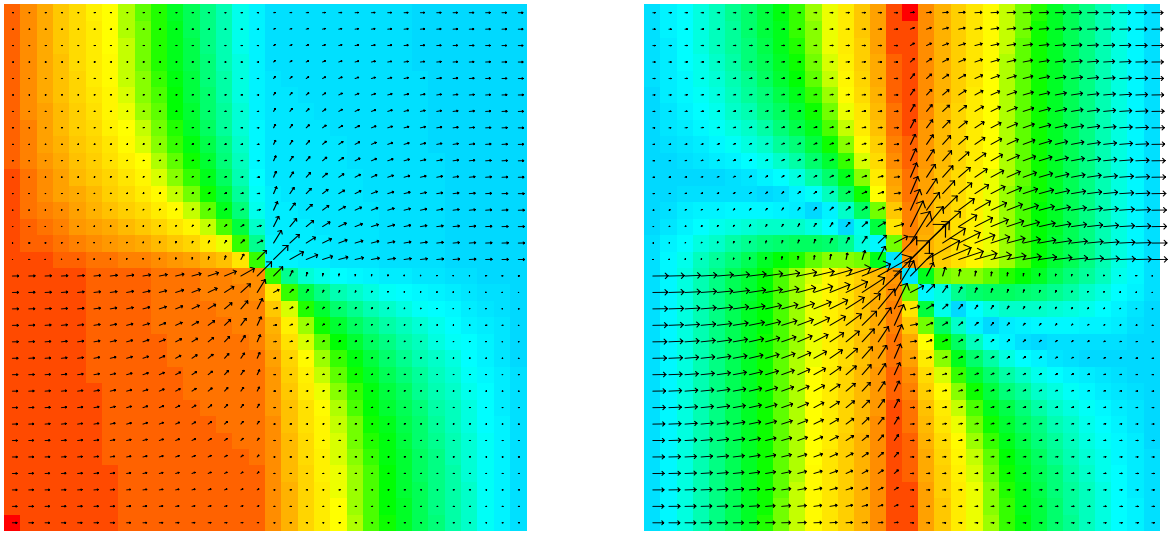

A. Computed pressure and velocity

B. Pressure and velocity error

Figure 3.4: Solution and error (magnified) for Example 3.3

the numerical error due to the non-matching grids is restricted to a small region around the interfaces. Superconvergence is preserved in the interior. In addition, we see that the interior velocity error depends on the smoothness of the solution in the whole domain Ω, but in a weaker sense, and that the interior velocity error is better than the velocity error calculated over the whole domain. These results also show the need of *a posteriori* error estimates and adaptive mesh refinement near the points of singularity to increase the overall accuracy of the solution.

4.0 *A POSTERIORI* ERROR ESTIMATES

In this chapter we study the effect of the upscaling error in *a posteriori* error estimators. Often the permeability data for problem (2.6)–(2.7) is generated using geostatistical modeling. As a result, this data is usually given at a very fine resolution. Due to limited computer resources one needs to approximate the problem on a very coarse scale. At this point, special care has to to be taken for the coefficients because fine-scale features of the data can have very large effects on the coarse-scale flow behavior. The process that calculates the coarse-scale data (*effective permeability* K_h) from a given fine-scale data is called *upscaling*. There are many different upscaling techniques: averaging (harmonic mean), Laplacian, multilevel, etc. All of them commit some error in modeling the coefficient K. Our goal is to include the modeling error due to upscaling in *a posteriori* error estimators. Since an adaptive mesh refinement algorithm involves computing solution on coarse grids, such upscaling error arises naturally and has to be taken into account.

We take the true permeability to be the one on the finest grid and on any coarser grid the approximate solution is found using the effective permeability. We extend the estimators in [70] to include this effect. We prove explicit upper bound for pressure, velocity and mortar pressure errors.

Equations (2.22)–(2.24) imply that $(\mathbf{u}, p, \lambda) \in \mathbf{V} \times W \times L^2(\Gamma)$ satisfies

$$A(\mathbf{u}, p, \lambda; \mathbf{v}, w, \mu) = L(\mathbf{v}, w, \mu) \quad \forall\ (\mathbf{v}, w, \mu) \in \mathbf{V} \times W \times L^2(\Gamma), \tag{4.1}$$

where

$$A(\mathbf{u}, p, \lambda; \mathbf{v}, w, \mu)$$
$$= \sum_{i=1}^{n} \left((K^{-1}\mathbf{u}, \mathbf{v})_{\Omega_i} - (p, \nabla \cdot \mathbf{v})_{\Omega_i} + \langle \lambda, \mathbf{v} \cdot \nu_i \rangle_{\Gamma_i} + \sigma (\nabla \cdot \mathbf{u}, w)_{\Omega_i} - \sigma \langle \mathbf{u} \cdot \nu_i, \mu \rangle_{\Gamma_i} \right)$$

and

$$L(\mathbf{v}, w, \mu) = \sigma(f, w) - \langle g, \mathbf{v} \cdot \nu \rangle_{\partial\Omega}.$$

Here $\sigma = 1$ or $\sigma = -1$. If $\sigma = -1$, $A(\cdot;\cdot)$ is a symmetric bilinear form, which we denote by $A^s(\cdot;\cdot)$. If $\sigma = 1$, we denote $A(\cdot;\cdot)$ by $A^c(\cdot;\cdot)$, which is non-symmetric, but coercive, since

$$A^c(\mathbf{v}, w, \mu; \mathbf{v}, w, \mu) = (K^{-1}\mathbf{v}, \mathbf{v}).$$

Note that the solution does not depend on the choice of σ. Different choices will be made for different arguments. Similarly, $(\mathbf{u}_h, p_h, \lambda_h) \in \mathbf{V}_h \times W_h \times M_h$ satisfies

$$A^h(\mathbf{u}_h, p_h, \lambda_h; \mathbf{v}, w, \mu) = L(\mathbf{v}, w, \mu) \quad \forall\ (\mathbf{v}, w, \mu) \in \mathbf{V}_h \times W_h \times M_h, \tag{4.2}$$

where $A^h(\cdot;\cdot)$ is a bilinear form similar to $A(\cdot;\cdot)$ with K_h^{-1} replacing K^{-1},

$$\begin{aligned} &A^h(\mathbf{u}, p, \lambda; \mathbf{v}, w, \mu) \\ &\quad = \sum_{i=1}^{n} \left((K_h^{-1}\mathbf{u}, \mathbf{v})_{\Omega_i} - (p, \nabla \cdot \mathbf{v})_{\Omega_i} + \langle \lambda, \mathbf{v} \cdot \nu_i \rangle_{\Gamma_i} + \sigma(\nabla \cdot \mathbf{u}, w)_{\Omega_i} - \sigma \langle \mathbf{u} \cdot \nu_i, \mu \rangle_{\Gamma_i} \right). \end{aligned}$$

We denote $A^h(\cdot;\cdot)$ by $A^{h,s}(\cdot;\cdot)$ if $\sigma = -1$, and by $A^{h,c}(\cdot;\cdot)$ if $\sigma = 1$.

Our goal is to derive *a posteriori* estimates of the error functions

$$\xi = \mathbf{u} - \mathbf{u}_h, \quad \eta = p - p_h, \quad \text{and} \quad \delta = \lambda - \lambda_h.$$

Using (4.1), $(\xi, \eta, \delta) \in \mathbf{V} \times W \times L^2(\Gamma)$ satisfies the residual equation

$$\begin{aligned} A^h(\xi, \eta, \delta; \mathbf{v}, w, \mu) &= L(\mathbf{v}, w, \mu) - A^h(\mathbf{u}_h, p_h, \lambda_h; \mathbf{v}, w, \mu) \\ &\quad + \sum_{i=1}^{n} ((K_h^{-1} - K^{-1})\mathbf{u}, \mathbf{v})_{\Omega_i}, \quad \forall\ (\mathbf{v}, w, \mu) \in \mathbf{V} \times W \times L^2(\Gamma), \end{aligned} \tag{4.3}$$

which, together with (4.2), implies the perturbed orthogonality condition

$$A^h(\xi, \eta, \delta; \mathbf{v}, w, \mu) = \sum_{i=1}^{n} ((K_h^{-1} - K^{-1})\mathbf{u}, \mathbf{v})_{\Omega_i} \quad \forall\ (\mathbf{v}, w, \mu) \in \mathbf{V}_h \times W_h \times M_h. \tag{4.4}$$

In addition to the projection operators defined in Chapter 2, we will make use of the interpolant $\mathcal{I}_h$ in the mortar space M_h for which the following approximation property holds true [32],

$$\|\mu - \mathcal{I}_h\mu\|_\tau \le C h_\tau^{3/2} \|\mu\|_{3/2,\tau}, \quad \forall \tau \in \mathcal{T}^{\Gamma,h}. \tag{4.5}$$

In the analysis below we will make use also of the well known Young's inequality

$$ab \leq \epsilon a^2 + \frac{1}{4\epsilon} b^2, \quad \forall \epsilon > 0. \tag{4.6}$$

We derive an upper bound on the error in terms of local residuals, i.e. we obtain an explicit estimator which involves only terms that depend explicitly on the input data and the computed solution and do not require the solution of additional finite element problems.

Let, for all $E \in \mathcal{T}_h$, $\tau \in \mathcal{T}^{\Gamma,h}$,

$$\omega_E^2 = \|K_h^{-1}\mathbf{u}_h + \nabla p_h\|_E^2 h_E^2 + \|f - \nabla \cdot \mathbf{u}_h\|_E^2 h_E^2 + \|\lambda_h - p_h\|_{\partial E \cap \Gamma}^2 h_E, \tag{4.7}$$

$$\omega_\tau^2 = \|[\mathbf{u}_h \cdot \nu]\|_\tau^2 h_\tau^3, \tag{4.8}$$

where for any $\mathbf{v} \in \mathbf{V}$, $\mathbf{v}|_{\Omega_i} = \mathbf{v}_i$,

$$[\mathbf{v} \cdot \nu]|_{\Gamma_{i,j}} = \mathbf{v}_i \cdot \nu_i + \mathbf{v}_j \cdot \nu_j$$

is the jump operator.

4.1 ERROR ESTIMATE FOR THE PRESSURE

We first derive an upper bound on the pressure error η.

Theorem 4.1. *Assume (2.5). Then there exists a constant C independent of h such that*

$$\|\eta\|^2 \leq C \left\{ \sum_{E \in \mathcal{T}_h} \omega_E^2 + \sum_{\tau \in \mathcal{T}^{\Gamma,h}} \omega_\tau^2 + \sum_{e \in \mathcal{T}_h|_{\partial\Omega}} \|g - \mathcal{Q}_h g\|_e^2 h_e + \sum_{E \in \mathcal{T}_h} \|(K_h^{-1} - K^{-1})\mathbf{u}_h\|_E^2 \right\}.$$

Note that $\mathcal{Q}_h$ is applied on $\partial\Omega$, where it is single valued.

Proof. The proof is based on a duality argument. Consider the auxiliary problem

$$\begin{aligned} -\nabla \cdot K\nabla w &= \eta \quad \text{in } \Omega, \\ w &= 0 \quad \text{on } \partial\Omega. \end{aligned}$$

The elliptic regularity assumption (2.5) implies that

$$\|w\|_2 \le C\|\eta\|. \tag{4.9}$$

Let $\mathbf{v} = -K\nabla w$ and $\mu = w|_\Gamma$. With (4.1), $(\mathbf{v}, w, \mu)$ satisfy

$$A^s(\mathbf{v}, w, \mu; \tilde{\mathbf{v}}, \tilde{w}, \tilde{\mu}) = -(\eta, \tilde{w}) \quad \forall\, (\tilde{\mathbf{v}}, \tilde{w}, \tilde{\mu}) \in \mathbf{V} \times W \times L^2(\Gamma).$$

Then, using (4.4) and (4.3),

$$\begin{aligned} \|\eta\|^2 &= -A^s(\mathbf{v}, w, \mu; \xi, \eta, \delta) = -A^s(\xi, \eta, \delta; \mathbf{v}, w, \mu) \\ &= -A^{h,s}(\xi, \eta, \delta; \mathbf{v}, w, \mu) + \sum_{i=1}^n ((K_h^{-1} - K^{-1})\xi, \mathbf{v})_{\Omega_i} \\ &= -A^{h,s}(\xi, \eta, \delta; \mathbf{v} - \Pi\mathbf{v}, w - \hat{w}, \mu - \mathcal{I}_h\mu) + \sum_{i=1}^n ((K_h^{-1} - K^{-1})\xi, \mathbf{v})_{\Omega_i} \\ &\qquad - \sum_{i=1}^n ((K_h^{-1} - K^{-1})\mathbf{u}, \Pi\mathbf{v})_{\Omega_i} \\ &= A^{h,s}(\mathbf{u}_h, p_h, \lambda_h; \mathbf{v} - \Pi\mathbf{v}, w - \hat{w}, \mu - \mathcal{I}_h\mu) + (f, w - \hat{w}) + \langle g, (\mathbf{v} - \Pi\mathbf{v}) \cdot \nu\rangle_{\partial\Omega} \\ &\qquad - \sum_{i=1}^n ((K_h^{-1} - K^{-1})\mathbf{u}_h, \mathbf{v})_{\Omega_i} \\ &= \sum_{E \in \mathcal{T}_h} \big((K_h^{-1}\mathbf{u}_h, \mathbf{v} - \Pi\mathbf{v})_E - (p_h, \nabla \cdot (\mathbf{v} - \Pi\mathbf{v}))_E - (\nabla \cdot \mathbf{u}_h, w - \hat{w})_E\big) \\ &\qquad + \sum_{i=1}^n \left(\langle \lambda_h, (\mathbf{v} - \Pi\mathbf{v}) \cdot \nu_i\rangle_{\Gamma_i} + \langle \mathbf{u}_h \cdot \nu_i, \mu - \mathcal{I}_h\mu\rangle_{\Gamma_i}\right) \\ &\qquad + (f, w - \hat{w}) + \langle g, (\mathbf{v} - \Pi\mathbf{v}) \cdot \nu\rangle_{\partial\Omega} - \sum_{E \in \mathcal{T}_h} ((K_h^{-1} - K^{-1})\mathbf{u}_h, \mathbf{v})_E. \end{aligned}$$

Applying Green's formula and using (2.15),

$$\begin{aligned}\|\eta\|^2 = \sum_{E\in\mathcal{T}_h} \left((K_h^{-1}\mathbf{u}_h + \nabla p_h, \mathbf{v} - \Pi\mathbf{v})_E + (f - \nabla\cdot\mathbf{u}_h, w - \hat{w})_E\right) \\ + \sum_{i=1}^{n} \langle \lambda_h - p_h, (\mathbf{v} - \Pi\mathbf{v})\cdot\nu_i\rangle_{\Gamma_i} + \sum_{\tau\in\mathcal{T}^{\Gamma,h}} \langle [\mathbf{u}_h\cdot\nu], \mu - \mathcal{I}_h\mu\rangle_\tau \\ + \langle g - \mathcal{Q}_h g, (\mathbf{v} - \Pi\mathbf{v})\cdot\nu\rangle_{\partial\Omega} - \sum_{E\in\mathcal{T}_h} ((K_h^{-1} - K^{-1})\mathbf{u}_h, \mathbf{v})_E.\end{aligned}$$

Using the Cauchy-Schwartz inequality and the approximation properties (2.18), (2.16), (2.20), (4.5),

$$\begin{aligned}\|\eta\|^2 \le C \Bigg\{ \sum_{E\in\mathcal{T}_h} \Big(\|K_h^{-1}\mathbf{u}_h + \nabla p_h\|_E h_E \|\mathbf{v}\|_{1,E} + \|f - \nabla\cdot\mathbf{u}_h\|_E h_E \|w\|_{1,E} \\ + \|\lambda_h - p_h\|_{\partial E\cap\Gamma} h_E^{1/2} \|\mathbf{v}\|_{1,E} \Big) + \sum_{\tau\in\mathcal{T}^{\Gamma,h}} \|[\mathbf{u}_h\cdot\nu]\|_\tau h_\tau^{3/2} \|\mu\|_{3/2,\tau} \\ + \sum_{e\in\mathcal{T}_h|_{\partial\Omega}} \|g - \mathcal{Q}_h g\|_e h_e^{1/2} \|\mathbf{v}\|_{1/2,e} + \sum_{E\in\mathcal{T}_h} \|(K_h^{-1} - K^{-1})\mathbf{u}_h\|_E \|\mathbf{v}\|_E \Bigg\}.\end{aligned}$$

An application of the discrete Cauchy–Schwartz inequality, the trace inequality (2.21), and (4.9) completes the proof. □

4.2 ERROR ESTIMATE FOR THE VELOCITY

We define the norm in the mortar space M_h by

$$\|\mu\|_{a_h} := a_h(\mu,\mu)^{1/2},$$

where $a_h : L^2(\Gamma)\times L^2(\Gamma) \to \mathbf{R}$ is the interface bilinear form defined in Section 5.1. It is shown in Chapter 5 (see (5.14) and the proof of Lemma 5.5) for RTN_0 ($k = 0$) rectangular elements and very general hanging interface nodes and mortar grid configurations satisfying (2.30) that

$$\sum_{\tau\in\mathcal{T}^{\Gamma,h}} \|\mu\|_{1/2,\tau}^2 \le C a_h(\mu,\mu), \quad \mu\in M_h. \tag{4.10}$$

We will also make use of the following construction. Define, for $\varphi \in L^2(\Gamma)$,

$$\mathbf{u}_h(\varphi) = \mathbf{u}_h^*(\varphi) + \bar{\mathbf{u}}_h, \quad p_h(\varphi) = p_h^*(\varphi) + \bar{p}_h$$

and note that $(\mathbf{u}_h(\varphi), p_h(\varphi)) \in \mathbf{V}_h \times W_h$ satisfy, for $1 \le i \le n$,

$$\begin{aligned}
(K^{-1}\mathbf{u}_h(\varphi), \mathbf{v})_{\Omega_i} &= (p_h(\varphi), \nabla \cdot \mathbf{v})_{\Omega_i} - \langle \varphi, \mathbf{v} \cdot \nu \rangle_{\Gamma_i} - \langle g, \mathbf{v} \cdot \nu \rangle_{\partial\Omega_i \setminus \Gamma_i}, \quad \mathbf{v} \in \mathbf{V}_{h,i}, \\
(\nabla \cdot \mathbf{u}_h(\varphi), w)_{\Omega_i} &= (f, w)_{\Omega_i}, \quad w \in W_{h,i}.
\end{aligned}$$

In particular, $\mathbf{u}_h(\lambda_h) = \mathbf{u}_h$ and $p_h(\lambda_h) = p_h$.

We recall some *a priori* error estimates from [9] which will motivate the saturation assumptions needed in the *a posteriori* error analysis.

Theorem 4.2. *For the solution to (2.25)–(2.27), if (2.30) holds, then*

$$\begin{aligned}
&\|\nabla \cdot (\mathbf{u} - \mathbf{u}_h)\| \le C \sum_{i=1}^{n} \|\nabla \cdot \mathbf{u}\|_{r,\Omega_i} h^r, \quad 1 \le r \le l+1, \\
&\|\mathbf{u} - \mathbf{u}_h\| \le C \sum_{i=1}^{n} (\|p\|_{r+1,\Omega_i} + \|\mathbf{u}\|_{r,\Omega_i}) h^r, \quad 1 \le r \le k+1, \\
&\|p - p_h\| \le C \sum_{i=1}^{n} (\|p\|_{r+1,\Omega_i} + \|\mathbf{u}\|_{r,\Omega_i} + \|\nabla \cdot \mathbf{u}\|_{r,\Omega_i}) h^r, \quad 1 \le r \le \min(k+1, l+1), \\
&\|\lambda - \lambda_h\|_{a_h} \le C \sum_{i=1}^{n} (\|p\|_{r+1,\Omega_i} + \|\mathbf{u}\|_{r,\Omega_i}) h^r, \quad 1 \le r \le k+1.
\end{aligned}$$

The *a priori* error bounds from Theorem 4.2 motivate the following assumption on the mortar error:

Saturation Assumption 4.1. *There exist a constant γ such that*

$$|||\lambda - \lambda_h||| := \left(\sum_{\tau \in \mathcal{T}^{\Gamma,h}} h_\tau^{-1} \|\lambda - \lambda_h\|_\tau^2 \right)^{1/2} \le \gamma \|\mathbf{u} - \mathbf{u}_h\|. \tag{4.11}$$

For further justification of (4.11), note that $|||\lambda - \lambda_h|||$ is closely related to the discrete $H^{1/2}(\Gamma)$ norm and, by (4.10), to $\|\lambda - \lambda_h\|_{a_h}$. Since $\mathbf{u}_h(\lambda)$ is the numerical solution based on the true interface data, we can assume that

$$\|\mathbf{u} - \mathbf{u}_h(\lambda)\| \leq \gamma_1 \|\mathbf{u} - \mathbf{u}_h\|,$$

and, using (5.13),

$$\begin{aligned} C\|\lambda - \lambda_h\|_{a_h} &\leq \|\mathbf{u}_h^*(\lambda) - \mathbf{u}_h^*(\lambda_h)\| = \|\mathbf{u}_h(\lambda) - \mathbf{u}_h(\lambda_h)\| = \|\mathbf{u}_h(\lambda) - \mathbf{u}_h\| \\ &\leq \|\mathbf{u} - \mathbf{u}_h(\lambda)\| + \|\mathbf{u} - \mathbf{u}_h\| \leq (1 + \gamma_1)\|\mathbf{u} - \mathbf{u}_h\|. \end{aligned}$$

Let $\mathbf{V}_h'$, W_h', and M_h' be the finite element spaces of one order higher than $\mathbf{V}_h$, W_h, and M_h, respectively. Let $\mathbf{u}_h' \in \mathbf{V}_h'$, $p_h' \in W_h'$, and $\lambda_h' \in M_h'$ be the mortar mixed finite element solution in these higher-order spaces to the equations with true permeability K (see (2.25)–(2.27)).

Saturation Assumption 4.2. *There exist constants $\beta < 1$ and $\beta_p < \infty$ such that*

$$\|\mathbf{u} - \mathbf{u}_h'\| \leq \beta \|\mathbf{u} - \mathbf{u}_h\|. \tag{4.12}$$

$$\|p - p_h'\| \leq \beta_p \|p - p_h\|. \tag{4.13}$$

Let

$$\xi' = \mathbf{u}_h' - \mathbf{u}_h, \quad \eta' = p_h' - p_h, \quad \text{and } \delta' = \lambda_h' - \lambda_h.$$

Similarly to (4.3) and (4.4), we have that $(\xi', \eta', \delta') \in \mathbf{V}_h' \times W_h' \times M_h'$ satisfies the residual equation

$$\begin{aligned} A(\xi', \eta', \delta'; \mathbf{v}_h', w_h', \mu_h') &= L(\mathbf{v}_h', w_h', \mu_h') - A^h(\mathbf{u}_h, p_h, \lambda_h; \mathbf{v}_h', w_h', \mu_h') \\ &\quad + \sum_{i=1}^{n} ((K_h^{-1} - K^{-1})\mathbf{u}_h, \mathbf{v}_h')_{\Omega_i}, \quad \forall\ (\mathbf{v}_h', w_h', \mu_h') \in \mathbf{V}_h' \times W_h' \times M_h', \end{aligned} \tag{4.14}$$

and the "orthogonality" condition

$$A(\xi', \eta', \delta'; \mathbf{v}, w, \mu) = \sum_{i=1}^{n} ((K_h^{-1} - K^{-1})\mathbf{u}_h, \mathbf{v})_{\Omega_i} \quad \forall\ (\mathbf{v}, w, \mu) \in \mathbf{V}_h \times W_h \times M_h. \tag{4.15}$$

The bounds on ξ and δ will be expressed in terms of weighted local residuals, for all $E \in \mathcal{T}_h$, $\tau \in \mathcal{T}^{\Gamma,h}$,

$$\tilde{\omega}_E^2 = h_E^{-2}\omega_E^2 = \|K_h^{-1}\mathbf{u}_h + \nabla p_h\|_E^2 + \|f - \nabla \cdot \mathbf{u}_h\|_E^2 + \|\lambda_h - p_h\|_{\partial E \cap \Gamma}^2 h_E^{-1}, \tag{4.16}$$

$$\tilde{\omega}_\tau^2 = h_\tau^{-2}\omega_\tau^2 = \|[\mathbf{u}_h \cdot \nu]\|_\tau^2 h_\tau. \tag{4.17}$$

Theorem 4.3. *Assume that the saturation assumptions (4.11), (4.12), and (4.13) hold. Then there exists a constant C independent of β such that*

$$\|\xi\|^2_{H(\mathrm{div})} \leq \frac{C}{(1-\beta)^2}\left\{\sum_{E\in\mathcal{T}_h}\tilde{\omega}_E^2 + \sum_{\tau\in\mathcal{T}^{\Gamma,h}}\tilde{\omega}_\tau^2 + \sum_{e\in\mathcal{T}_{h|\partial\Omega}}\|g-\mathcal{Q}_h g\|_e^2 h_e^{-1} + \sum_{E\in\mathcal{T}_h}\|(K_h^{-1}-K^{-1})\mathbf{u}_h\|_E^2\right\}.$$

Proof. The bound on $\|\nabla\cdot\xi\|$ is trivial. Indeed, for all $E\in\mathcal{T}_h$,

$$\|\nabla\cdot\xi\|_E = \|\nabla\cdot(\mathbf{u}-\mathbf{u}_h)\|_E = \|f-\nabla\cdot\mathbf{u}_h\|_E \leq \tilde{\omega}_E.$$

To bound $\|\xi\|$, since

$$\|\mathbf{u}-\mathbf{u}_h'\| = \|\mathbf{u}-\mathbf{u}_h-(\mathbf{u}_h'-\mathbf{u}_h)\| \geq \|\xi\| - \|\xi'\|,$$

condition (4.12) implies that

$$\|\xi\| \leq \frac{1}{1-\beta}\|\xi'\|, \tag{4.18}$$

so, it is enough to bound $\|\xi'\|$. Using (4.15) and (4.14),

$$\begin{aligned}
\|K^{-1/2}\xi'\|^2 &= A^c(\xi',\eta',\delta';\xi',\eta',\delta') = A^c(\xi',\eta',\delta';\xi'-\Pi\xi',\eta',\delta')\\
&\quad + \sum_{i=1}^n((K_h^{-1}-K^{-1})\mathbf{u}_h,\Pi\xi')_{\Omega_i}\\
&= L^c(\xi'-\Pi\xi',\eta',\delta') - A^{h,c}(\mathbf{u}_h,p_h,\lambda_h;\xi'-\Pi\xi',\eta',\delta')\\
&\quad + \sum_{i=1}^n((K_h^{-1}-K^{-1})\mathbf{u}_h,\xi')_{\Omega_i}\\
&= -\sum_{E\in\mathcal{T}_h}\big((K^{-1}\mathbf{u}_h,\xi'-\Pi\xi')_E - (p_h,\nabla\cdot(\xi'-\Pi\xi'))_E + (\nabla\cdot\mathbf{u}_h,\eta')_E\big)\\
&\quad - \sum_{i=1}^n(\langle\lambda_h,(\xi'-\Pi\xi')\cdot\nu_i\rangle_{\Gamma_i} - \langle\mathbf{u}_h\cdot\nu_i,\delta'\rangle_{\Gamma_i})\\
&\quad + (f,\eta') - \langle g,(\xi'-\Pi\xi')\cdot\nu\rangle_{\partial\Omega} + \sum_{E\in\mathcal{T}_h}((K_h^{-1}-K^{-1})\mathbf{u}_h,\xi')_E.
\end{aligned}$$

The use of Green's formula and (2.15) gives

$$\begin{aligned}\|K^{-1/2}\xi'\|^2 = &-\sum_{E\in\mathcal{T}_h}\left((K^{-1}\mathbf{u}_h+\nabla p_h,\xi'-\Pi\xi')_E-(f-\nabla\cdot\mathbf{u}_h,\eta')_E\right)\\ &-\sum_{i=1}^{n}\langle\lambda_h-p_h,(\xi'-\Pi\xi')\cdot\nu_i\rangle_{\Gamma_i}-\sum_{\tau\in\mathcal{T}^{\Gamma,h}}\langle[\mathbf{u}_h\cdot\nu],\delta'\rangle_\tau\\ &-\langle g-\mathcal{Q}_h g,(\xi'-\Pi\xi')\cdot\nu\rangle_{\partial\Omega}+\sum_{E\in\mathcal{T}_h}((K_h^{-1}-K^{-1})\mathbf{u}_h,\xi')_E\\ &=T_1+\cdots+T_6.\end{aligned}\tag{4.19}$$

For T_1, using the Cauchy–Schwartz inequality, (2.18), (2.11), and (4.6), we have

$$\begin{aligned}(K^{-1}\mathbf{u}_h+\nabla p_h,\xi'-\Pi\xi')_E&\le\|K^{-1}\mathbf{u}_h+\nabla p_h\|_E\|\xi'-\Pi\xi'\|_E\\ &\le C\|K^{-1}\mathbf{u}_h+\nabla p_h\|_E h_E\|\xi'\|_{1,E}\le C\|K^{-1}\mathbf{u}_h+\nabla p_h\|_E\|\xi'\|_E\\ &\le C\left(\frac{1}{4\varepsilon_1}\|K^{-1}\mathbf{u}_h+\nabla p_h\|_E^2+\varepsilon_1\|\xi'\|_E^2\right).\end{aligned}\tag{4.20}$$

Similarly for T_2,

$$(f-\nabla\cdot\mathbf{u}_h,\eta')_E\le\frac{1}{2}\|f-\nabla\cdot\mathbf{u}_h\|_E^2+\frac{1}{2}\|\eta'\|_E^2.\tag{4.21}$$

To bound T_3, the use of (2.20), (2.21), and (2.11) gives, for $e\in\Gamma_i$, $e\in\partial E$,

$$\begin{aligned}\langle\lambda_h-p_h,(\xi'-\Pi\xi')\cdot\nu_i\rangle_e&\le C\|\lambda_h-p_h\|_e h_E^{1/2}\|\xi'\|_{1,E}\\ &\le C\|\lambda_h-p_h\|_e h_E^{-1/2}\|\xi'\|_E\le C\left(\frac{1}{4\varepsilon_3}\|\lambda_h-p_h\|_e^2h_E^{-1}+\varepsilon_3\|\xi'\|_E^2\right),\end{aligned}\tag{4.22}$$

where we applied (4.6) at the last inequality. Similarly for T_5,

$$\langle g-\mathcal{Q}_h g,(\xi'-\Pi\xi')\cdot\nu\rangle_e\le C\left(\frac{1}{4\varepsilon_5}\|g-\mathcal{Q}_h g\|_e^2h_e^{-1}+\varepsilon_5\|\xi'\|_E^2\right).\tag{4.23}$$

To bound T_4, use (4.6) to get,

$$\begin{aligned}\sum_{\tau\in\mathcal{T}^{\Gamma,h}}\langle[\mathbf{u}_h\cdot\nu],\delta'\rangle_\tau&\le\sum_{\tau\in\mathcal{T}^{\Gamma,h}}\left(h_\tau^{1/2}\|[\mathbf{u}_h\cdot\nu]\|_\tau\right)\left(h_\tau^{-1/2}\|\delta'\|_\tau\right)\\ &\le\sum_{\tau\in\mathcal{T}^{\Gamma,h}}\left(\frac{1}{4\varepsilon_4}\|[\mathbf{u}_h\cdot\nu]\|_\tau^2h_\tau+\varepsilon_4\|\delta'\|_\tau^2h_\tau^{-1}\right).\end{aligned}\tag{4.24}$$

Finally, for T_6, another application of (4.6) gives,

$$((K_h^{-1}-K^{-1})\mathbf{u}_h,\xi')_E\le\left(\frac{1}{4\varepsilon_6}\|(K_h^{-1}-K^{-1})\mathbf{u}_h\|_E^2+\varepsilon_6\|\xi'\|_E^2\right).\tag{4.25}$$

Combining (2.4) with (4.19)–(4.24) for small enough ε_1, ε_3, ε_5, and ε_6,

$$\begin{aligned}\|\xi'\|^2 \leq C \Bigg\{ \sum_{E\in\mathcal{T}_h} \big(&\|K^{-1}\mathbf{u}_h + \nabla p_h\|_E^2 + \|f - \nabla\cdot\mathbf{u}_h\|_E^2 + \|\lambda_h - p_h\|_{\partial E\cap\Gamma}^2 h_E^{-1} \\ &+ \|(K_h^{-1} - K^{-1})\mathbf{u}_h\|_E^2 + \|\eta'\|_E^2\big) \\ + \sum_{\tau\in\mathcal{T}^{\Gamma,h}} \Big(\frac{1}{4\varepsilon_4}\|[\mathbf{u}_h\cdot\nu]\|_\tau^2 h_\tau + \varepsilon_4\|\delta'\|_\tau^2 h_\tau^{-1}\Big) &+ \sum_{e\in\mathcal{T}_h|_{\partial\Omega}} \|g - \mathcal{Q}_h g\|_e^2 h_e^{-1} \Bigg\}.\end{aligned} \tag{4.26}$$

Using the definitions of the weighted local residuals (4.16) and (4.17), we obtain

$$\begin{aligned}\|\xi'\|^2 \leq C \Bigg\{ &\sum_{E\in\mathcal{T}_h} \tilde{\omega}_E^2 + \sum_{\tau\in\mathcal{T}^{\Gamma,h}} \tilde{\omega}_\tau^2 + \sum_{e\in\mathcal{T}_h|_{\partial\Omega}} \|g - \mathcal{Q}_h g\|_e^2 h_e^{-1} + \sum_{E\in\mathcal{T}_h} \|(K_h^{-1} - K^{-1})\mathbf{u}_h\|_E^2 \\ &+ \|\eta'\|^2 + \varepsilon_4 \sum_{\tau\in\mathcal{T}^{\Gamma,h}} \|\delta'\|_\tau^2 h_\tau^{-1} \Bigg\}.\end{aligned} \tag{4.27}$$

Due to (4.13), the bound on $\|\eta\|$ from Theorem 4.1 applies to $\|\eta'\|$ as well. It remains to estimate $|||\delta'|||^2 = \sum_{\tau\in\mathcal{T}^{\Gamma,h}} \|\delta'\|_\tau^2 h_\tau^{-1}$. Using (4.11) (with a constant γ' in the case of the higher order spaces) and (4.12), we have

$$\begin{aligned}|||\delta'||| &\leq |||\lambda - \lambda_h||| + |||\lambda - \lambda_h'||| \leq \gamma\|\mathbf{u} - \mathbf{u}_h\| + \gamma'\|\mathbf{u} - \mathbf{u}_h'\| \\ &\leq (\gamma + \gamma'\beta)\|\mathbf{u} - \mathbf{u}_h\|.\end{aligned} \tag{4.28}$$

Using (4.28), (4.18), and taking ε_4 in (4.27) small enough completes the proof. □

Remark 4.1. *Due to the approximation property (2.19) of $\mathcal{Q}_h$ the third term in the bound of Theorem 4.3 and is of higher order than the other terms. Therefore its effect becomes negligible for small h.*

4.3 NUMERICAL SIMULATIONS

In this section we present a numerical test illustrating the need to include the upscaling error in the *a posteriori* error estimators. We compare two error estimators. The first one is based on ω_E and ω_τ, defined in (4.7) and (4.8). The second one contains, in addition to the previous two, the upscaling term $\|(K_h^{-1} - K^{-1})\mathbf{u}_h\|_E$. Note that we employ the pressure error estimator from Theorem 4.1.

These estimators are used as local error indicators that drive an adaptive mesh refinement process. The following algorithm describes the adaptive procedure.

Grid Refinement Algorithm

1. Solve the problem on a coarse subdomain and mortar grid.
2. For each subdomain Ω_i:
   a. Compute $\omega_i = \left(\sum_{E \in \mathcal{T}_{h,i}} \omega_E^2 + \sum_{\tau \in \mathcal{T}^{\Gamma_i,h}} \omega_\tau^2 \right)^{1/2}$, or, alternatively,
   $$\omega_{i,upsc} = \left(\sum_{E \in \mathcal{T}_{h,i}} \omega_E^2 + \sum_{\tau \in \mathcal{T}^{\Gamma_i,h}} \omega_\tau^2 + \sum_{E \in \mathcal{T}_{h,i}} \|(K_h^{-1} - K^{-1})\mathbf{u}_h\|_E^2 \right)^{1/2};$$
   b. If $\omega_i > .5 \max_{1 \le j \le n} \omega_j$ ($\omega_{i,upsc} > .5 \max_{1 \le j \le n} \omega_{j,upsc}$, resp.), refine $\mathcal{T}_{h,i}$.
3. For each interface $\Gamma_{i,j}$, if either Ω_i or Ω_j has been refined, refine $\mathcal{T}_{h,i,j}$.
4. Solve the problem on the refined grid. If either the desired error tolerance or the maximum refinement level has been reached, exit; otherwise, go to Step 2.

Example 4.1.

We test a problem with a highly oscillating tensor

$$K = \begin{cases} 105 - 100 \sin(20\pi x) \sin(20\pi y), & x, y \in [0, 1/2] \text{ or } x, y \in [1/2, 1], \\ 105 - 100 \sin(2\pi x) \sin(2\pi y), & \text{otherwise.} \end{cases}$$

The unit square domain is decomposed into 6×6 subdomains. The coarse grid in each subdomain is 2×2 with a single mortar element on each interface. Left-to-right flow is imposed through boundary conditions: Dirichlet on the left and right edge and no-flow on the rest of the boundary. The computed magnitude of the velocity after three refinements for the

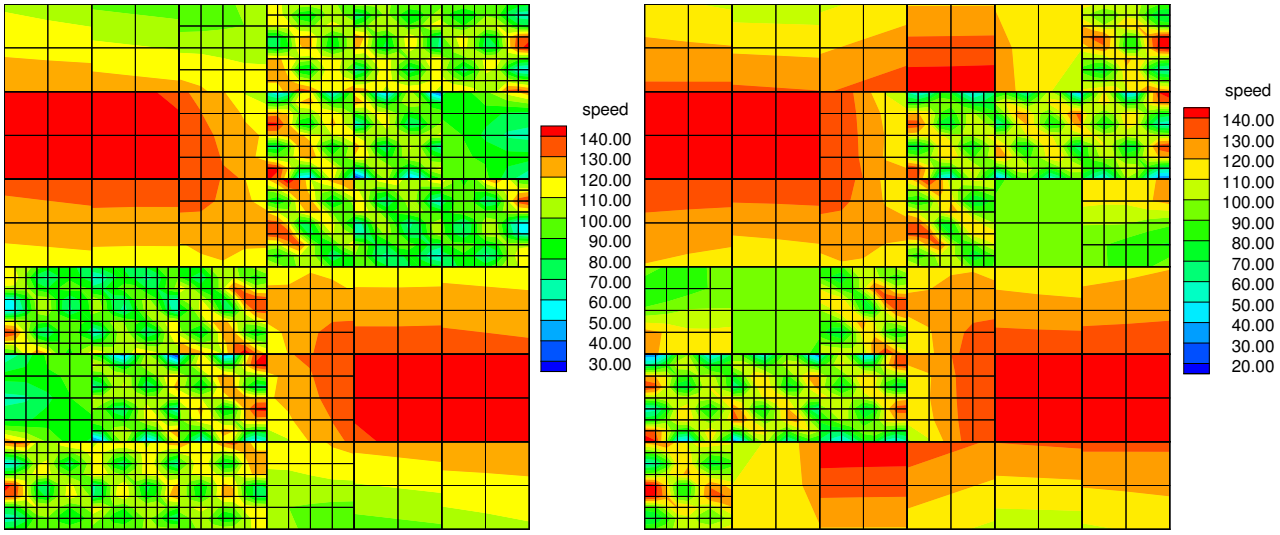

A. With upscaling term B. Without upscaling term

Figure 4.1: Computed magnitude of the velocity on the fourth grid level with and without the upscaling term for Example 4.1

two estimators are shown in Figure 4.1. Note that in the case of $\omega_{i,upsc}$, the highly oscillating velocity is well resolved by the fine computational grid in the lower-left and the upper-right regions, while the mesh produced by ω_i on the same level only partially captures these oscillations. Furthermore, it can be seen in Figure 4.2 that three more levels of refinement are needed for ω_i to achieve comparable resolution, though even on that level there are parts of the oscillating regions that are not refined at all. Clearly, the overall quality of the grids generated by $\omega_{i,upsc}$ is superior to the ones produced by ω_i. The computed pressures after three refinements with $\omega_{i,upsc}$ and six refinements with ω_i are shown in Figure 4.3. Since the pressure is smooth, it is resolved well by both estimators.

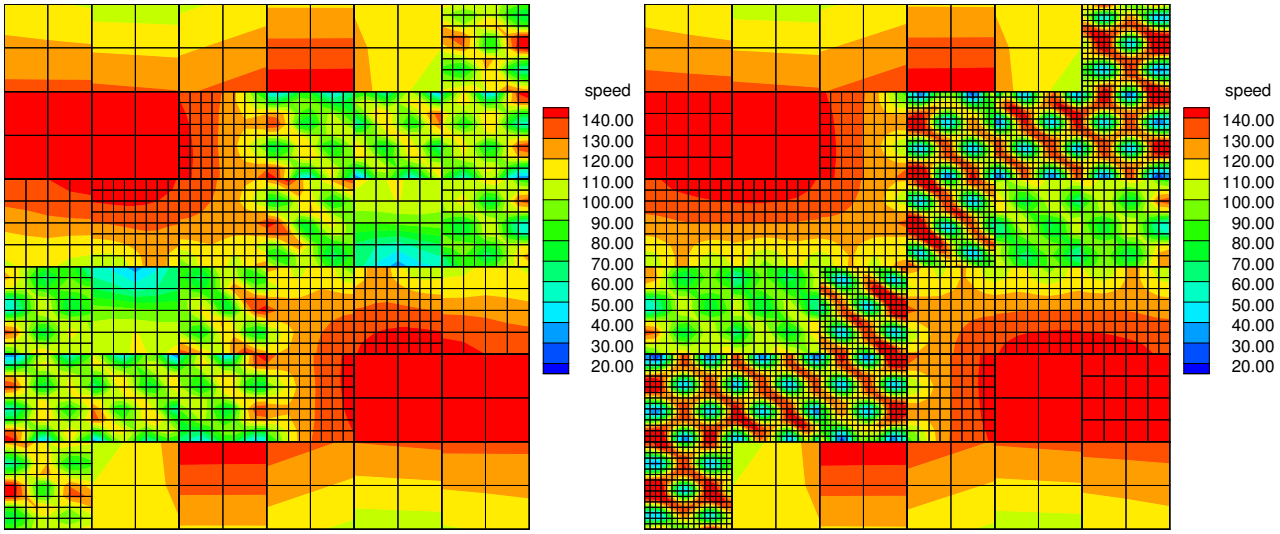

A. Level 6 B. Level 7

Figure 4.2: Computed magnitude of the velocity on the sixth and seventh grid levels without the upscaling term for Example 4.1

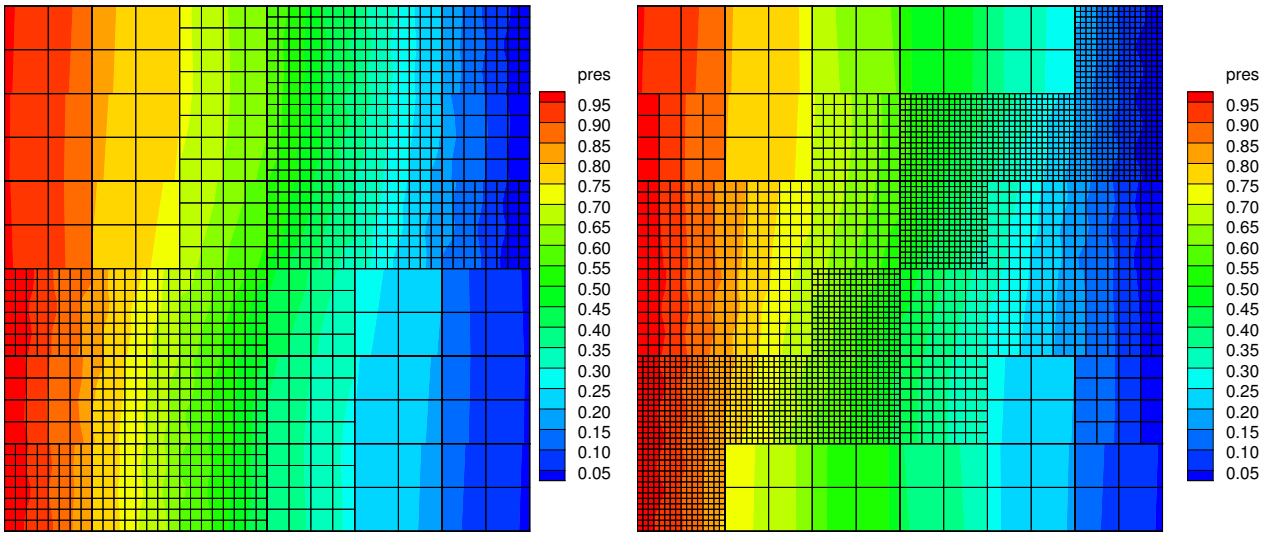

A. On level 4, with upscaling term B. On level 7, without upscaling term

Figure 4.3: Computed pressure for Example 4.1

5.0 BALANCING DOMAIN DECOMPOSITION

This chapter deals with the problem of solving efficiently the algebraic system arising in mortar mixed finite element discretizations of problem (2.1)–(2.3). A non-overlapping domain decomposition algorithm developed for matching grids by Glowinski and Wheeler [43, 34] and later extended to non-matching grids [74, 69] is employed as a solver. The method reduces the global system to an interface problem which is symmetric and positive definite in the case of elliptic equations and can be solved iteratively via a preconditioned conjugate gradient method. This approach is very suitable for parallel implementation since the dominant cost is solving subdomain problems. The feasibility of the domain decomposition solver depends critically on the rate of convergence of the interface iteration and ultimately on the conditioning of the interface operator.

We extend the balancing preconditioner for mixed finite elements developed by Cowsar, Mandel, and Wheeler [33] to the case of non-matching multiblock grids in [59]. A key ingredient in our analysis is a characterization for the mortar bilinear form as a $H^{1/2}$-norm of an interpolant of the mortar interface data. Our theoretical results for the mortar balancing preconditioner provide, as in the case of matching grids, a quasi-optimal condition number bound $O((1+\log(\tilde{H}/h))^2)$ which is independent of the jump in coefficients between subdomains. Here h is the discretization parameter and $\tilde{H}$ is the characteristic size of the subdomains. This bound also indicates very weak dependence on the number of subdomains, which has been confirmed experimentally.

We assume that there exist positive constants c, C, and α_i such that

$$c\alpha_i \xi^T \xi \leq \xi^T K(x) \xi \leq C\alpha_i \xi^T \xi, \quad \forall \xi \in \mathbf{R}^d, \ \forall x \in \Omega_i, \ i = 1, \ldots, n. \tag{5.1}$$

In this chapter we will use $\|w\|^2_{1,G}$ and $\|w\|^2_{1/2,S}$ to mean the scaled Sobolev norms

$$\|w\|^2_{1,G} = |w|^2_{1,G} + \frac{1}{\tilde{H}^2}\|w\|^2_G, \quad \|w\|^2_{1/2,S} = |w|^2_{1/2,S} + \frac{1}{\tilde{H}}\|w\|^2_S,$$

where

$$|w|^2_{1,G} = \int_G |\nabla w(x)|^2\, dx, \quad |w|^2_{1/2,S} = \int_S \int_S \frac{|w(t) - w(s)|^2}{|t-s|^d}\, dt\, ds.$$

It will be convenient to treat the local operators $\mathcal{Q}_{h,i}$ as operators from M_h to $\mathbf{V}_{h,i}\cdot\nu_i|_{\Gamma_i}$, implicitly assuming that, for a function $\mu \in M_h$, $\mathcal{Q}_{h,i}\mu = \mathcal{Q}_{h,i}N_i\mu$, where $N_i : M_h \to M_{h,i} \equiv M_h|_{\Gamma_i}$ is the the restriction operator. Similarly $\mathcal{Q}^T_{h,i}$, the L^2-orthogonal projector from $\mathbf{V}_{h,i}\cdot\nu_i|_{\Gamma_i}$ onto $M_{h,i}$, will be understood as an operator from $\mathbf{V}_{h,i}\cdot\nu_i|_{\Gamma_i}$ to M_h, implicitly assuming that $\mathcal{Q}^T_{h,i}\mathbf{v}_i\cdot\nu_i = N_i^T\mathcal{Q}^T_{h,i}\mathbf{v}_i\cdot\nu_i$, where $N_i^T : M_{h,i} \to M_h$ is the extension-by-zero operator. In addition, given a function in $M_{h,i}$ we assume by default that it is extended by zero to the whole M_h.

5.1 REDUCTION TO AN INTERFACE PROBLEM

Define bilinear forms $a_{h,i} : L^2(\Gamma)\times L^2(\Gamma) \to \mathbf{R}$, $1 \le i \le n$, and $a_h : L^2(\Gamma)\times L^2(\Gamma) \to \mathbf{R}$ by

$$a_{h,i}(\lambda,\mu) = -\langle \mathbf{u}^*_{h,i}(\lambda)\cdot\nu_i, \mu\rangle_{\Gamma_i}, \quad a_h(\lambda,\mu) = \sum_{i=1}^n a_{h,i}(\lambda,\mu), \tag{5.2}$$

where, for $\lambda \in L^2(\Gamma)$, $(\mathbf{u}^*_{h,i}(\lambda), p^*_{h,i}(\lambda)) \in \mathbf{V}_{h,i}\times W_{h,i}, 1 \le i \le n$, solve

$$(K^{-1}\mathbf{u}^*_{h,i}(\lambda), \mathbf{v})_{\Omega_i} = (p^*_{h,i}(\lambda), \nabla\cdot\mathbf{v})_{\Omega_i} - \langle\lambda, \mathbf{v}\cdot\nu_i\rangle_{\Gamma_i},\ \mathbf{v}\in\mathbf{V}_{h,i}, \tag{5.3}$$

$$(\nabla\cdot\mathbf{u}^*_{h,i}(\lambda), w)_{\Omega_i} = 0,\ w \in W_{h,i}. \tag{5.4}$$

Define a linear functional $g_h : L^2(\Gamma) \to \mathbf{R}$ by

$$g_h(\mu) = \sum_{i=1}^n \langle \bar{\mathbf{u}}_{h,i}\cdot\nu_i, \mu\rangle_{\Gamma_i}, \tag{5.5}$$

where $(\bar{\mathbf{u}}_{h,i}, \bar{p}_{h,i}) \in \mathbf{V}_{h,i}\times W_{h,i}, 1 \le i \le n$, solve

$$(K^{-1}\bar{\mathbf{u}}_{h,i}, \mathbf{v})_{\Omega_i} = (\bar{p}_{h,i}, \nabla\cdot\mathbf{v})_{\Omega_i} - \langle g, \mathbf{v}\cdot\nu_i\rangle_{\partial\Omega_i\setminus\Gamma_i},\ \mathbf{v}\in\mathbf{V}_{h,i}, \tag{5.6}$$

$$(\nabla\cdot\bar{\mathbf{u}}_{h,i}, w)_{\Omega_i} = (f, w)_{\Omega_i},\ w \in W_{h,i}. \tag{5.7}$$

It is straightforward to show (see [43]) that the solution $(\mathbf{u}_h, p_h, \lambda_h)$ of (2.25)–(2.27) satisfies

$$a_h(\lambda_h, \mu) = g_h(\mu), \quad \mu \in M_h, \tag{5.8}$$

with

$$\mathbf{u}_h = \mathbf{u}_h^*(\lambda_h) + \bar{\mathbf{u}}_h, \qquad p_h = p_h^*(\lambda_h) + \bar{p}_h,$$

where $\mathbf{u}_h^*(\lambda) \in \mathbf{V}_h$ is such that $\mathbf{u}_h^*(\lambda)|_{\Omega_i} = \mathbf{u}_{h,i}^*(\lambda)$, with similar definitions for $p_h^*(\lambda)$, $\bar{\mathbf{u}}_h$, and $\bar{p}_h$.

We introduce linear maps $A_{h,i} : M_h \to M_h$, $i = 1, \ldots, n$, corresponding to the bilinear forms $a_{h,i}(\cdot, \cdot)$ and satisfying

$$\langle A_{h,i}\lambda, \mu \rangle = a_{h,i}(\lambda, \mu), \quad \forall \lambda, \mu \in M_h. \tag{5.9}$$

Note that (5.2) and (5.9) imply

$$A_{h,i}\lambda = -\mathcal{Q}_{h,i}^T \mathbf{u}_{h,i}^*(\lambda) \cdot \nu_i, \tag{5.10}$$

hence the operators $A_{h,i}$ are Dirichlet-to-Neumann maps. It is clear from (5.3) that $\mathbf{u}_{h,i}^*(\lambda) = \mathbf{u}_{h,i}^*(\mathcal{Q}_{h,i}\lambda)$, which combined with (5.10) implies that

$$A_{h,i} = \mathcal{Q}_{h,i}^T \overline{A_{h,i}} \mathcal{Q}_{h,i}, \tag{5.11}$$

where $\overline{A_{h,i}}$ are the local non-mortar Dirichlet-to-Neumann maps from $\mathbf{V}_{h,i} \cdot \nu_i|_{\Gamma_i}$ to $\mathbf{V}_{h,i} \cdot \nu_i|_{\Gamma_i}$.

The interface problem (5.8) can now be written as

$$A_h \lambda = \bar{g}_h, \tag{5.12}$$

where

$$A_h = \sum_{i=1}^{n} A_{h,i} : M_h \to M_h$$

and $\bar{g}_h \in M_h$ is the Riesz representation of g_h. The operator A_h is a mortar version of the Poincaré-Steklov operator [5]. It can be viewed algebraically as the Schur complement with respect to the mortar unknowns.

The following lemma has been shown in [74, 9] (see also [34, 33] for the conforming grids case).

Lemma 5.1. *The interface bilinear form $a_h(\cdot,\cdot)$ is symmetric and positive semi-definite in $L^2(\Gamma)\times L^2(\Gamma)$. If (2.30) holds, then $a_h(\cdot,\cdot)$ is positive definite in $M_h\times M_h$.*

The proof is based on the representation

$$a_{h,i}(\lambda,\mu)=(K^{-1}\mathbf{u}_h^*(\lambda),\mathbf{u}_h^*(\mu))_{\Omega_i}, \tag{5.13}$$

which follows easily from (5.2) and (5.3).

Another useful characterization for $a_{h,i}(\cdot,\cdot)$ has been shown in [74] (see also [33]). There exist positive constants c and C such that

$$c\alpha_i|\mathcal{I}^{\partial\Omega_i}\mathcal{Q}_{h,i}\mu|^2_{1/2,\partial\Omega_i}\le a_{h,i}(\mu,\mu)\le C\alpha_i|\mathcal{I}^{\partial\Omega_i}\mathcal{Q}_{h,i}\mu|^2_{1/2,\partial\Omega_i},\quad \forall\mu\in M_h, \tag{5.14}$$

where α_i is the constant from (5.1) and $\mathcal{I}^{\partial\Omega_i}$ is a continuous piecewise linear interpolant on the trace of the $\mathcal{T}_{h,i}$ on the boundary introduced in [33]. The interpolant $\mathcal{I}^{\partial\Omega_i}$ is defined in Section 5.4 for the case of RT_0. See [33] for a general definition.

Due to Lemma 5.1, the interface problem (5.12) can be solved using a preconditioned conjugate gradient (PCG) method. One evaluation of the operator $A_h:\lambda\rightarrow A_h\lambda$ is required on each PCG iteration. It involves the following steps.

1. Project (L^2-orthogonally) mortar data onto the subdomain grids

$$\lambda\xrightarrow{\mathcal{Q}_{h,i}}\mathcal{Q}_{h,i}\lambda.$$

2. Solve in parallel subdomain problems (5.3)–(5.4) with Dirichlet data $\mathcal{Q}_{h,i}\lambda$ on the interior interfaces to compute the fluxes $\mathbf{u}_{h,i}^*(\lambda)\cdot\nu_i$.

3. Project the fluxes back to the mortar space

$$\mathbf{u}_{h,i}^*(\lambda)\cdot\nu_i\xrightarrow{Q_{h,i}^T}\mathbf{u}_{h,i}^m$$

and compute the jump across each interface $\Gamma_{i,j}$

$$[\mathbf{u}_h^m]_{ij}=\mathbf{u}_{h,i}^m+\mathbf{u}_{h,j}^m.$$

The projection Steps 1 and 3 are relatively inexpensive. The dominant cost is in Step 2.

5.2 BALANCING PRECONDITIONER

The balancing preconditioner is based on the Neumann-Neumann preconditioner developed in [18, 36, 52]. The latter can be expressed in operator form as

$$B_{NN}^{-1} = \sum_{i=1}^{n} A_{h,i}^{+}, \tag{5.15}$$

where $A_{h,i}^{+}$ is the Moore-Penrose pseudo-inverse of $A_{h,i}$. The evaluation of B_{NN}^{-1} requires solving subdomain problems $A_{h,i}\lambda_i = r_i$ with Neumann boundary data r_i: find $\mathbf{u}_{h,i} \in V_{h,i}$, $p_{h,i} \in W_{h,i}$, $\lambda_i \in M_{h,i}$ such that

$$\begin{aligned}
&(K^{-1}\mathbf{u}_{h,i}, \mathbf{v})_{\Omega_i} = (p_{h,i}, \nabla \cdot \mathbf{v})_{\Omega_i} - \langle \lambda_i, \mathbf{v} \cdot \nu_i \rangle_{\Gamma_i}, \ \ \mathbf{v} \in \mathbf{V}_{h,i}, \\
&(\nabla \cdot \mathbf{u}_{h,i}, w)_{\Omega_i} = 0, \ \ w \in W_{h,i}, \\
&\langle \mathbf{u}_{h,i} \cdot \nu_i, \mu \rangle_{\Gamma_i} = \langle r_i, \mu \rangle_{\Gamma_i}, \ \ \mu \in M_{h,i}.
\end{aligned}$$

The preconditioner (5.15) has two drawbacks: the local problems may not be solvable and the convergence deteriorates for large number of subdomains due to lack of global exchange of information. The balancing preconditioner [54, 55, 33] was developed to overcome these problems. The idea is to balance residuals so that local problems $A_{h,i}\lambda_i = r_i$ are solvable (modulo Null $A_{h,i}$) and the result does not depend on the specific choice of local solutions. We note that $A_{h,i}\lambda_i = r_i$ is solvable if

$$r_i \perp \text{Null} A_{h,i} = \begin{cases} \{\text{const}\} & \text{if full Neumann,} \\ \emptyset & \text{otherwise.} \end{cases}$$

Define a partition of unity D_i such that $D_i\lambda$ is nonzero only on Γ_i and

$$\sum_{i=1}^{n} D_i\lambda = \lambda, \quad \forall \lambda \in M_h. \tag{5.16}$$

Define spaces Z_i such that Null $A_{h,i} \subseteq Z_i$. We take $Z_i = \{\text{const}\}$ for $i = 1, \ldots, n$. The coarse space is defined as follows:

$$M_H = \{\lambda \in M_h : \lambda = \sum_{i=1}^{n} D_i\zeta_i, \ \ \zeta_i \in Z_i\}.$$

Clearly $\dim M_H \leq n$. A residual r is said to be *balanced* (local problems are solvable) if

$$\langle r, \mu_H \rangle = 0, \quad \mu_H \in M_H.$$

Balancing r means replacing it with

$$r^{bal} = r - A_h r_H,$$

where $r_H \in M_H$ is found by solving a coarse problem

$$a_h(r_H, \mu_H) = \langle r, \mu_H \rangle, \quad \mu_H \in M_H.$$

Algorithm (Balancing Preconditioner)

Given $r \in M_h$, define $B_{bal}^{-1} r$ as follows:

1. Solve a coarse problem:

$$a_h(r_H, \mu_H) = \langle r, \mu_H \rangle, \quad \mu_H \in M_H,$$

and balance the residual:

$$r^{bal} = r - A_h r_H.$$

2. Distribute r^{bal} to subdomains: $r_i = D_i^T r^{bal}$.
3. Solve local Neumann problems for $\lambda_i \in M_{h,i}$:

$$A_{h,i} \lambda_i = r_i.$$

4. Average local solutions: $\lambda = \sum_{i=1}^{n} D_i \lambda_i$.
5. Solve a coarse problem:

$$a_h(\lambda_H, \mu_H) = \langle r, \mu_H \rangle - a_h(\lambda, \mu_H), \quad \mu_H \in M_H,$$

and balance local solutions:

$$B_{bal}^{-1} r = \lambda + \lambda_H.$$

Note that the coarse solves in Step 1 and Step 5 provide global exchange of information across subdomains. In addition, Step 1 guarantees that the local problems in Step 3 are solvable, and, due to Step 5, the result of the preconditioner is independent of the specific

choice of local solutions. The dominant cost is in Step 3 which requires solving subdomain problems in parallel. The preconditioning cost is comparable to the cost of performing one unpreconditioned iteration, thus one preconditioned iteration is twice as expensive as one unpreconditioned iteration.

5.3 ANALYSIS OF THE CONDITION NUMBER

We start with several technical lemmas. The first lemma establishes that the balancing preconditioner operator is symmetric and positive definite and gives an abstract bound on the condition number. The proof follows closely the proof of Theorem 3.2 in [54] and is omitted here.

Lemma 5.2. *B_{bal} is symmetric and positive definite and*

$$cond(B_{bal}^{-1}A_h) \leq \sup \left\{ \frac{\sum_{j=1}^n a_{h,j}(\sum_{i=1}^n D_i\lambda_i, \sum_{i=1}^n D_i\lambda_i)}{\sum_{i=1}^n a_{h,i}(\lambda_i,\lambda_i)} : \lambda_i \in M_{h,i} \text{ and } \lambda_i \perp \text{Null } A_{h,i} \right\}.$$

The proof of the following lemma which gives a bound on the condition number of the preconditioned system follows from the proof of Theorem 3.3 in [55].

Lemma 5.3. *For subdomain Ω_i, define the weighting map D_i as*

$$(D_i\lambda_i)(x) = \frac{\alpha_i}{\alpha_i + \alpha_j}\lambda_i(x), \quad x \in \Gamma_{i,j},$$

and assume that there exists a number R so that

$$\frac{1}{\alpha_j}a_{h,j}(\lambda_i,\lambda_i) \leq \frac{1}{\alpha_i}R\, a_{h,i}(\lambda_i,\lambda_i)$$

for all $i,j = 1,\ldots,n$ and all $\lambda_i \in M_{h,i}$ such that $\int_{\Gamma_i}\lambda_i\zeta_i\,ds = 0, \forall\,\zeta_i \in$ Null $A_{h,i}$. Then there exists a constant C independent of h, $\tilde{H}$, and R such that

$$cond(B_{bal}^{-1}A_h) \leq CR.$$

We make the following explicit assumption about the computational grids. There exist positive constants c and C independent of h and $\tilde{H}$ such that, for any $\lambda \in M_h$,

$$c\|\mathcal{I}^{\partial\Omega_i}\mathcal{Q}_{h,i}\lambda\|_{1/2,\Gamma_{i,j}} \leq \|\mathcal{I}^{\partial\Omega_j}\mathcal{Q}_{h,j}\lambda\|_{1/2,\Gamma_{i,j}} \leq C\|\mathcal{I}^{\partial\Omega_i}\mathcal{Q}_{h,i}\lambda\|_{1/2,\Gamma_{i,j}}, \quad 1 \leq i,j \leq n. \tag{5.17}$$

Remark 5.1. *It is shown in Section 5.4, Lemma 5.5, that (5.17) holds in the case of RT_0 spaces under mild and easily satisfied in practice assumptions on the computational grids. These assumptions allow for a great amount of independence in constructing the subdomain grids, including large grid-size ratios (with constants possibly depending on these ratios).*

The following lemma is an extension of Lemma 6.4 in [33] to non-matching grids.

Lemma 5.4. *Assume that (5.17) holds. Then there exists a constant C independent of $\tilde{H}$ and h such that*

$$\|\mathcal{I}^{\partial\Omega_j}\mathcal{Q}_{h,j}\lambda_i\|^2_{1/2,\partial\Omega_j} \leq C(1+\log(\tilde{H}/h))^2\|\mathcal{I}^{\partial\Omega_i}\mathcal{Q}_{h,i}\lambda_i\|^2_{1/2,\partial\Omega_i} \quad \forall\lambda_i \in M_{h,i}.$$

Proof. By Lemma 4.3 of [20], we have

$$\|\mathcal{I}^{\partial\Omega_j}\mathcal{Q}_{h,j}\lambda_i\|^2_{1/2,\partial\Omega_j} \leq C(1+\log(\tilde{H}/h))^2\|\mathcal{I}^{\partial\Omega_j}\mathcal{Q}_{h,j}\lambda_i\|^2_{1/2,\Gamma_{i,j}}.$$

By (5.17),

$$\|\mathcal{I}^{\partial\Omega_j}\mathcal{Q}_{h,j}\lambda_i\|_{1/2,\Gamma_{i,j}} \leq C\|\mathcal{I}^{\partial\Omega_i}\mathcal{Q}_{h,i}\lambda_i\|_{1/2,\Gamma_{i,j}}.$$

Combining the above inequalities with the obvious inequality

$$\|\mathcal{I}^{\partial\Omega_i}\mathcal{Q}_{h,i}\lambda_i\|_{1/2,\Gamma_{i,j}} \leq \|\mathcal{I}^{\partial\Omega_i}\mathcal{Q}_{h,i}\lambda_i\|_{1/2,\partial\Omega_i}$$

completes the proof. □

We assume that $\partial\Omega_i \cap \partial\Omega$ is either empty or of size $\mathcal{O}(\tilde{H})$ so that the Poincaré inequality holds uniformly for all Ω_i and there exists a constant C independent of h and $\tilde{H}$ such that

$$\|w\|^2_{\Omega_i} \leq C\tilde{H}^2|w|^2_{1,\Omega_i}, \quad \|w\|^2_{\partial\Omega_i} \leq C\tilde{H}|w|^2_{1/2,\partial\Omega_i} \tag{5.18}$$

for all $w \in H^1(\Omega_i)$ if $\partial\Omega_i \cap \partial\Omega$ is non-empty and for all $w \in H^1(\Omega_i)$, $\langle w, 1\rangle_{\Gamma_i} = 0$, if $\partial\Omega_i \cap \partial\Omega$ is empty.

We are now ready to state the main result.

Theorem 5.1. *If* (5.17) *holds and the weights* D_i *satisfy*

$$(D_i\lambda)(x) = \frac{\alpha_i}{\alpha_i + \alpha_j}\lambda(x), \quad x \in \Gamma_{i,j}, \quad \text{for all } \lambda \in M_h,$$

then there exists a constant C *independent of* h, $\tilde{H}$, *and jumps in* K, *such that*

$$cond(B_{bal}^{-1}A_h) \leq C(1 + \log(\tilde{H}/h))^2.$$

Proof. Let $\lambda_i \in M_{h,i}$ be such that $\lambda_i \perp \text{Null } A_{h,i}$. With (5.14) we have

$$\begin{aligned} a_{h,j}(\lambda_i, \lambda_i) &\leq C\alpha_j |\mathcal{I}^{\partial\Omega_j}\mathcal{Q}_{h,j}\lambda_i|^2_{1/2,\partial\Omega_j} \leq C\alpha_j \|\mathcal{I}^{\partial\Omega_j}\mathcal{Q}_{h,j}\lambda_i\|^2_{1/2,\partial\Omega_j} \\ &\leq C\alpha_j(1 + \log(\tilde{H}/h))^2 \|\mathcal{I}^{\partial\Omega_i}\mathcal{Q}_{h,i}\lambda_i\|^2_{1/2,\partial\Omega_i}, \end{aligned}$$

using Lemma 5.4 for the last inequality. Note that it easily follows from the definitions of $\mathcal{Q}_{h,i}$ and $\mathcal{I}^{\partial\Omega_i}$ that

$$\langle \mathcal{I}^{\partial\Omega_i}\mathcal{Q}_{h,i}\lambda_i, 1\rangle_{\Gamma_i} = \langle \mathcal{Q}_{h,i}\lambda_i, 1\rangle_{\Gamma_i} = \langle \lambda_i, 1\rangle_{\Gamma_i} = 0$$

so that the Poincaré inequality (5.18) implies

$$\|\mathcal{I}^{\partial\Omega_i}\mathcal{Q}_{h,i}\lambda_i\|^2_{1/2,\partial\Omega_i} \leq C|\mathcal{I}^{\partial\Omega_i}\mathcal{Q}_{h,i}\lambda_i|^2_{1/2,\partial\Omega_i}.$$

Therefore we have

$$\begin{aligned} a_{h,j}(\lambda_i, \lambda_i) &\leq C\alpha_j(1 + \log(\tilde{H}/h))^2 |\mathcal{I}^{\partial\Omega_i}\mathcal{Q}_{h,i}\lambda_i|^2_{1/2,\partial\Omega_i} \\ &\leq C\frac{\alpha_j}{\alpha_i}(1 + \log(\tilde{H}/h))^2 a_{h,i}(\lambda_i, \lambda_i), \end{aligned}$$

using (5.14) for the last inequality. The proof is completed by applying Lemma 5.3. □

Remark 5.2. *The above theorem implies in the case of non-matching grids a bound for the balancing preconditioner which is similar to the bounds obtained for matching grids [55, 33].*

5.4 ON GRID ASSUMPTION (5.17)

Here we justify the assumption (5.17) on the computational grids. We show that it holds in the case of RT_0 rectangular subdomain discretizations for a fairly general grid configuration. We start by defining the piecewise linear interpolant $\mathcal{I}^{\partial\Omega_i}$ for the RT_0 spaces. More general definition is given in [33]. Let $\hat{\mathcal{T}}_{h,i}$ be a refinement of $\mathcal{T}_{h,i}|_{\Gamma_i}$ with vertices at the element centers (primary vertices) and the element vertices (secondary vertices) of $\mathcal{T}_{h,i}|_{\Gamma_i}$. Note that the primary vertices coincide with the degrees of freedom of $\mathbf{V}_{h,i}\cdot\nu_i|_{\Gamma_i}$ and, correspondingly, the pressure Lagrange multipliers on Γ_i. Let $U_{h,i}$ be the space of continuous piecewise linear functions subordinate to the partition $\hat{\mathcal{T}}_{h,i}$. For $\phi\in\mathbf{V}_{h,i}\cdot\nu_i|_{\Gamma_i}$, define $\mathcal{I}^{\partial\Omega_i}\phi\in U_{h,i}$ as follows:

$$\mathcal{I}^{\partial\Omega_i}\phi(x)=\begin{cases}\phi(x), & \text{if } x \text{ is a primary vertex of } \hat{\mathcal{T}}_{h,i};\\ \text{the area-weighted average of values of } \phi \text{ at all adjacent primary vertices,}\\ \qquad \text{if } x \text{ is a secondary vertex of } \hat{\mathcal{T}}_{h,i};\\ \text{the linear interpolation of vertex values,} & \text{if } x \text{ is a not a vertex of } \hat{\mathcal{T}}_{h,i}.\end{cases}$$

To simplify the presentation below, we call two non-negative functions $f_1(\cdot)$ and $f_2(\cdot)$ with the same domain D equivalent and write

$$f_1\simeq f_2$$

if there exist positive constants c and C independent of h and $\tilde{H}$ such that

$$cf_1(\phi)\le f_2(\phi)\le Cf_1(\phi),\quad \forall\phi\in D.$$

It is easy to see that for any $\hat{p}\in U_{h,i}$ and for any $\tau^i\in\hat{\mathcal{T}}_{h,i}$

$$|\hat{p}|^2_{1,\tau^i}\simeq|\tau^i|^{1-2/(d-1)}\sum_{\substack{\text{vertices}\\ v_l,v_k\in\tau^i}}(\hat{p}(v_l)-\hat{p}(v_k))^2, \tag{5.19}$$

$$|\hat{p}|^2_{0,\tau^i}\simeq|\tau^i|\sum_{\substack{\text{vertices}\\ v_l\in\tau^i}}\hat{p}(v_l)^2. \tag{5.20}$$

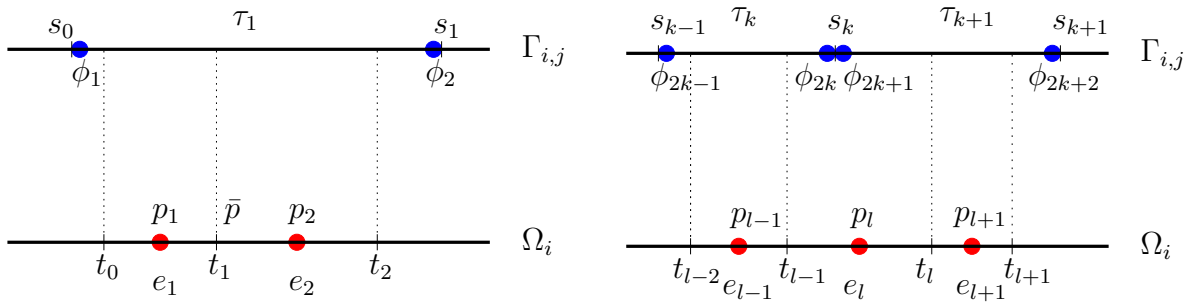

Figure 5.1: Grids on the mortar and neighboring subdomain along the interface $\Gamma_{i,j}$

Lemma 5.5. *Consider $d = 2$, RT_0 subdomain discretizations on rectangular grids, and discontinuous piecewise linear mortar spaces. Assume that every element of $\mathcal{T}_{h,i,j}$ contains at least one element of $\mathcal{T}_{h,i}|_{\Gamma_{i,j}}$ and that at least one element of $\mathcal{T}_{h,i,j}$ contains at least two elements of $\mathcal{T}_{h,i}|_{\Gamma_{i,j}}$. Assume that the same relation holds for $\mathcal{T}_{h,i,j}$ and $\mathcal{T}_{h,j}|_{\Gamma_{i,j}}$ (see Figure 5.1). Then, for any $\lambda \in M_h$,*

$$\|\mathcal{I}^{\partial\Omega_i}\mathcal{Q}_{h,i}\lambda\|_{1/2,\Gamma_{i,j}} \simeq \|\mathcal{I}^{\partial\Omega_j}\mathcal{Q}_{h,j}\lambda\|_{1/2,\Gamma_{i,j}}.$$

Proof. First, consider an element τ_1 of $\mathcal{T}_{h,i,j}$ that contains at least two elements, e_1, e_2, of $\mathcal{T}_{h,i}|_{\Gamma_{i,j}}$. Denote the vertices of τ_1 by v_1, v_2 with coordinates s_0, s_1, respectively, and the coordinates of the endpoints of e_1, e_2 by t_0, t_1, t_2 (see Figure 5.1, left). Let, for a given $\lambda \in M_h$,

$$\lambda(v_m) = \phi_m, \quad m = 1, 2, \qquad p_l = \mathcal{Q}_{h,i}\lambda|_{e_l}, \quad l = 1, 2.$$

By definition, the value of $\mathcal{I}^{\partial\Omega_i}\mathcal{Q}_{h,i}\lambda$ at the midpoint of e_l (primary vertex) is p_l. Denote by $\bar{p}$ the value of $I^{\partial\Omega_i}\mathcal{Q}_{h,i}\lambda$ at the secondary vertex between e_1 and e_2. We have

$$\bar{p} = \frac{|e_2|p_1 + |e_1|p_2}{|e_1| + |e_2|}, \quad p_1 - \bar{p} = \frac{|e_1|}{|e_1| + |e_2|}(p_1 - p_2), \quad \bar{p} - p_2 = \frac{|e_2|}{|e_1| + |e_2|}(p_1 - p_2),$$

hence it is enough to consider in (5.19) and (5.20) only the values of $\mathcal{I}^{\partial\Omega_i}\mathcal{Q}_{h,i}\lambda$ at the primary vertices. For p_1, p_2 we obtain

$$\begin{pmatrix} p_1 \\ p_2 \end{pmatrix} = A_0 \begin{pmatrix} \phi_1 \\ \phi_2 \end{pmatrix}, \quad A_0 = \begin{pmatrix} \alpha_1 & \alpha_2 \\ \beta_1 & \beta_2 \end{pmatrix}, \tag{5.21}$$

where

$$\alpha_1 = \frac{2s_1 - t_0 - t_1}{2(s_1 - s_0)},\ \alpha_2 = \frac{t_0 + t_1 - 2s_0}{2(s_1 - s_0)}, \quad \beta_1 = \frac{2s_1 - t_1 - t_2}{2(s_1 - s_0)},\ \beta_2 = \frac{t_1 + t_2 - 2s_0}{2(s_1 - s_0)}.$$

Note that $\alpha_1 + \alpha_2 = 1$, $\beta_1 + \beta_2 = 1$, and hence

$$\det A_0 = \alpha_1 - \beta_1 = \frac{t_2 - t_0}{2(s_1 - s_0)} \geq C > 0,$$

which gives

$$\begin{pmatrix} \phi_1 \\ \phi_2 \end{pmatrix} = A_0^{-1} \begin{pmatrix} p_1 \\ p_2 \end{pmatrix}, \tag{5.22}$$

where the elements of A_0^{-1} do not depend on h. We also have

$$p_1 - p_2 = (\alpha_1 - \beta_1)(\phi_1 - \phi_2). \tag{5.23}$$

Proceeding inductively, assume that we have expressed $p_1, \ldots, p_{l-1}$ in terms of $\phi_1, \ldots, \phi_{2k}$, as well as differences of two consecutive p's in terms of differences of ϕ's and vice versa. Consider two neighboring elements, τ_k, τ_{k+1}, of $\mathcal{T}_{h,i,j}$, each containing an element of $\mathcal{T}_{h,i}|_{\Gamma_{i,j}}$ (e_{l-1} and e_{l+1}, respectively) (see Figure 5.1, right). Denote the vertices of τ_k and τ_{k+1} by v_{2k-1}, v_{2k} and v_{2k+1}, v_{2k+2}, respectively, with coordinates s_{k-1}, s_k, s_{k+1}. Denote the coordinates of the endpoints of e_{l-1}, e_l, e_{l+1} by $t_{l-2}, t_{l-1}, t_l, t_{l+1}$. Let

$$\lambda(v_m) = \phi_m,\ m = 2k-1, \ldots, 2k+2, \quad p_n = \mathcal{Q}_{h,i}\lambda|_{e_n},\ n = l-1, l, l+1.$$

Then we have

$$\begin{aligned} p_{l-1} &= a_{l,1}\phi_{2k-1} + a_{l,2}\phi_{2k}, \\ p_l &= b_{l,1}\phi_{2k-1} + b_{l,2}\phi_{2k} + b_{l,3}\phi_{2k+1} + b_{l,4}\phi_{2k+2}, \\ p_{l+1} &= c_{l,1}\phi_{2k+1} + c_{l,2}\phi_{2k+2}, \end{aligned} \tag{5.24}$$

where

$$\begin{aligned} a_{l,1} &= \frac{(2s_k - t_{l-2} - t_{l-1})}{2(s_k - s_{k-1})}, & a_{l,2} &= \frac{(t_{l-2} + t_{l-1} - 2s_{k-1})}{2(s_k - s_{k-1})}, \\ b_{l,1} &= \frac{(s_k - t_{l-1})^2}{2(t_l - t_{l-1})(s_k - s_{k-1})}, & b_{l,2} &= \frac{(s_k - t_{l-1})(t_{l-1} + s_k - 2s_{k-1})}{2(t_l - t_{l-1})(s_k - s_{k-1})}, \\ b_{l,3} &= \frac{(t_l - s_k)(2s_{k+1} - s_k - t_l)}{2(t_l - t_{l-1})(s_{k+1} - s_k)}, & b_{l,4} &= \frac{(t_l - s_k)^2}{2(t_l - t_{l-1})(s_{k+1} - s_k)}, \\ c_{l,1} &= \frac{(2s_{k+1} - t_l - t_{l+1})}{2(s_{k+1} - s_k)}, & c_{l,2} &= \frac{(t_l + t_{l+1} - 2s_k)}{2(s_{k+1} - s_k)}. \end{aligned}$$

Note that the coefficients in (5.24) can be bounded above and below by constants independent of h and dependent on the grid-size ratio. We can rewrite the last two equations of (5.24) as

$$\begin{pmatrix} p_l \\ p_{l+1} \end{pmatrix} = \begin{pmatrix} b_{l,1}\phi_{2k-1} + b_{l,2}\phi_{2k} \\ 0 \end{pmatrix} + A_l \begin{pmatrix} \phi_{2k+1} \\ \phi_{2k+2} \end{pmatrix}, \quad A_l = \begin{pmatrix} b_{l,3} & b_{l,4} \\ c_{l,1} & c_{l,2} \end{pmatrix}. \tag{5.25}$$

Note that

$$a_{l,1} + a_{l,2} = 1, \quad b_{l,1} + b_{l,2} + b_{l,3} + b_{l,4} = 1, \quad c_{l,1} + c_{l,2} = 1. \tag{5.26}$$

Since

$$\det A_l = \frac{(t_l - s_k)(t_{l+1} - s_k)}{2(t_l - t_{l-1})(s_{k+1} - s_k)} \geq C > 0,$$

$$\begin{pmatrix} \phi_{2k+1} \\ \phi_{2k+2} \end{pmatrix} = A_l^{-1} \left[\begin{pmatrix} p_l \\ p_{l+1} \end{pmatrix} - \begin{pmatrix} b_{l,1}\phi_{2k-1} + b_{l,2}\phi_{2k} \\ 0 \end{pmatrix} \right]. \tag{5.27}$$

Thus, ϕ_{2k+1} and ϕ_{2k+2} are linear combinations of $p_1, \ldots, p_{l+1}$ with coefficients independent of h. Using (5.26), it follows from (5.24) that

$$\begin{pmatrix} p_{l-1} - p_l \\ p_l - p_{l+1} \end{pmatrix} = (\phi_{2k-1} - \phi_{2k}) \begin{pmatrix} a_{l,1} - b_{l,1} \\ b_{l,1} \end{pmatrix} + B_l \begin{pmatrix} \phi_{2k} - \phi_{2k+1} \\ \phi_{2k+1} - \phi_{2k+2}, \end{pmatrix}, \tag{5.28}$$

where

$$B_l = \begin{pmatrix} b_{l,3} + b_{l,4} & b_{l,4} \\ b_{l,1} + b_{l,2} & c_{l,2} - b_{l,4} \end{pmatrix}. \tag{5.29}$$

Using (5.26), we get

$$\det B_l = b_{l,3}c_{l,2} - b_{l,4}c_{l,1} = \det A_l,$$

so

$$\begin{pmatrix} \phi_{2k} - \phi_{2k+1} \\ \phi_{2k+1} - \phi_{2k+2} \end{pmatrix} = B_l^{-1} \left[\begin{pmatrix} p_{l-1} - p_l \\ p_l - p_{l+1} \end{pmatrix} - (\phi_{2k-1} - \phi_{2k}) \begin{pmatrix} a_{l,1} - b_{l,1} \\ b_{l,1} \end{pmatrix} \right]. \tag{5.30}$$

Therefore, $(\phi_{2k} - \phi_{2k+1})$ and $(\phi_{2k+1} - \phi_{2k+2})$ can be expressed as linear combinations of the differences $(p_n - \ p_{n+1}), n = 1, \ldots, l$.

Applying the inequality $(a+b)^2 \leq 2(a^2 + b^2)$ and combining (5.20), (5.21), (5.24), and (5.27) implies

$$|\mathcal{I}^{\partial\Omega_i} \mathcal{Q}_{h,i} \lambda|_{0,\Gamma_{i,j}} \simeq |\lambda|_{0,\Gamma_{i,j}}. \tag{5.31}$$

Combining (5.19), (5.23),(5.28), and (5.30) gives

$$|\mathcal{I}^{\partial\Omega_i}\mathcal{Q}_{h,i}\lambda|_{1,\Gamma_{i,j}} \simeq |\lambda|_{1,\Gamma_{i,j}}. \tag{5.32}$$

Similar arguments imply

$$|\mathcal{I}^{\partial\Omega_j}\mathcal{Q}_{h,j}\lambda|_{0,\Gamma_{i,j}} \simeq |\lambda|_{0,\Gamma_{i,j}} \tag{5.33}$$

and

$$|\mathcal{I}^{\partial\Omega_j}\mathcal{Q}_{h,j}\lambda|_{1,\Gamma_{i,j}} \simeq |\lambda|_{1,\Gamma_{i,j}}. \tag{5.34}$$

The interpolation theory of Sobolev spaces [53] and bounds (5.31), (5.32), (5.33), and (5.34) imply the statement of the lemma. □

Remark 5.3. *The proof of the above lemma is also valid in the case of continuous piecewise linear mortars.*

Remark 5.4. *The above argument can be generalized to three-dimensional rectangular-type RT_0 discretizations in a relatively straightforward way.*

5.5 NUMERICAL SIMULATIONS

We present four computational experiments confirming the theoretical results of Section 5.3 on the behavior of the balancing preconditioner. In Examples 5.1 and 5.3 we study the dependence of the condition number on h for a smooth and a highly heterogeneous problem, respectively. Example 5.2 is designed to investigate the effect of jumps in the coefficients. In Example 5.4 we consider the effect of the number of subdomains. In all cases one processor is assigned per subdomain. The runs in Examples 5.1, 5.2, and 5.3 are performed on the unit square divided into four subdomains ($\tilde{H} = 1/2$). The runs in Example 5.4 are performed on a sequence of domain decompositions ranging from 2×2 to 5×5 subdomains.

In Examples 5.1 and 5.3 the condition number and number of CG iterations with and without preconditioning are reported for several levels of grid refinements starting with the grids shown in Figure 5.2A. The largest ratio of the subdomain grid sizes in these examples is 5/2. We also consider a second case in Example 5.1 where the ratio is 11/2 (see

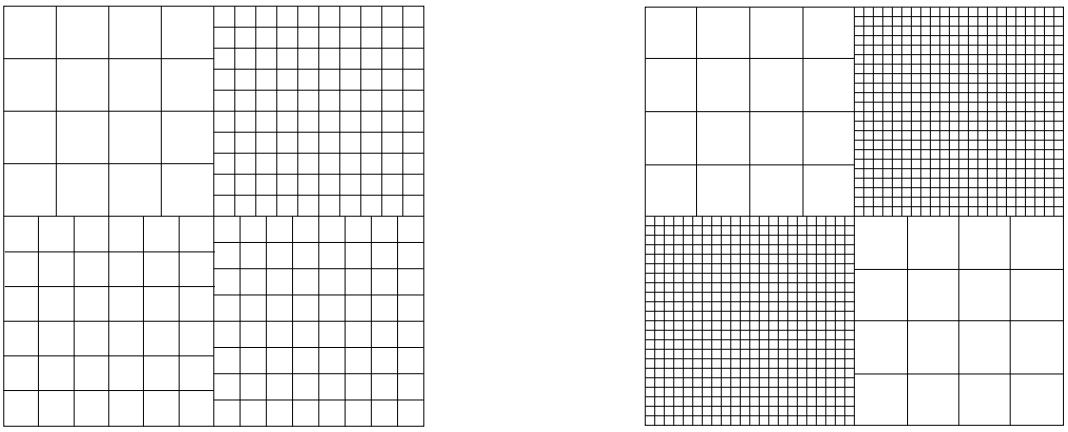

A. Case 1 B. Case 2

Figure 5.2: Initial grids for Example 5.1

Figure 5.2B). The two cases are denoted by Case 1 and Case 2. The mortars are chosen to be discontinuous for Examples 5.1, 5.2 and 5.4) or continuous (for Example 5.2) piecewise linears on an interface grid obtained by coarsening by two the trace of the coarser of the neighboring subdomain grids.

Example 5.1.

The problem in the first test has analytical solution $p(x, y) = x^3y^2 + \sin(xy)$ and a smooth permeability tensor

$$K = \begin{pmatrix} 10 + 5\cos(xy) & 0 \\ 0 & 1 \end{pmatrix}.$$

The condition number and number of iterations for Case 1 and Case 2 are given in Table 5.1, Figure 5.3 and Figure 5.4. As expected from the theory, the condition number in the case of balancing preconditioner grows very slowly as h gets smaller and the number of PCG iterations stays almost the same. A comparison of the results from Case 1 and Case 2 indicates that the condition number and number of iterations are almost independent of the grid size ratio.

Example 5.2.

In this test we study the dependence of the behavior of the balancing preconditioner on jumps in the coefficient. A different permeability function is assigned on each subdomain

Table 5.1: Condition number and number of iterations for Example 5.1

$1/h$	*BalCG*		*CG*	
	cond.	*iter.*	*cond.*	*iter.*
4	4.54520	11	9.04823	14
8	5.90177	11	17.0075	18
16	7.54221	12	33.5087	25
32	9.44828	12	66.7478	36

Case 1

$1/h$	*BalCG*		*CG*	
	cond.	*iter.*	*cond.*	*iter.*
4	2.30058	8	10.7644	12
8	2.83097	9	21.1122	19
16	3.37244	9	41.7829	29
32	4.11108	9	83.2505	41

Case 2

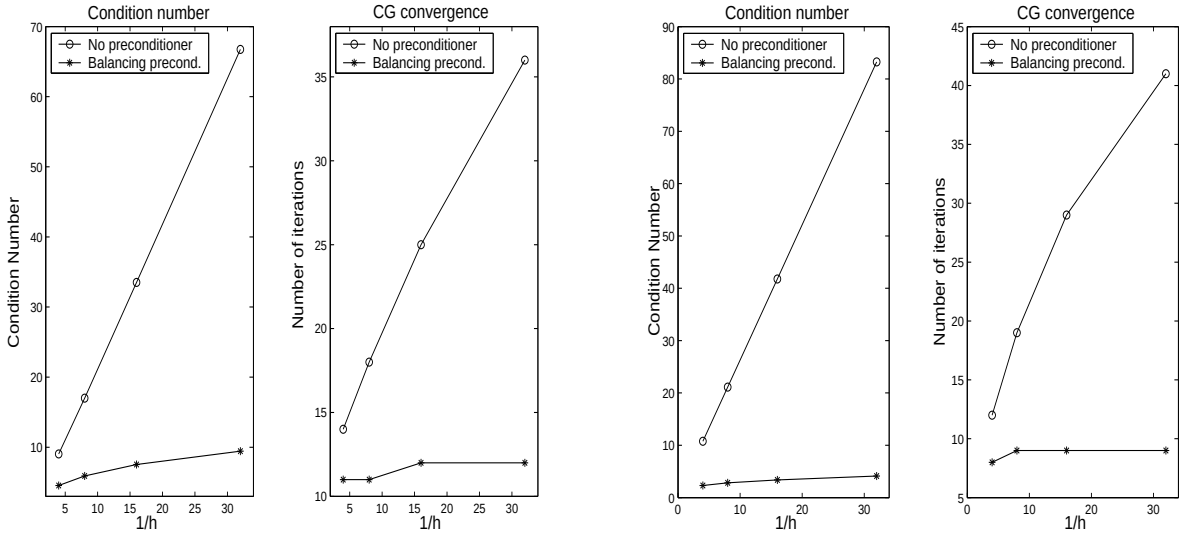

A. Case 1

B. Case 2

Figure 5.3: Condition number and number of iterations for Example 5.1

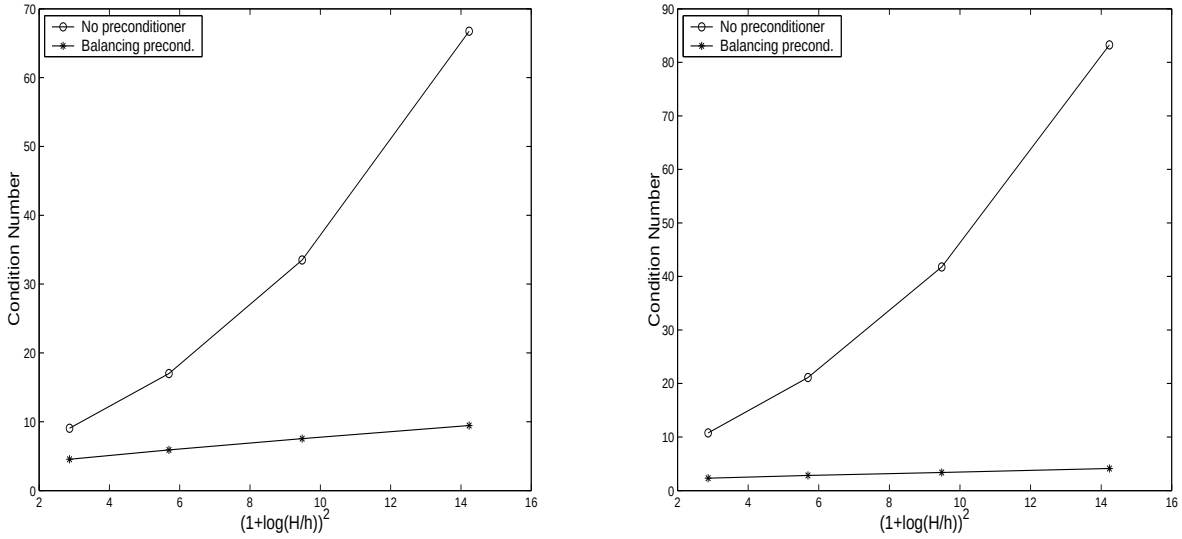

A. Case 1 B. Case 2

Figure 5.4: Dependence of the condition number on $(1 + \log(\tilde{H}/h))^2$ in Example 5.1

as shown in Figure 5.5 (left). A series of runs is performed changing each function so that the jumps between subdomains get larger. The behavior of the CG iteration is illustrated in Figure 5.6. We note that both the condition number and the number of iterations remain bounded when jumps become larger which is consistent with the bound given in Theorem 5.1. We also compare in Figure 5.5 (right) the residual reductions in the unpreconditioned and the preconditioned CG iterations. The preconditioning accelerates the residual reduction and removes the oscillations observed in the unpreconditioned case.

Example 5.3.

In the next test we simulate flow through highly heterogeneous porous media. The permeability field and the computed solution on the first level of refinement (left-to-right flow is imposed through boundary conditions) are given in Figure 5.7. For each level of refinement the permeability field is projected onto the corresponding computational grids. The condition number and the number of iterations (see Table 5.2 and Figure 5.8) once again grow very slowly as h gets smaller. On Figure 5.9 we compare the residual reductions in the unpreconditioned and the preconditioned CG iterations.

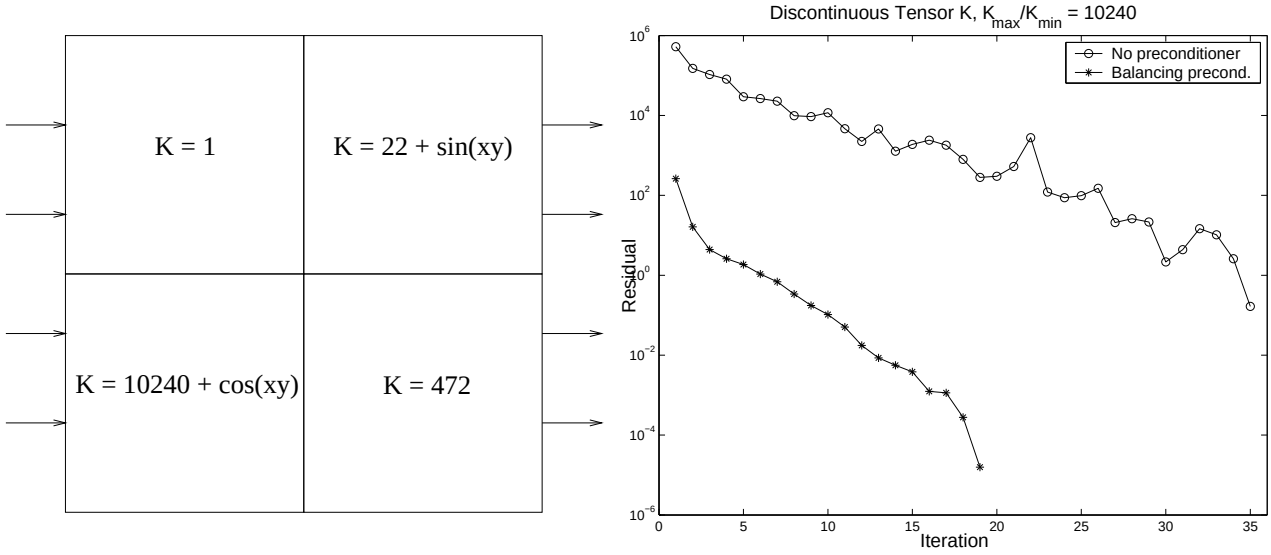

Figure 5.5: Permeability values (left) and residual reduction (right) for the initial level in Example 5.2

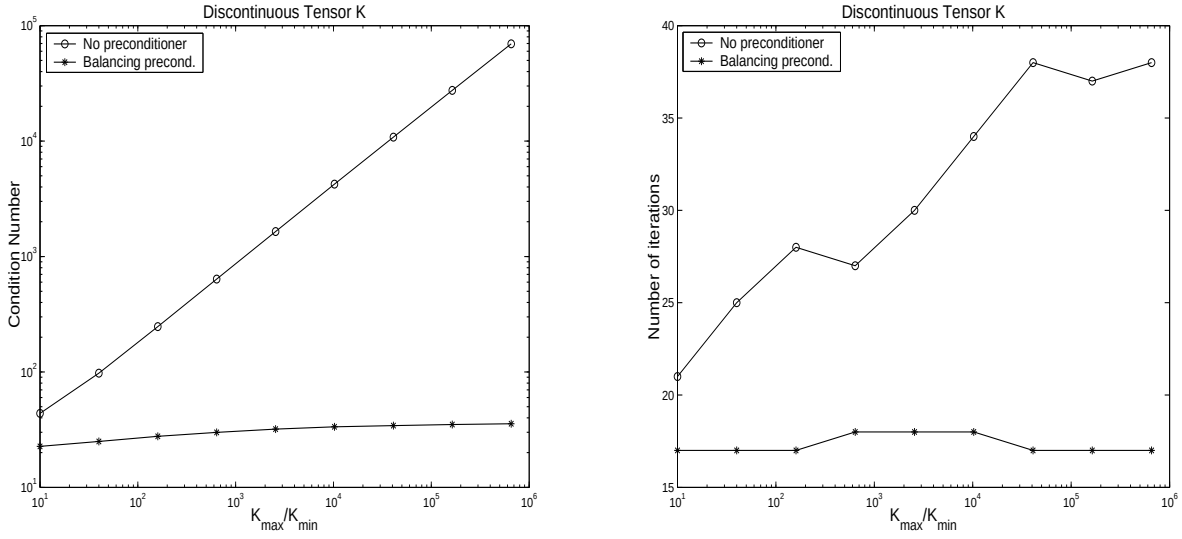

Figure 5.6: Dependence of CG convergence on jumps in coefficients in Example 5.2

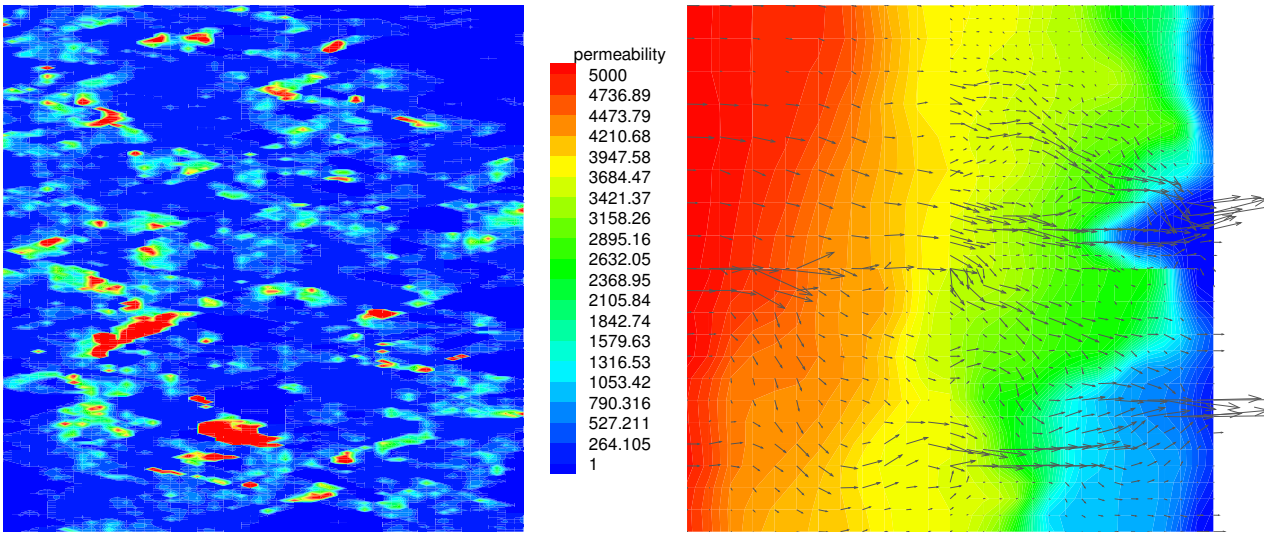

Figure 5.7: Permeability field and computed pressure (shade) and velocity (arrows) in Example 5.3

Table 5.2: Condition number and number of iterations for Example 5.3

$1/h$	*BalCG*		*CG*	
	cond.	*iter.*	*cond.*	*iter.*
4	63.4544	17	222.195	25
8	53.8312	27	338.236	47
16	90.2661	34	2313.30	94
32	192.754	38	14049.8	207
64	336.072	50	65824.2	492

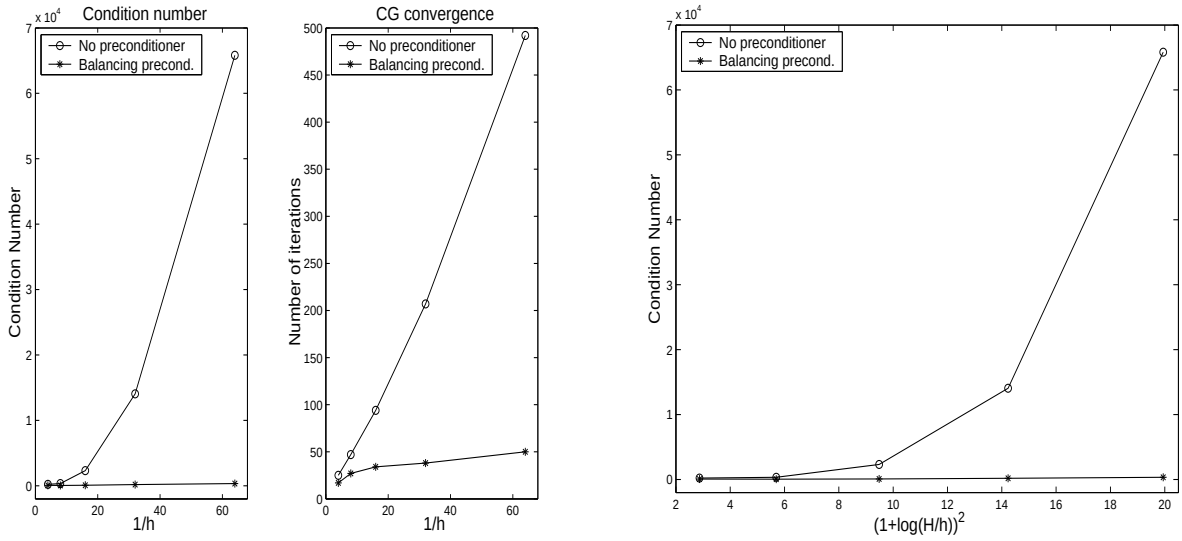

Figure 5.8: Condition number and number of iterations for Example 5.3

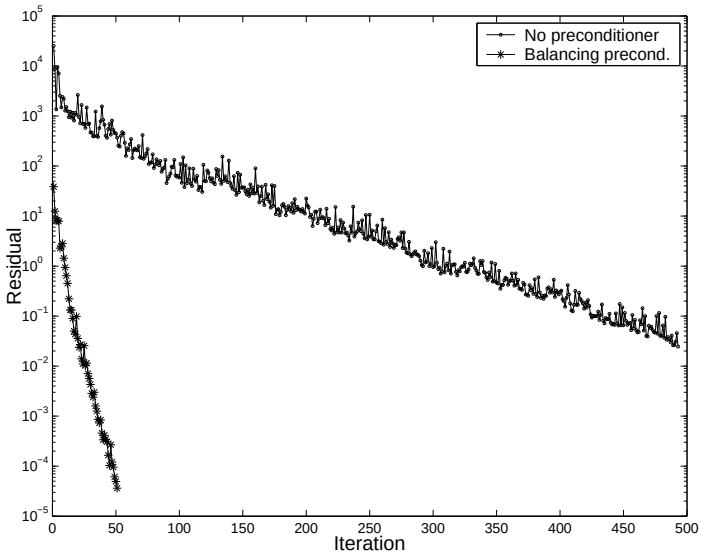

Figure 5.9: Residual reduction for Example 5.3

Example 5.4.

Lastly, we study the dependence of the behavior of the balancing preconditioner on the number of subdomains. We solve a problem with analytical solution

$$p(x, y, z) = x^3y^4 + x^2 + \sin(xy)\cos(y)$$

Table 5.3: Condition number and number of iterations for Example 5.4

Num	*BalCG*		*CG*	
Proc.	*cond.*	*iter.*	*cond.*	*iter.*
4	8.16598	13	38.2574	23
9	12.2771	16	111.967	38
16	13.2133	19	225.357	55
25	13.4436	20	379.496	72

and a smooth permeability tensor

$$K = \begin{pmatrix} (x+1)^2 + y^2 & 0 & 0 \\ 0 & (x+1)^2 & 0 \\ 0 & 0 & 1 \end{pmatrix}$$

on a sequence of domain decompositions from 2×2 to 5×5 subdomains. The ratio $\tilde{H}/h$ is kept constant with subdomain grids chosen 14×18 or 12×20 in a checkerboard fashion. The condition number and number of iterations are given in Table 5.3 and Figure 5.10. The results are consistent with the theory and indicate very good parallel scalability of the balancing preconditioner.

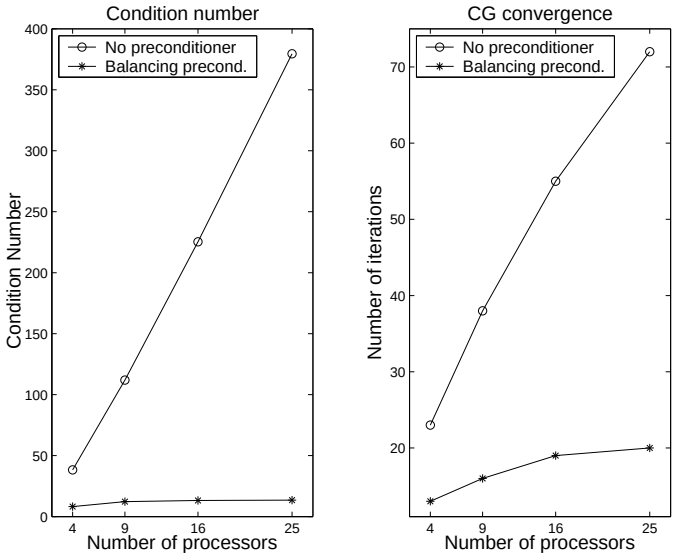

Figure 5.10: Condition number and number of iterations for Example 5.4

6.0 MULTISCALE MORTAR MIXED FINITE ELEMENT METHOD

In this chapter we develop multiscale mortar mixed finite element discretizations for second order elliptic equations. Our method is similar to the variational multiscale method [48, 49, 22, 10, 7, 3, 8, 4] and multiscale finite elements [46, 47, 30].

The new method is based on domain decomposition theory and mortar finite elements. We partition the computational domain into a series of small subdomains (or coarse elements), over which we pose the original problem. We allow for geometrically non-conforming domain decompositions. We connect the subdomains together using a low degree-of-freedom mortar space defined on a coarse scale mortar grid. The mortar provides a natural Dirichlet pressure boundary condition for the subdomain problems, which can be solved easily because of their relatively small size. The (weak) velocity flux mismatch provides a criterion for updating the mortar pressure, and we iterate to convergence. By using a higher order mortar approximation, we are able to compensate for the coarseness of the grid scale and maintain good (fine scale) overall accuracy. This approach is more flexible than the variational multiscale method and multiscale finite elements, because it is easy to improve global accuracy by simply refining the local mortar grid where needed. That is, we can easily exploit adaptive meshing strategies to improve where necessary the strength of the global coupling.

6.1 FORMULATION OF THE METHOD

Let the mortar interface mesh $\mathcal{T}_{H,i,j}$ be a quasi-uniform finite element partition of $\Gamma_{i,j}$ with maximal element diameter $H_{i,j}$. Let $H = \max_{1\le i,j\le n} H_{i,j}$. Define $\mathcal{T}^{\Gamma,H} = \cup_{1\le i<j\le n}\mathcal{T}_{H,i,j}$. For

any $\tau \in \mathcal{T}_{H,i,j}$, let

$$E_\tau = \{E \in \mathcal{T}_h : \partial E \cap \tau \neq \emptyset\}.$$

Denote by $M_{H,i,j} \subset L^2(\Gamma_{i,j})$ the mortar space on $\Gamma_{i,j}$, containing either the continuous or discontinuous piecewise polynomials of degree m on $\mathcal{T}_{H,i,j}$, where m is at least $k+1$. Now let

$$M_H = \bigoplus_{1 \le i < j \le n} M_{H,i,j}$$

be the mortar finite element space on Γ. We require that the following condition be satisfied [9].

Assumption 6.1. *Assume that there exists a constant C, independent of h and H, such that*

$$\|\mu\|_{\Gamma_{i,j}} \le C(\|\mathcal{Q}_{h,i}\mu\|_{\Gamma_{i,j}} + \|\mathcal{Q}_{h,j}\mu\|_{\Gamma_{i,j}}), \quad \mu \in M_H, \ \ 1 \le i < j \le n. \tag{6.1}$$

Condition (6.1) says that the mortar space cannot be too rich compared to the normal traces of the subdomain velocity spaces. Therefore in the sequel, we tacitly assume that $h \le H \le 1$. Condition (6.1) is not very restrictive, and it is easily satisfied in practice (see, e.g., [74, 59]). In the case of RT_0 spaces, (6.1) holds under the assumptions on the grids in Lemmas 5.5, 6.4, or 6.5.

In the following we treat any function $\mu \in M_H$ as extended by zero on $\partial\Omega$.

In the multiscale mixed finite element approximation of (2.22)–(2.23). we seek $\mathbf{u}_h \in \mathbf{V}_h$, $p_h \in W_h$, $\lambda_H \in M_H$ such that, for $1 \le i \le n$,

$$(K^{-1}\mathbf{u}_h, \mathbf{v})_{\Omega_i} = (p_h, \nabla \cdot \mathbf{v})_{\Omega_i} - \langle \lambda_H, \mathbf{v} \cdot \nu_i \rangle_{\Gamma_i} - \langle g, \mathbf{v} \cdot \nu_i \rangle_{\partial\Omega_i \setminus \Gamma}, \quad \mathbf{v} \in \mathbf{V}_{h,i}, \tag{6.2}$$

$$(\nabla \cdot \mathbf{u}_h, w)_{\Omega_i} = (f, w)_{\Omega_i}, \qquad w \in W_{h,i}, \tag{6.3}$$

$$\sum_{i=1}^{n} \langle \mathbf{u}_h \cdot \nu_i, \mu \rangle_{\Gamma_i} = 0, \qquad \mu \in M_H. \tag{6.4}$$

Strictly within each block Ω_i, we have a standard mixed finite element method, and (6.3) enforces local conservation over each grid cell. Moreover, $\mathbf{u}_h \cdot \nu$ is continuous on any element edge (or face) $e \not\subset \Gamma \cup \partial\Omega$, and (6.4) enforces weak continuity of flux across these interfaces with respect to the mortar space M_H.

The above method was defined in [9], except that H was comparable to h ($H = \mathcal{O}(h)$) and $m = k+1$ was one more than the degree of approximating polynomials in $\mathbf{V}_h$. Here, we weaken the discretization on Γ by taking larger elements of size H but compensating with a higher degree of approximation. The theoretical results of [9] are no longer valid, since asymptotically we now take $H = \mathcal{O}(h^\alpha)$, with $\alpha < 1$.

6.1.1 A domain decomposition formulation

Similarly to Section 5.1, define a bilinear form $a_H : L^2(\Gamma) \times L^2(\Gamma) \to \mathbf{R}$ by

$$a_H(\lambda, \mu) = \sum_{i=1}^{n} a_{H,i}(\lambda, \mu) = -\sum_{i=1}^{n} \langle \mathbf{u}_h^*(\lambda) \cdot \nu_i, \mu \rangle_{\Gamma_i},$$

where $(\mathbf{u}_h^*(\lambda), p_h^*(\lambda)) \in \mathbf{V}_h \times W_h$ solves (5.3)–(5.4) for each $1 \le i \le n$. Also define a linear functional $g_H : L^2(\Gamma) \to \mathbf{R}$ by

$$g_H(\mu) = \sum_{i=1}^{n} g_{H,i}(\mu) = \sum_{i=1}^{n} \langle \bar{\mathbf{u}}_h \cdot \nu_i, \mu \rangle_{\Gamma_i},$$

where $(\bar{\mathbf{u}}_h, \bar{p}_h) \in \mathbf{V}_h \times W_h$ solves, for $1 \le i \le n$, (5.6)–(5.7). It is straightforward to show (see [43, 9]) that the solution of

$$a_H(\lambda_H, \mu) = g_H(\mu), \quad \mu \in M_H, \tag{6.5}$$

generates the solution of (6.2)–(6.4) via

$$\mathbf{u}_h = \mathbf{u}_h^*(\lambda_H) + \bar{\mathbf{u}}_h, \qquad p_h = p_h^*(\lambda_H) + \bar{p}_h.$$

The following is proved in [9].

Lemma 6.1. *The interface bilinear form $a_H(\cdot, \cdot)$ is symmetric and positive semi-definite on $L^2(\Gamma)$. If (6.1) holds, then $a_H(\cdot, \cdot)$ is positive definite on M_H. Moreover,*

$$a_{H,i}(\mu, \mu) = (K^{-1}\mathbf{u}_h^*(\mu), \mathbf{u}_h^*(\mu))_{\Omega_i} \ge 0. \tag{6.6}$$

The substructuring domain decomposition algorithm described in Chapter 5 is used to solve the linear system of equations resulting from (6.2)–(6.4) very efficiently in parallel. It solves the mortar interface problem (6.5) using the CG method with balancing preconditioner. See Chapter 5 for more details.

6.1.2 Equivalent formulation

Here we present an equivalent formulation which is useful in the analysis. Define the space of weakly continuous velocities to be

$$\mathbf{V}_h^0 = \left\{ \mathbf{v} \in \mathbf{V}_h : \sum_{i=1}^n \langle \mathbf{v}|_{\Omega_i} \cdot \nu_i, \mu \rangle_{\Gamma_i} = 0, \quad \forall \mu \in M_H \right\}.$$

We note that we can eliminate λ_H from the mixed method (6.2)–(6.4) by restricting $\mathbf{V}_h$ to $\mathbf{V}_h^0$; that is, the problem is equivalent to finding $\mathbf{u}_h \in \mathbf{V}_h^0$ and $p_h \in W_h$ such that

$$(K^{-1}\mathbf{u}_h, \mathbf{v}) = \sum_{i=1}^n (p_h, \nabla \cdot \mathbf{v})_{\Omega_i} - \langle g, \mathbf{v} \cdot \nu \rangle_{\partial\Omega}, \quad \mathbf{v} \in \mathbf{V}_h^0, \tag{6.7}$$

$$\sum_{i=1}^n (\nabla \cdot \mathbf{u}_h, w)_{\Omega_i} = (f, w), \qquad w \in W_h. \tag{6.8}$$

To analyze (6.7)–(6.8) one needs to establish approximation properties for $\mathbf{V}_h^0$:

Lemma 6.2. *Under hypothesis (6.1), there exists a projection operator* $\Pi_0 : H^{1/2+\varepsilon}(\Omega) \cap \mathbf{V} \to \mathbf{V}_h^0$ *such that*

$$(\nabla \cdot (\Pi_0 \mathbf{q} - \mathbf{q}), w)_\Omega = 0, \quad w \in W_h, \tag{6.9}$$

and

$$\|\Pi_0 \mathbf{q} - \Pi \mathbf{q}\| \le C \sum_{i=1}^n \|\mathbf{q}\|_{r+1/2,\Omega_i} h^r H^{1/2}, \qquad 0 \le r \le k+1, \tag{6.10}$$

$$\|\Pi_0 \mathbf{q} - \mathbf{q}\| \le C \sum_{i=1}^n (\|\mathbf{q}\|_{r,\Omega_i} h^r + \|\mathbf{q}\|_{r+1/2,\Omega_i} h^r H^{1/2}), \quad 1 \le r \le k+1, \tag{6.11}$$

$$\|\Pi_0 \mathbf{q} - \mathbf{q}\| \le C \sum_{i=1}^n \|\mathbf{q}\|_{r,\Omega_i} h^{r-1/2} H^{1/2}, \qquad 1 \le r \le k+1. \tag{6.12}$$

The proof of this lemma can be found in [9, §3], with a straightforward modification of the argument for the two scales h and H. It is now easy to prove solvability of our method.

Lemma 6.3. *If (6.1) holds, then there exists a unique solution of (6.2)–(6.4).*

The proof of this lemma can be found in [11, §3].

6.2 *A PRIORI* ERROR ESTIMATES

The proofs of the theorems presented in Sections 6.2 and 6.3 can be found in [11].

Subtracting (6.7)–(6.8) from (2.22)–(2.23) gives the following equations for the error (recall that $\lambda = p$):

$$(K^{-1}(\mathbf{u}-\mathbf{u}_h),\mathbf{v}) = \sum_{i=1}^{n}((p-p_h,\nabla\cdot\mathbf{v})_{\Omega_i} - \langle p,\mathbf{v}\cdot\nu_i\rangle_{\Gamma_i}), \quad \mathbf{v}\in\mathbf{V}_h^0, \tag{6.13}$$

$$\sum_{i=1}^{n}(\nabla\cdot(\mathbf{u}-\mathbf{u}_h),w)_{\Omega_i} = 0, \qquad w\in W_h. \tag{6.14}$$

6.2.1 *A priori* estimates for the velocity

Theorem 6.1. *For the velocity* $\mathbf{u}_h$ *of the mixed method* (6.2)–(6.4)*, if* (6.1) *holds, then there exists a positive constant* C*, independent of* h *and* H*, such that*

$$\|\nabla\cdot(\mathbf{u}-\mathbf{u}_h)\| \le C\sum_{i=1}^{n}\|\nabla\cdot\mathbf{u}\|_{r,\Omega_i}h^r, \quad 0\le r\le l+1, \tag{6.15}$$

$$\|\mathbf{u}-\mathbf{u}_h\| \le C\sum_{i=1}^{n}(\|p\|_{s+1/2,\Omega_i}H^{s-1/2} + \|\mathbf{u}\|_{r,\Omega_i}h^r \tag{6.16}$$

$$+ \|\mathbf{u}\|_{r+1/2,\Omega_i}h^rH^{1/2}), \quad 1\le r\le k+1,\ 0<s\le m+1.$$

Remark 6.1. A straightforward modification of the argument in [9, §4] produces error estimates for $\|\mathbf{u}-\mathbf{u}_h\|$ of order $\mathcal{O}(H^sh^{-1/2}+h^r)$, which at its limits is $\mathcal{O}(H^{m+1}h^{-1/2}+h^{k+1})$. This is asymptotically undesirable as $h\to 0$. In our improved estimate, we obtain a balancing of the terms in (6.16) when $H=\mathcal{O}(h^{r/(s-1/2)})$, which at its limits is $H=\mathcal{O}(h^{(k+1)/(m+1/2)})$. For the lowest order Raviart-Thomas-Nedelec space RTN_0 [60, 57], $k=l=0$ and so if, say, $m=2$, then we should take the asymptotic scaling $H=\mathcal{O}(h^{2/5})$, which maintains the optimal convergence rate $\mathcal{O}(h)$.

If we restrict to the case of diagonal tensor K and Raviart-Thomas-Nedelec (RTN) spaces [60, 57] on rectangular grids, we can obtain superconvergence of the velocity at certain discrete points. For a function ψ and a (say 3-D) rectangular element E, let $|||\psi|||^2_{i,E}$ denote the approximate integral of $|\psi|^2$ using exact integration in x_i and the $k+1$ point Gauss rule in the other directions. Then let

$$|||\mathbf{q}|||^2 = \sum_{i=1}^{3} \sum_{E \in \mathcal{T}_h} |||q_i|||^2_{i,E}, \tag{6.17}$$

and note that if $\mathbf{v} \in \mathbf{V}_h$, then $|||\mathbf{v}||| = \|\mathbf{v}\|_\Omega$.

Theorem 6.2. *Assume that the tensor K is diagonal and the mixed finite element spaces are* RTN *on rectangular grids. For the velocity $\mathbf{u}_h$ of the mixed method (6.2)–(6.4), if (6.1) holds, then there exists a positive constant C, independent of h and H, such that*

$$|||\mathbf{u} - \mathbf{u}_h||| \leq C \sum_{i=1}^{n} (\|p\|_{s+1/2,\Omega_i} H^{s-1/2} + \|\mathbf{u}\|_{r+1/2,\Omega_i} h^r H^{1/2}), \tag{6.18}$$

where $1/2 \leq r \leq k+1$, $0 < s \leq m+1$.

Remark 6.2. For RTN_0 ($k = l = 0$), the terms in (6.18) are balanced if $H = \mathcal{O}(h^{1/m})$, giving the superconvergence error $\mathcal{O}(h^{1+1/(2m)})$. For $m = 2$, this is $H = \mathcal{O}(h^{1/2})$, which differs slightly from the optimal choice $\mathcal{O}(h^{2/5})$ from the Remark 6.1.

6.2.2 *A priori* estimates for the pressure

Theorem 6.3. *Assume full H^2-regularity of the problem on Ω. For the pressure p_h of the mixed method (6.2)–(6.4), if (6.1) holds, then there exists a positive constant C, independent of h and H, such that*

$$\begin{aligned} \|\hat{p} - p_h\| \leq C \sum_{i=1}^{n} (&\|p\|_{s+1/2,\Omega_i} H^{s+1/2} + \|\nabla \cdot \mathbf{u}\|_{t,\Omega_i} h^t H \\ &+ \|\mathbf{u}\|_{r,\Omega_i} h^r H + \|\mathbf{u}\|_{r+1/2,\Omega_i} h^r H^{3/2}), \end{aligned} \tag{6.19}$$

$$\|p - p_h\| \leq C \sum_{i=1}^{n} \|p\|_{t,\Omega_i} h^t + \|\hat{p} - p_h\|, \tag{6.20}$$

where $1 \leq r \leq k+1$, $0 < s \leq m+1$, and $0 \leq t \leq l+1$.

Remark 6.3. Again, a straightforward modification of the argument in [9] produces an undesirable superconvergence error estimate of order $\mathcal{O}(H^{m+2}h^{-1/2}+H^{3/2}h^{k+1/2}+h^{l+2})$ instead of $\mathcal{O}(H^{m+3/2}+H(h^{l+1}+h^{k+1}))$. A balancing of the terms in (6.19) implies for spaces with $l=k$ that $H=\mathcal{O}(h^{(k+1)/(m+1/2)})$, which gives superconvergence of order $\mathcal{O}(h^{(k+1)(m+3/2)/(m+1/2)})$. For $k=0$ and $m=2$, we should take the asymptotic scaling $H=\mathcal{O}(h^{2/5})$, which gives $\mathcal{O}(h^{7/5})$. If $H=\mathcal{O}(h^{1/m})$, as in Remark 6.2, then we expect an error of $\mathcal{O}(h^{1+1/m})$ when $k=l=0$.

6.2.3 *A priori* estimates for the mortar pressure

Let $\|\cdot\|_{a_H}$ be the semi-norm induced by $a_H(\cdot,\cdot)$ on $L^2(\Gamma)$, which is

$$\|\mu\|_{a_H}=a_H(\mu,\mu)^{1/2},\quad \mu\in L^2(\Gamma).$$

Theorem 6.4. *For the mortar pressure λ_H of the mixed method (6.2)–(6.4), if (6.1) holds, then there exists a positive constant C, independent of h and H, such that*

$$\|p-\lambda_H\|_{a_H}\le C\left(\sum_{i=1}^{n}(\|p\|_{r+1,\Omega_i}+\|\mathbf{u}\|_{r,\Omega_i})h^r+\|\mathbf{u}-\mathbf{u}_h\|\right),\quad 1\le r\le k+1. \tag{6.21}$$

In the case of diagonal tensor K and RTN *spaces on rectangular type grids,*

$$\|p-\lambda_H\|_{a_H}\le C\left(\sum_{i=1}^{n}\|\mathbf{u}\|_{r+1,\Omega_i}h^{r+1}+|||\mathbf{u}-\mathbf{u}_h|||\right),\quad 0\le r\le k+1. \tag{6.22}$$

6.3 *A POSTERIORI* ESTIMATES

We next present several *a posteriori* error bounds, which depend only on the input data and the computed solution. The error estimators are utilized in an adaptive mesh refinement procedure to obtain the numerical solution on appropriate subdomain and mortar grids in the next section (see §6.5).

In this section we assume full H^2-regularity of the problem (2.1)–(2.3). We want to derive *a posteriori* estimates of the error functions

$$\xi=\mathbf{u}-\mathbf{u}_h,\quad \eta=p-p_h,\quad \text{and}\quad \delta=\lambda-\lambda_H. \tag{6.23}$$

6.3.1 Some saturation assumptions

In the case of RTN_0 ($k = 0$) rectangular elements with linear mortars it was shown in Chapter 5 (see (5.14) and the proof of Lemma 5.5) that

$$\sum_{\tau \in \mathcal{T}^{\Gamma,H}} \|\mu\|^2_{1/2,\tau} \leq C a_H(\mu,\mu), \quad \mu \in M_H. \tag{6.24}$$

The proof can be generalized in a relatively straightforward way to the other mixed finite element spaces under consideration and to higher order elements. One such generalization is given in Section 6.4

The *a priori* error bounds from Theorems 6.1 and 6.4 motivate the following assumption on the mortar error.

Saturation Assumption 6.1. *There exist a constant C such that*

$$|||\lambda - \lambda_H||| := \left(\sum_{\tau \in \mathcal{T}^{\Gamma,H}} \sum_{E \in E_\tau} h_E^{-1} \|\lambda - \lambda_H\|^2_{\partial E \cap \tau} \right)^{1/2} \leq C \|\mathbf{u} - \mathbf{u}_h\|. \tag{6.25}$$

For additional justification of (6.25), see Section 4.2.

Let $\mathbf{V}_h'$, W_h', and M_H' be the finite element spaces of index one higher (i.e., of approximation order one more) than $\mathbf{V}_h$, W_h, and M_H, respectively. Let $\mathbf{u}_h' \in \mathbf{V}_h'$, $p_h' \in W_h'$, and $\lambda_H' \in M_H'$ be the multiscale mortar mixed finite element solution in these higher-order spaces (see (6.2)–(6.4)). The *a priori* error estimates from Theorems 6.1 and 6.3 motivate the following assumption.

Saturation Assumption 6.2. *There exist constants $\beta < 1$, $\beta_{\mathrm{div}} < 1$, and $C < \infty$ such that*

$$\|\mathbf{u} - \mathbf{u}_h'\| \leq \beta \|\mathbf{u} - \mathbf{u}_h\|, \tag{6.26}$$

$$\|\nabla \cdot (\mathbf{u} - \mathbf{u}_h')\| \leq \beta_{\mathrm{div}} \|\nabla \cdot (\mathbf{u} - \mathbf{u}_h)\|, \tag{6.27}$$

$$\|p - p_h'\| \leq \beta_p \|p - p_h\|. \tag{6.28}$$

It is a common practice to include saturation assumptions in the literature dealing with *a posteriori* results. They simply state that *a priori* error bounds in Theorems 6.1, 6.3, and 6.4 are asymptotically close to the true error, and that the mesh sizes h and H are small enough so that the higher order approximation leads to more accurate solution than the lower order approximation.

6.3.2 Explicit residual-based estimators

We proceed in this subsection with the presentation of explicit residual-based upper and lower bounds on the error.

6.3.2.1 Upper bounds Denote, for all $E \in \mathcal{T}_h$, $\tau \in \mathcal{T}^{\Gamma,H}$,

$$\omega_E^2 = \|K^{-1}\mathbf{u}_h + \nabla p_h\|_E^2 h_E^2 + \|f - \nabla \cdot \mathbf{u}_h\|_E^2 h_E^2 + \|\lambda_H - p_h\|_{\partial E \cap \Gamma}^2 h_E, \tag{6.29}$$

$$\omega_\tau^2 = \sum_{E \in E_\tau} \|[\mathbf{u}_h \cdot \nu]\|_{\partial E \cap \tau}^2 H_\tau^3. \tag{6.30}$$

We have an upper bound on the pressure error η.

Theorem 6.5. *There exists a constant C, independent of h and H, such that*

$$\|\eta\|^2 \leq C \left(\sum_{E \in \mathcal{T}_h} \omega_E^2 + \sum_{\tau \in \mathcal{T}^{\Gamma,H}} \omega_\tau^2 + \sum_{e \in \mathcal{T}_{h|\partial\Omega}} \|g - \mathcal{Q}_h g\|_e^2 h_e \right). \tag{6.31}$$

Remark 6.4. Due to the approximation property (2.19) of $\mathcal{Q}_h$, the last term in the bound of Theorem 6.5 is of higher order than the other terms. Therefore its effect becomes negligible for small h.

The bound on ξ is expressed in terms of $h_E^{-1}\omega_E$ and $H_\tau^{-1}\omega_\tau$.

Theorem 6.6. *Assume that the saturation assumptions (6.25), (6.26), and (6.28) hold. Then there exist a constant C, independent of β, h, and H, such that*

$$\|\xi\|_{H(\mathrm{div};\Omega)}^2 \leq \frac{C}{(1-\beta)^2} \left(\sum_{E \in \mathcal{T}_h} h_E^{-2}\omega_E^2 + \sum_{\tau \in \mathcal{T}^{\Gamma,H}} H_\tau^{-2}\omega_\tau^2 + \sum_{e \in \mathcal{T}_{h|\partial\Omega}} \|g - \mathcal{Q}_h g\|_e^2 h_e^{-1} \right).$$

6.3.2.2 Lower bounds Next, we establish lower bounds on the error, which indicate that the residual error estimators can be used effectively in an adaptive mesh refinement algorithm.

Theorem 6.7. *There exists a constant C, independent of h and H, such that*

$$\sum_{E\in\mathcal{T}_h}\omega_E^2+\sum_{\tau\in\mathcal{T}^{\Gamma,H}}\omega_\tau^2\le C\left(\|\eta\|^2+\sum_{E\in\mathcal{T}_h}h_E^2\|\xi\|^2_{H(\mathrm{div};E)}+\sum_{E\in\mathcal{T}_h}h_E\|\delta\|^2_{\partial E\cap\Gamma}\right.\\ \left.+\sum_{\tau\in\mathcal{T}^{\Gamma,H}}\sum_{E\in E_\tau}h_E^{-1}H_\tau^3\|\xi\|^2_{H(\mathrm{div};E)}\right). \tag{6.32}$$

Moreover, the following local bounds hold for any $E\in\mathcal{T}_h$, $e\in\partial E$, and $\tau\in\mathcal{T}^{\Gamma,H}$:

$$\|K^{-1}\mathbf{u}_h+\nabla p_h\|_E^2h_E^2+\|f-\nabla\cdot\mathbf{u}_h\|_E^2h_E^2\le C(\|\eta\|_E^2+\|\xi\|^2_{H(\mathrm{div};E)}h_E^2), \tag{6.33}$$

$$\sum_{E\in E_\tau}\|[\mathbf{u}_h\cdot\nu]\|^2_{\partial E\cap\tau}H_\tau^3\le C\sum_{E\in E_\tau}h_E^{-1}H_\tau^3\|\xi\|^2_{H(\mathrm{div};E)}, \tag{6.34}$$

$$\|\lambda_H-p_h\|_e^2h_E\le C(\|\eta\|_E^2+\|\xi\|^2_{H(\mathrm{div};E)}h_E^2+\|\delta\|_e^2h_E). \tag{6.35}$$

Remark 6.5. Generally, the terms after $\|\eta\|^2$ in (6.32) are of higher order. From Remarks 6.1 and 6.3, when $l=k$, the choice $H=\mathcal{O}(h^{(k+1)/(m+1/2)})$ gives optimal *a priori* errors of order $\mathcal{O}(h^{k+1})$ for p in L^2 and $\mathbf{u}$ in $H(\mathrm{div};\Omega)$, as well as for the mortar $\lambda=p$ in the a_H-norm (which bounds the L^2-norm). Thus for C_1 and C_2 independent of h,

$$C_1\left(\sum_{E\in\mathcal{T}_h}\omega_E^2+\sum_{\tau\in\mathcal{T}^{\Gamma,H}}\omega_\tau^2+\mathcal{O}(h^{2(k+1)+\alpha})\right)\\ \le\|\eta\|^2\le C_2\left(\sum_{E\in\mathcal{T}_h}\omega_E^2+\sum_{\tau\in\mathcal{T}^{\Gamma,H}}\omega_\tau^2+\mathcal{O}(h^{2(k+1)+1})\right), \tag{6.36}$$

where $\alpha=\min(1,3(k+1)/(m+1/2)-1)$. In the case of RTN_0 ($k=0$) and quadratic mortars ($m=2$), the optimal choice is $H=\mathcal{O}(h^{2/5})$, and $\alpha=1/5>0$. Similarly, for linear mortars ($m=1$) with $H=\mathcal{O}(h^{2/3})$, $\alpha=1>0$. Whenever $\alpha>0$, the error in $\|\eta\|^2$ is dominated above and below by our local residual estimators $\sum_{E\in\mathcal{T}_h}\omega_E^2+\sum_{\tau\in\mathcal{T}^{\Gamma,H}}\omega_\tau^2$ for small enough h, up to C_1 and C_2, and so this quantity is an efficient and reliable indicator of the pressure error.

6.3.3 Error estimators based on solving local problems

In this subsection we present an implicit error estimator which requires solving local (element) boundary value problems. These problems approximate the local residual equations satisfied by the true error. The motivation for considering implicit estimators comes from the unknown generic constants that appear in the explicit estimators. We show that the implicit estimator provides both optimal upper and lower bounds for the velocity error.

6.3.3.1 Global approximation to the error Following the approach in [73], we first construct a global approximation to the error based on higher order finite element spaces. For $\mathbf{v} \in \mathbf{V}_i$, let

$$r(\mathbf{v}) = -\langle g, \mathbf{v} \cdot \nu \rangle_{\partial\Omega_i \setminus \Gamma} - (K^{-1}\mathbf{u}_h, \mathbf{v})_{\Omega_i} + (p_h, \nabla \cdot \mathbf{v})_{\Omega_i} - \langle \lambda_H, \mathbf{v} \cdot \nu_i \rangle_{\Gamma_i}. \tag{6.37}$$

Using (2.22)–(2.24), the true error satisfies the residual equations

$$(K^{-1}\xi, \mathbf{v})_{\Omega_i} - (\eta, \nabla \cdot \mathbf{v})_{\Omega_i} + \langle \delta, \mathbf{v} \cdot \nu_i \rangle_{\Gamma_i} = r(\mathbf{v}), \quad \mathbf{v} \in \mathbf{V}_i, \tag{6.38}$$

$$(\nabla \cdot \xi, w)_{\Omega_i} = (f - \nabla \cdot \mathbf{u}_h, w)_{\Omega_i}, \qquad w \in W_i, \tag{6.39}$$

$$\sum_{i=1}^{n} \langle \xi \cdot \nu_i, \mu \rangle_{\Gamma_i} = -\sum_{i=1}^{n} \langle \mathbf{u}_h \cdot \nu_i, \mu \rangle_{\Gamma_i}, \qquad \mu \in M. \tag{6.40}$$

Recall from Subsection 6.3.1 that $\mathbf{V}_h' \times W_h' \times M_H'$ is the mortar mixed finite element space of index order one higher than $\mathbf{V}_h \times W_h \times M_H$. Let

$$\xi' = \mathbf{u}_h' - \mathbf{u}_h, \quad \eta' = p_h' - p_h, \quad \text{and} \quad \delta' = \lambda_H' - \lambda_H. \tag{6.41}$$

Then $(\xi', \eta', \delta') \in \mathbf{V}_h' \times W_h' \times M_H'$ is the finite element approximation to (ξ, η, δ) satisfying

$$(K^{-1}\xi', \mathbf{v})_{\Omega_i} - (\eta', \nabla \cdot \mathbf{v})_{\Omega_i} + \langle \delta', \mathbf{v} \cdot \nu_i \rangle_{\Gamma_i} = r(\mathbf{v}), \quad \mathbf{v} \in \mathbf{V}_{h,i}', \tag{6.42}$$

$$(\nabla \cdot \xi', w)_{\Omega_i} = (f - \nabla \cdot \mathbf{u}_h, w)_{\Omega_i}, \qquad w \in W_{h,i}', \tag{6.43}$$

$$\sum_{i=1}^{n} \langle \xi' \cdot \nu_i, \mu \rangle_{\Gamma_i} = -\sum_{i=1}^{n} \langle \mathbf{u}_h \cdot \nu_i, \mu \rangle_{\Gamma_i}, \qquad \mu \in M_H'. \tag{6.44}$$

The saturation assumptions (4.12) and (6.27) imply

$$\frac{1}{1+\beta}\|\xi'\| \leq \|\xi\| \leq \frac{1}{1-\beta}\|\xi'\|, \tag{6.45}$$

$$\frac{1}{1+\beta_{\text{div}}}\|\nabla\cdot\xi'\| \leq \|\nabla\cdot\xi\| \leq \frac{1}{1-\beta_{\text{div}}}\|\nabla\cdot\xi'\|, \tag{6.46}$$

so it is enough to estimate ξ', since we do not wish to compute $\mathbf{u}_h'$.

6.3.3.2 Local (element) approximation to the error For any $E \in \mathcal{T}_h$, the true error satisfies the local equations

$$(K^{-1}\xi, \mathbf{v})_E - (\eta, \nabla\cdot\mathbf{v})_E = r_E(\mathbf{v}) - \langle p, \mathbf{v}\cdot\nu_E\rangle_{\partial E}, \quad \mathbf{v} \in \mathbf{V}(E), \tag{6.47}$$

$$(\nabla\cdot\xi, w)_E = (f - \nabla\cdot\mathbf{u}_h, w)_E, \quad w \in W(E), \tag{6.48}$$

where

$$r_E(\mathbf{v}) = -(K^{-1}\mathbf{u}_h, \mathbf{v})_E + (p_h, \nabla\cdot\mathbf{v})_E. \tag{6.49}$$

We construct a higher order local approximation of the error by solving element sub-problems: Find $\psi' \in \mathbf{V}_h'(E)$ and $\theta' \in W_h'(E)$ such that

$$(K^{-1}\psi', \mathbf{v})_E - (\theta', \nabla\cdot\mathbf{v})_E = r_E(\mathbf{v}) - \langle p_A, \mathbf{v}\cdot\nu_E\rangle_{\partial E}, \quad \mathbf{v} \in \mathbf{V}_h'(E), \tag{6.50}$$

$$(\nabla\cdot\psi', w)_E = (f - \nabla\cdot\mathbf{u}_h, w)_E, \quad w \in W_h'(E). \tag{6.51}$$

where $p_A = g$ on $\partial\Omega$, $p_A = \lambda_H$ on $\partial E \cap \Gamma$, and $p_A = \tilde{p}_h$ on $\partial E \cap \mathcal{E}_h$, where $\tilde{p}_h \in \Lambda_h(\partial E) = \mathbf{V}_h(E)\cdot\nu$ is the Lagrange multiplier for $\mathbf{V}_h$ and W_h in the standard hybrid formulation of the mixed method [14, 26], which can be defined from $\mathbf{u}_h$ and p_h as

$$\langle \tilde{p}_h, \mathbf{v}\cdot\nu_E\rangle_{\partial E} = -(K^{-1}\mathbf{u}_h, \mathbf{v})_E + (p_h, \nabla\cdot\mathbf{v})_E, \quad \mathbf{v} \in \mathbf{V}_h(E). \tag{6.52}$$

Note that (6.2) implies that $\tilde{p}_h$ is single-valued on $\mathcal{E}_h$. Let $\tilde{p}'$ be the Lagrange multiplier for the higher order spaces $\mathbf{V}_h'$ and W_h' satisfying

$$\langle \tilde{p}', \mathbf{v}\cdot\nu_E\rangle_{\partial E} = -(K^{-1}\mathbf{u}_h', \mathbf{v})_E + (p_h', \nabla\cdot\mathbf{v})_E, \quad \mathbf{v} \in V_h'(E). \tag{6.53}$$

Again, $\tilde{p}'$ is single-valued on $\mathcal{E}_h$.

We need one last saturation assumption.

Saturation Assumption 6.3. *There exist a constant C such that*

$$\left(\sum_{e\in\mathcal{E}_h} h_e^{-1}\|\tilde{p}' - \tilde{p}_h\|_e^2\right)^{1/2} \leq C\|\mathbf{u}-\mathbf{u}_h\|. \tag{6.54}$$

The assumption (6.54) is motivated by the *a priori* error estimate for the Lagrange multiplier [26]

$$\left(\sum_{e\in\mathcal{E}_h} h_e^{-1}\|\bar{p} - \tilde{p}_h\|_e^2\right)^{1/2} \leq Ch^{k+1},$$

where $\bar{p}$ is the L^2-projection of p onto $\mathbf{V}_h\cdot\nu|_{\mathcal{E}_h}$.

Theorem 6.8. *If the saturation assumptions (6.25), (6.26), (6.27), and (6.54) hold, then there exist constants C_1 and C_2, independent of β and β_{div}, such that*

$$C_1\left[\|\psi'\|_{H(\text{div};\Omega)} + \left(\sum_{\tau\in\mathcal{T}^{\Gamma,H}}\sum_{E\in E_\tau}\|[\mathbf{u}_h\cdot\nu]\|^2_{\partial E\cap\tau}h_E\right)^{1/2}\right] \leq \|\xi\|_{H(\text{div};\Omega)} \tag{6.55}$$

$$\leq \frac{C_2}{(1-\beta_{max})^2}\left[\|\psi'\|_{H(\text{div};\Omega)} + \left(\sum_{\tau\in\mathcal{T}^{\Gamma,H}}\sum_{E\in E_\tau}\|[\mathbf{u}_h\cdot\nu]\|^2_{\partial E\cap\tau}h_E\right)^{1/2}\right],$$

where $\beta_{max} = \max\{\beta, \beta_{\text{div}}\}$.

6.4 EQUIVALENCE OF NORMS IN THE MULTISCALE CASE

In this section we prove equivalence of some norms for the case of multiscale mortar mixed finite element method. We will follow the notations from Section 5.4.

It is easy to see that for any $\lambda\in M_H$ and for any $\tau\in\mathcal{T}^{\Gamma,H}$

$$|\lambda|^2_{0,\tau} \simeq |\tau| \sum_{\substack{\text{nodes}\\ v_l\in\tau}} \lambda(v_l)^2, \tag{6.56}$$

$$|\lambda|^2_{1,\tau} \simeq |\tau|^{1-2/(d-1)} \sum_{\substack{\text{nodes}\\ v_l, v_k\in\tau}} (\lambda(v_l)-\lambda(v_k))^2. \tag{6.57}$$

Lemma 6.4. *Consider $d = 2$, RT_0 subdomain discretizations on rectangular grids, and discontinuous piecewise linear mortar spaces. Assume that the local and mortar grids are nested and the local grid is uniform, i.e., every element of $\mathcal{T}_{H,i,j}$ contains n elements ($n \geq 2$) of equal length of $\mathcal{T}_{h,i}|_{\Gamma_{i,j}}$ (see Figure 6.1). Then, for any $\lambda \in M_H$,*

$$\|\mathcal{I}^{\partial\Omega_i}\mathcal{Q}_{h,i}\lambda\|_{1/2,\Gamma_{i,j}} \simeq \|\lambda\|_{1/2,\Gamma_{i,j}}.$$

Proof. Fix an element τ of $\mathcal{T}_{H,i,j}$ and let it contain n elements, $e_1, \cdots, e_n$, of $\mathcal{T}_{h,i}|_{\Gamma_{i,j}}$. Denote the vertices of τ by v_1, v_2 with coordinates s_0, s_1, respectively, and the coordinates of the endpoints of $\{e_k\}|_{k=1}^n$ by $\{t_k\}|_{k=0}^n$ (see Figure 6.1). Let, for a given $\lambda \in M_H$,

$$\lambda(v_l) = \phi_l, \quad l = 1, 2, \qquad p_k = \mathcal{Q}_{h,i}\lambda|_{e_k}, \quad k = 1, \cdots, n.$$

Using arguments similar to the ones used in the proof of Lemma 5.5, we can exclude the values of $I^{\partial\Omega_i}\mathcal{Q}_{h,i}\lambda$ at the secondary vertices and consider in (6.56) and (6.57) only the primary vertices. For $p_k, k = 1, \cdots, n$ we obtain

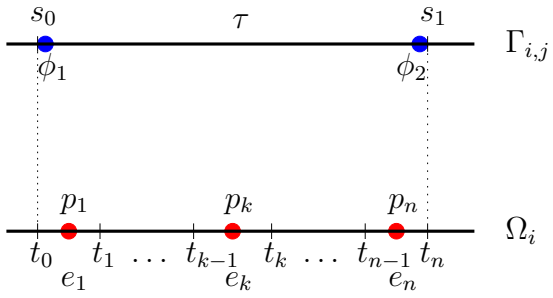

Figure 6.1: Grids on the linear mortar and neighboring subdomain along the interface $\Gamma_{i,j}$

$$p_k = \frac{1}{t_k - t_{k-1}} \int_{t_{k-1}}^{t_k} \lambda(s)\, ds.$$

Writing λ in terms of the basis functions and mapping the element τ to the reference element [0,1], we get (see command lines 1 and 2 in Figure A.1) the following system of equations

$$p_k = \left(\frac{1 - 2k + 2n}{2n}\right)\phi_1 + \left(\frac{-1 + 2k}{2n}\right)\phi_2 \equiv a_{k,1}\phi_1 + a_{k,2}\phi_2, \quad k = 1, \cdots, n. \tag{6.58}$$

Note that

$$a_{k,1} = a_{n+1-k,2}, \quad k = 1, \cdots, n.$$

Applying the inequality $(a+b)^2 \leq 2(a^2+b^2)$ results in

$$p_k^2 \leq 2\left(\frac{1-2k+2n}{2n}\right)^2 \phi_1^2 + 2\left(\frac{2k-1}{2n}\right)^2 \phi_2^2 \leq 2\phi_1^2 + 2\phi_2^2, \quad k = 1, \cdots, n. \tag{6.59}$$

Using (5.20), (6.59), and (6.56), we get

$$|\hat{p}|_{0,\tau}^2 = \sum_{k=1}^{n} |\hat{p}|_{0,e_k}^2 \simeq \sum_{k=1}^{n} h p_k^2 \leq 2hn(\phi_1^2 + \phi_2^2) = 2H(\phi_1^2 + \phi_2^2) \simeq |\lambda|_{0,\tau}^2 \tag{6.60}$$

Proving the other direction is more involved. We would like to express ϕ_1, ϕ_2 in terms of **all** $p_1, \cdots, p_n$. To do so, rewrite (6.58) in matrix form

$$A\vec{\phi} = \vec{p}, \quad \vec{\phi} = \begin{bmatrix} \phi_1 \\ \phi_2 \end{bmatrix}, \quad \vec{p} = \begin{bmatrix} p_1, \cdots, p_n \end{bmatrix}^T, \quad A = [a_{k,l}]_{n\times 2}. \tag{6.61}$$

The system (6.61) is overdetermined (if $n > 2$) and we solve the normal equations instead, i.e.,

$$B\vec{\phi} = \vec{c} \quad \text{with } B \equiv A^T A, \quad \vec{c} \equiv A^T \vec{p}. \tag{6.62}$$

Using Mathematica, we get the following expressions for the elements of B (see command line 4 in Figure A.1):

$$b_{1,1} = b_{2,2} = \sum_{k=1}^{n} a_{k,1}^2 = \frac{(2n+1)(2n-1)}{12n}, \quad b_{1,2} = b_{2,1} = \sum_{k=1}^{n} a_{k,1}a_{k,2} = \frac{1+2n^2}{12n}.$$

Solving (6.62) gives (see command lines 6 and 7 in Figure A.1)

$$\phi_l = \beta_{l,1}c_1 + \beta_{l,2}c_2 = \sum_{k=1}^{n} d_{k,l}p_k, \qquad l = 1, 2,$$

where

$$d_{k,1} = \beta_{1,1}a_{k,1} + \beta_{1,2}a_{k,2} = \frac{-1+3n-6kn+4n^2}{n(n-1)(n+1)},$$
$$d_{k,2} = \beta_{2,1}a_{k,1} + \beta_{2,2}a_{k,2} = -\frac{1+3n-6kn+2n^2}{n(n-1)(n+1)},$$
$$B^{-1} = \begin{bmatrix} \beta_{1,1}\beta_{1,2} \\ \beta_{2,1}\beta_{2,2} \end{bmatrix}.$$

Applying the discrete Cauchy-Schwartz inequality results in

$$\phi_l^2 \le \left(\sum_{k=1}^{n} d_{k,l}^2\right)\left(\sum_{k=1}^{n} p_k^2\right) = \frac{4n^2-1}{n^3-n}\left(\sum_{k=1}^{n} p_k^2\right) \le \frac{5}{n}\left(\sum_{k=1}^{n} p_k^2\right), \quad l = 1, 2,$$

where we used command lines 9 through 12 from Figure A.2. Then, using (6.56) and (5.20), we obtain

$$|\lambda|_{0,\tau}^2 \simeq H(\phi_1^2 + \phi_2^2) \le H\frac{10}{n}\left(\sum_{k=1}^{n} p_k^2\right) = 10\sum_{k=1}^{n} h p_k^2 \simeq |\hat{p}|_{0,\tau}^2. \tag{6.63}$$

Combination of (6.60) and (6.63) gives

$$|\mathcal{I}^{\partial\Omega_i}\mathcal{Q}_{h,i}\lambda|_{0,\Gamma_{i,j}} \simeq |\lambda|_{0,\Gamma_{i,j}}. \tag{6.64}$$

To prove similar connection between the H^1 semi-norms, we use (6.58) to obtain

$$p_k - p_{k+1} = \frac{1}{n}(\phi_1 - \phi_2), \qquad k = 1, \cdots, n-1.$$

After an application of (5.19) and (6.57), we get

$$|\hat{p}|_{1,\tau}^2 = \sum_{k=1}^{n} |\hat{p}|_{1,e_k}^2 \simeq \sum_{k=1}^{n-1} \frac{1}{h}(p_k - p_{k+1})^2 \simeq \frac{1}{H}(\phi_1 - \phi_2)^2 \simeq |\lambda|_{1,\tau}^2,$$

i.e.,

$$|\mathcal{I}^{\partial\Omega_i}\mathcal{Q}_{h,i}\lambda|_{1,\Gamma_{i,j}} \simeq |\lambda|_{1,\Gamma_{i,j}}. \tag{6.65}$$

The interpolation theory of Sobolev spaces [53] and bounds (6.64) and (6.65) imply the statement of the lemma. □

Next we prove a similar statement for quadratic mortar spaces.

Lemma 6.5. *Consider $d = 2$, RT_0 subdomain discretizations on rectangular grids, and discontinuous piecewise quadratic mortar spaces. Assume that the local and mortar grids are nested and the local grid is uniform, i.e., every element of $\mathcal{T}_{H,i,j}$ contains n elements ($n \ge 3$) of equal length of $\mathcal{T}_{h,i}|_{\Gamma_{i,j}}$ (see Figure 6.2). Then, for any $\lambda \in M_H$,*

$$\|\mathcal{I}^{\partial\Omega_i}\mathcal{Q}_{h,i}\lambda\|_{1/2,\Gamma_{i,j}} \simeq \|\lambda\|_{1/2,\Gamma_{i,j}}.$$

Proof. Fix an element τ of $\mathcal{T}_{H,i,j}$ and assume it contains n elements, $e_1, \cdots, e_n$, of $\mathcal{T}_{h,i}|_{\Gamma_{i,j}}$. Denote the vertices of τ by v_1, v_3 with coordinates s_0, s_1, respectively, and the midpoint of τ by v_2. Denote also the coordinates of the endpoints of $\{e_k\}|_{k=1}^n$ by $\{t_k\}|_{k=0}^n$ (see Figure 6.2). For a given $\lambda \in M_H$, let

$$\lambda(v_l) = \phi_l, \quad l = 1, 2, 3, \qquad p_k = \mathcal{Q}_{h,i}\lambda|_{e_k}, \quad k = 1, \cdots, n.$$

We write

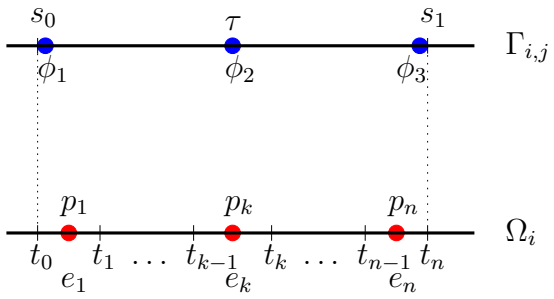

Figure 6.2: Grids on the quadratic mortar and neighboring subdomain along the interface $\Gamma_{i,j}$

$$\lambda(s) = \sum_{l=1}^{3} \phi_l \, f_l\left(\frac{s - s_0}{s_1 - s_0}\right)$$

where

$$f_1(x) = (1 - 2x)(1 - x), \quad f_2(x) = 4x(1 - x), \quad f_3(x) = x(2x - 1)$$

are the basis functions on the reference element [0,1]. Then, for p_k we obtain

$$p_k = \frac{1}{t_k - t_{k-1}} \int_{t_{k-1}}^{t_k} \lambda(s)\, ds \equiv a_{k,1}\phi_1 + a_{k,2}\phi_2 + a_{k,3}\phi_3, \quad k = 1, \cdots, n, \tag{6.66}$$

where (see command lines 1 through 3 in Figure A.3)

$$a_{k,1} = \frac{4 + 12k^2 + 9n + 6n^2 - 6k(2 + 3n)}{6n^2}, \tag{6.67}$$

$$a_{k,2} = -\frac{2(2 + 6k^2 + 3n - 6k(1 + n))}{3n^2}, \tag{6.68}$$

$$a_{k,3} = \frac{4 + 12k^2 + 3n - 6k(2 + n)}{6n^2}. \tag{6.69}$$

Note that

$$a_{k,1} = a_{n+1-k,3} \quad \text{and} \quad a_{k,2} = a_{n+1-k,2}, \quad k = 1, \cdots, n.$$

It is easy to see that $|a_{k,l}| \le 1$ and $|a_{k,1}| + |a_{k,2}| + |a_{k,3}| \le \frac{5}{4}$, $k = 1, \cdots, n, l = 1, 2, 3$, so that we get

$$p_k^2 \le \frac{5}{4} \sum_{l=1}^{3} \phi_l^2. \tag{6.70}$$

Using (5.20), (6.70), and (6.56), we obtain

$$|\hat{p}|_{0,\tau}^2 \simeq \sum_{k=1}^{n} h p_k^2 \le \frac{5}{4} hn \sum_{l=1}^{3} \phi_l^2 = \frac{5}{4} H \sum_{l=1}^{3} \phi_l^2 \simeq |\lambda|_{0,\tau}^2. \tag{6.71}$$

Next, we want to express ϕ_1, ϕ_2, ϕ_3 in terms of **all** $p_1, \cdots, p_n$. Rewrite (6.66) in matrix form

$$A\vec{\phi} = \vec{p}, \quad \vec{\phi} = \begin{bmatrix} \phi_1 \\ \phi_2 \\ \phi_3 \end{bmatrix}, \quad \vec{p} = \begin{bmatrix} p_1, \cdots, p_n \end{bmatrix}^T, \quad A = [a_{k,l}]_{n \times 3}.$$

Form the normal equations for this overdetermined (if $n > 3$) system,

$$B\vec{\phi} = \vec{c} \quad \text{with } B \equiv A^T A, \quad \vec{c} \equiv A^T \vec{p}. \tag{6.72}$$

We obtain for the elements of B (see command line 5 in Figure A.3):

$$b_{1,1} = b_{3,3} = \sum_{k=1}^{n} a_{k,1}^2 = \frac{16 - 35n^2 + 24n^4}{180n^3}, \quad b_{2,2} = \sum_{k=1}^{n} a_{k,2}^2 = \frac{4(4 - 5n^2 + 6n^4)}{45n^3}$$

$$b_{1,2} = b_{2,1} = b_{3,2} = b_{2,3} = \sum_{k=1}^{n} a_{k,1} a_{k,2} = \frac{(4 + n^2)(-2 + 3n^2)}{45n^3},$$

$$b_{1,3} = b_{3,1} = \sum_{k=1}^{n} a_{k,1} a_{k,3} = -\frac{-16 + 5n^2 + 6n^4}{180n^3}.$$

The solution of (6.72) can be written as a linear combination of $\{p_k\}|_{k=1}^n$,

$$\phi_l = \sum_{m=1}^{3} \beta_{l,m} c_m = \sum_{k=1}^{n} d_{k,l} p_k, \qquad l = 1, 2, 3,$$

with

$$d_{k,l} = \sum_{m=1}^{3} \beta_{l,m} a_{k,m}, \quad B^{-1} = [\beta_{k,l}]_{3 \times 3}.$$

For the values of $d_{k,l}, k = 1, \cdots, n, l = 1, 2, 3$, we get (see command lines 7 and 8 in Figure A.4)

$$\begin{aligned} d_{k,1} &= \frac{4 - 12n + 24kn - 7n^2 - 30kn^2 + 30k^2n^2 + 18n^3 - 36kn^3 + 9n^4}{n(n-1)(n+1)(n-2)(n+2)} \\ d_{k,2} &= -\frac{-8 + 20n^2 - 30kn^2 + 30k^2n^2 + 15n^3 - 30kn^3 + 3n^4}{n(n-1)(n+1)(n-2)(n+2)} \\ d_{k,3} &= \frac{4 + 12n - 24kn + 17n^2 - 30kn^2 + 30k^2n^2 + 12n^3 - 24kn^3 + 3n^4}{n(n-1)(n+1)(n-2)(n+2)}. \end{aligned}$$

An application of the discrete Cauchy-Schwartz inequality leads to

$$\phi_l^2 \leq \left(\sum_{k=1}^{n} d_{k,l}^2\right)\left(\sum_{k=1}^{n} p_k^2\right) \equiv e_l \left(\sum_{k=1}^{n} p_k^2\right), \quad l = 1, 2, 3.$$

A simple calculation gives (see command lines 10 through 15 in Figures A.5 and A.6)

$$e_1 = e_3 = \frac{4 - 17n^2 + 9n^4}{4n - 5n^3 + n^5} \leq \frac{14.5}{n}, \quad e_2 = \frac{16 - 20n^2 + 9n^4}{4(4n - 5n^3 + n^5)} \leq \frac{4}{n}.$$

Using (6.56) and (5.20), we get

$$|\lambda|_{0,\tau}^2 \simeq H\left(\sum_{l=1}^{3} \phi_l^2\right) \leq H\frac{33}{n}\left(\sum_{k=1}^{n} p_k^2\right) = 33\sum_{k=1}^{n} h p_k^2 \simeq |\hat{p}|_{0,\tau}^2. \tag{6.73}$$

Combining (6.71) and (6.73) gives

$$|\mathcal{I}^{\partial\Omega_i}\mathcal{Q}_{h,i}\lambda|_{0,\Gamma_{i,j}} \simeq |\lambda|_{0,\Gamma_{i,j}}. \tag{6.74}$$

To prove equivalence of the H^1 semi-norms, we use (6.66)–(6.69) to obtain (see command lines 16 through 18 in Figure A.6)

$$p_k - p_{k+1} = r_{k,1}(\phi_1 - \phi_2) + r_{k,2}(\phi_2 - \phi_3), \qquad k = 1, \cdots, n-1, \tag{6.75}$$

where

$$r_{k,1} = \frac{3n - 4k}{n^2}, \quad r_{k,2} = \frac{4k - n}{n^2}, \qquad k = 1, \cdots, n-1.$$

Applying the inequality $(a+b)^2 \leq 2(a^2 + b^2)$ and using that $|r_{k,l}| \leq \frac{3}{n}$, we get

$$(p_k - p_{k+1})^2 \leq \frac{18}{n^2}\left((\phi_1 - \phi_2)^2 + (\phi_2 - \phi_3)^2\right), \qquad k = 1, \cdots, n-1.$$

Then, using (5.19) and (6.57), we obtain

$$|\hat{p}|_{1,\tau}^2 \simeq \sum_{k=1}^{n-1} \frac{1}{h}(p_k - p_{k+1})^2 \leq \frac{18}{nh}\left((\phi_1 - \phi_2)^2 + (\phi_2 - \phi_3)^2\right) \simeq |\lambda|_{1,\tau}^2. \tag{6.76}$$

For a similar inequality in the other direction, we write equations (6.75) in matrix form

$$R\vec{\delta} = \vec{\Delta}, \quad \vec{\delta} = \begin{bmatrix} \phi_1 - \phi_2 \\ \phi_2 - \phi_3 \end{bmatrix}, \quad \vec{\Delta} = \begin{bmatrix} p_1 - p_2, \cdots, p_{n-1} - p_n \end{bmatrix}^T, \quad R = [r_{k,l}]_{(n-1)\times 2}.$$

Again, we solve the normal equations

$$S\vec{\delta} = \vec{q} \quad \text{with } S \equiv R^T R, \quad \vec{q} \equiv R^T \vec{\Delta}. \tag{6.77}$$

The matrix S has elements (see command line 19 in Figure A.6)

$$s_{1,1} = s_{2,2} = \sum_{k=1}^{n-1} r_{k,1}^2 = \frac{(n-1)(7n-8)}{3n^3}, \quad s_{1,2} = s_{2,1} = \sum_{k=1}^{n-1} r_{k,1} r_{k,2} = \frac{(n-1)(8-n)}{3n^3}.$$

Solving (6.77) gives (see command lines 22 and 23 in Figure A.6)

$$\phi_l - \phi_{l+1} = \gamma_{l,1} q_1 + \gamma_{l,2} q_2 = \sum_{k=1}^{n-1} t_{k,l}(p_k - p_{k+1}), \qquad l = 1, 2,$$

where

$$\begin{aligned} t_{k,1} &= \gamma_{1,1} r_{k,1} + \gamma_{1,2} r_{k,2} = \frac{n(5n - 6k - 4)}{4(n-1)(n-2)}, \\ t_{k,2} &= \gamma_{2,1} r_{k,1} + \gamma_{2,2} r_{k,2} = \frac{n(-n + 6k - 4)}{4(n-1)(n-2)}, \\ S^{-1} &= [\gamma_{k,l}]_{2\times 2}. \end{aligned}$$

Next, we apply the discrete Cauchy-Schwartz inequality and use command lines 24 through 27 in Figure A.7 to get

$$\begin{aligned} (\phi_l - \phi_{l+1})^2 &\leq \left(\sum_{k=1}^{n-1} t_{k,l}^2\right)\left(\sum_{k=1}^{n-1}(p_k - p_{k+1})^2\right) = \frac{n^2(7n-8)}{16(n-1)(n-2)} \sum_{k=1}^{n-1}(p_k - p_{k+1})^2 \\ &\leq 1.5n \sum_{k=1}^{n-1}(p_k - p_{k+1})^2, \qquad l = 1, 2. \end{aligned}$$

Then, we use (6.57) and (5.19) to obtain

$$|\lambda|^2_{1,\tau} \simeq \frac{1}{H}\left((\phi_1-\phi_2)^2+(\phi_2-\phi_3)^2+(\phi_1-\phi_3)^2\right) \leq \frac{3}{H}\left((\phi_1-\phi_2)^2+(\phi_2-\phi_3)^2\right)$$
$$\leq \frac{9}{h}\sum_{k=1}^{n-1}(p_k-p_{k+1})^2 \simeq |\hat{p}|^2_{1,\tau} \tag{6.78}$$

Combination of (6.76) and (6.78) gives

$$|\mathcal{I}^{\partial\Omega_i}\mathcal{Q}_{h,i}\lambda|_{1,\Gamma_{i,j}} \simeq |\lambda|_{1,\Gamma_{i,j}}. \tag{6.79}$$

The interpolation theory of Sobolev spaces [53] and bounds (6.74) and (6.79) imply the statement of the lemma. □

Remark 6.6. *The proofs of the above two lemmas are also valid in the case of continuous piecewise mortars.*

Under the the assumptions on the grids in Lemmas 6.4 or 6.5, and using (5.14), we can conclude that the assumption (6.1) holds.

6.5 NUMERICAL SIMULATIONS

In this section we present several numerical tests confirming the theoretical convergence rates and illustrating the behavior of the method. The examples are on the unit square (cube for Example 6.3), and use the lowest order Raviart-Thomas-Nedelec spaces [60, 57], RTN_0, on rectangles (for which $k = l = 0$). The boundary conditions are Dirichlet on the left and right edges and Neumann on the rest of the boundary. Unless otherwise noted, the domain is divided into four (eight for Example 6.3) subdomains with interfaces along the $x = 1/2$ and $y = 1/2$ (and $z = 1/2$ for Example 6.3) lines.

We employ the non-overlapping domain decomposition algorithm from Section 6.1.1 for the solution of the algebraic problem. In particular, we employ the CG method for solving the symmetric and positive definite interface coarse scale mortar problem (5.8), which results from the multiscale algebraic system. The balancing preconditioner of Chapter 5 is used for accelerating the convergence of the CG iteration. As a result both the condition number

of the interface problem and the number of interface iterations grow only very slowly when increasing the dimension of the mortar problem, either through refining the mortar grid or through increasing the number of subdomains. In the numerical experiments we report the rates of convergence of the numerical solution to the true solution, as well as the number of interface iterations and estimated condition number. In some cases, see Tables 6.4 and 6.8, the condition number is larger on the coarsest grid than on the finer grids. This is due to an underestimation of the smallest eigenvalue on the coarsest grid.

The convergence rates are established by running each test case on several levels of grid refinement and computing a least squares fit to the error. We consider both matching and non-matching initial grids. For initial matching grids, we use a 2×2 ($2 \times 2 \times 2$ for Example 6.3) subdomain grid (so, initially $h = 1/4$). For initial non-matching grids, we use 2×2 or 3×3 subdomain grids alternated in a checkerboard fashion. We test both continuous and discontinuous quadratic mortars ($m = 2$) and compare the results to the cases of linear mortars ($m = 1$), continuous or discontinuous, respectively. The initial mortar grids on all interfaces have one element (so, initially $H = 1/2$). For the case of quadratic mortars, on each level of grid refinement we divide each subdomain element diameter h by four and halve each mortar element diameter H so that $H = h^{1/2}$ (see Remarks 6.1–6.3). For the case of linear mortars we halve both subdomain and mortar element diameters, so $H = 2h$ on each level.

For each test case we report on some of the possible combinations between mortar types (continuous or discontinuous) and grid types (matching or non-matching). The results for the rest of the combinations are similar.

Table 6.1: Theoretical convergence rates for quadratic and linear mortars.

m	H	$\|\|p - p_h\|\|$	$\|\|\mathbf{u} - \mathbf{u}_h\|\|$	$\|\|\|p - p_h\|\|\|$	$\|\|\|\mathbf{u} - \mathbf{u}_h\|\|\|$	$\|\|\|p - \lambda_H\|\|\|$	
						full K	*diag K*
2	$h^{1/2}$	1	1	1.5	1.25	1.25	1.5
1	$2h$	1	1	2	1.5	1.5	2

The theoretical convergence rates for the above choices of subdomain and mortar grids

are given in Table 6.1. The second pressure error in the tables, $|||p - p_h|||$, is the discrete L^2-norm induced by the midpoint rule on $\mathcal{T}_h$, which is $\mathcal{O}(h^2)$-close to $\|\hat{p} - p_h\|$. The discrete velocity error $|||\mathbf{u} - \mathbf{u}_h|||$ is defined in (6.17) above. The discrete interface pressure error $|||p - \lambda_H|||$ is computed by adding for each block Ω_i the discrete L^2-norm of $p - \mathcal{Q}_{h,i}\lambda_H$ induced by the midpoint rule on the traces of $\mathcal{T}_{h,i}$ on $\partial\Omega_i \cap \Gamma$. This is essentially the L^2-norm, and we expect it to be $1/2$ power of H better than $\|p - \lambda_H\|_{a_H}$, since the latter is essentially $\|p - \lambda_H\|_{H^{1/2}(\Gamma)}$ (see [33], [74], and Remark 6.1 in [9]).

Example 6.1.

In the first example we solve a problem with known analytic solution

$$p(x, y) = x^3y^4 + x^2 + \sin(xy)\cos(y)$$

and full tensor coefficient

$$K = \begin{pmatrix} (x+1)^2 + y^2 & \sin(xy) \\ \sin(xy) & (x+1)^2 \end{pmatrix}.$$

Convergence rates, number of interface iterations, and condition number of the interface operator for this test case are given in Tables 6.2–6.5. We observe that the convergence rates are at least as good as predicted by the theory. For all four cases we obtain optimal order $\mathcal{O}(h)$ for both the pressure and the velocity L^2-error.

The discrete pressure error $|||p - p_h||| \approx \|\hat{p} - p_h\|$ is superconvergent of order $\mathcal{O}(h^2)$ for both quadratic and linear mortars, even though Theorem 6.3 predicts only $\mathcal{O}(h^{3/2})$ for quadratic mortars. By Theorem 6.2, the discrete velocity error $|||\mathbf{u} - \mathbf{u}_h|||$ is superconvergent of order $\mathcal{O}(h^{5/4})$ for quadratic mortars and $\mathcal{O}(h^{3/2})$ for linear mortars. Again, we observe higher than expected superconvergence for the case of quadratic mortars. Lastly, the discrete interface pressure error $|||p - \lambda_H||| \approx H^{1/2}\|p - \lambda_H\|_{a_H}$ is also better than expected, achieving convergence of $\mathcal{O}(h^2)$.

Based on comparing the results from linear and quadratic mortars, we observe that in certain cases for fine meshes the quadratic mortars are more efficient: we achieve the same accuracy with less computational work. For example, in the case of continuous mortars, for the finest level of grid refinement, the accuracy is comparable but there is more than a

Table 6.2: Number of iterations, condition number, discrete norm errors and convergence rates for Example 6.1: continuous quadratic mortars and matching grids.

$1/h$	*iter.*	*cond.*	$\|\|p-p_h\|\|$	$\|\|\mathbf{u}-\mathbf{u}_h\|\|$	$\|\|\|p-p_h\|\|\|$	$\|\|\|\mathbf{u}-\mathbf{u}_h\|\|\|$	$\|\|\|p-\lambda_H\|\|\|$
4	4	1.20E+0	3.38E-1	3.00E-1	6.87E-2	2.13E-2	5.81E-2
16	12	2.37E+1	7.98E-2	6.93E-2	4.21E-3	1.89E-3	3.50E-3
64	14	2.17E+1	1.99E-2	1.72E-2	2.59E-4	1.97E-4	2.17E-4
256	16	2.73E+1	4.97E-3	4.31E-3	1.61E-5	2.43E-5	1.37E-5
rate			$\mathcal{O}(h^{1.01})$	$\mathcal{O}(h^{1.02})$	$\mathcal{O}(h^{2.01})$	$\mathcal{O}(h^{1.63})$	$\mathcal{O}(h^{2.01})$
theory			$\mathcal{O}(h)$	$\mathcal{O}(h)$	$\mathcal{O}(h^{1.5})$	$\mathcal{O}(h^{1.25})$	$\mathcal{O}(h^{1.25})$

Table 6.3: Number of iterations, condition number, discrete norm errors and convergence rates for Example 6.1: continuous linear mortars and matching grids.

$1/h$	*iter.*	*cond.*	$\|\|p-p_h\|\|$	$\|\|\mathbf{u}-\mathbf{u}_h\|\|$	$\|\|\|p-p_h\|\|\|$	$\|\|\|\mathbf{u}-\mathbf{u}_h\|\|\|$	$\|\|\|p-\lambda_H\|\|\|$
4	4	2.44E+0	3.38E-1	3.00E-1	6.87E-2	2.13E-2	5.81E-2
8	7	9.91E+0	1.62E-1	1.41E-1	1.70E-2	6.33E-3	1.41E-2
16	13	2.38E+1	7.98E-2	6.93E-2	4.21E-3	1.88E-3	3.50E-3
32	19	3.48E+1	3.98E-2	3.45E-2	1.04E-3	5.88E-4	8.67E-4
64	23	4.40E+1	1.99E-2	1.72E-2	2.59E-4	1.93E-4	2.16E-4
128	23	5.54E+1	9.94E-3	8.62E-3	6.46E-5	6.53E-5	5.38E-5
256	23	6.76E+1	4.97E-3	4.31E-3	1.61E-5	2.27E-5	1.35E-5
rate			$\mathcal{O}(h^{1.01})$	$\mathcal{O}(h^{1.02})$	$\mathcal{O}(h^{2.01})$	$\mathcal{O}(h^{1.65})$	$\mathcal{O}(h^{2.01})$
theory			$\mathcal{O}(h)$	$\mathcal{O}(h)$	$\mathcal{O}(h^{2})$	$\mathcal{O}(h^{1.5})$	$\mathcal{O}(h^{1.5})$

30% reduction in the number of interface problem iterations needed for quadratic mortars (see the lines for $1/h = 256$ in Tables 6.2 and 6.3). In the case of discontinuous mortars, both linear and quadratic mortars are very efficient, with the number of interface iterations remaining almost unchanged with the grid refinement. We will see from Example 6.5 below that for heterogeneous problems with large variations in the velocity, discontinuous quadratic

Table 6.4: Number of iterations, condition number, discrete norm errors and convergence rates for Example 6.1: discontinuous quadratic mortars and non-matching grids.

$1/h$	*iter.*	*cond.*	$\|\|p-p_h\|\|$	$\|\|\mathbf{u}-\mathbf{u}_h\|\|$	$\|\|\|p-p_h\|\|\|$	$\|\|\|\mathbf{u}-\mathbf{u}_h\|\|\|$	$\|\|\|p-\lambda_H\|\|\|$
4	8	1.88E+1	2.64E-1	2.03E-1	4.62E-2	2.13E-2	4.45E-2
16	7	2.45E+0	6.37E-2	4.86E-2	2.83E-3	1.82E-3	2.72E-3
64	7	2.34E+0	1.59E-2	1.21E-2	1.75E-4	1.59E-4	1.69E-4
256	8	3.03E+0	3.98E-3	3.03E-3	1.09E-5	1.68E-5	1.06E-5
rate			$\mathcal{O}(h^{1.01})$	$\mathcal{O}(h^{1.01})$	$\mathcal{O}(h^{2.01})$	$\mathcal{O}(h^{1.72})$	$\mathcal{O}(h^{2.01})$
theory			$\mathcal{O}(h)$	$\mathcal{O}(h)$	$\mathcal{O}(h^{1.5})$	$\mathcal{O}(h^{1.25})$	$\mathcal{O}(h^{1.25})$

Table 6.5: Number of iterations, condition number, discrete norm errors and convergence rates for Example 6.1: discontinuous linear mortars and non-matching grids.

$1/h$	*iter.*	*cond.*	$\|\|p-p_h\|\|$	$\|\|\mathbf{u}-\mathbf{u}_h\|\|$	$\|\|\|p-p_h\|\|\|$	$\|\|\|\mathbf{u}-\mathbf{u}_h\|\|\|$	$\|\|\|p-\lambda_H\|\|\|$
4	4	1.31E+0	2.63E-1	2.04E-1	4.54E-2	2.35E-2	4.55E-2
8	7	1.79E+0	1.28E-1	9.82E-2	1.14E-2	7.44E-3	1.14E-2
16	7	2.12E+0	6.37E-2	4.86E-2	2.82E-3	2.30E-3	2.86E-3
32	7	2.61E+0	3.18E-2	2.43E-2	7.01E-4	7.29E-4	7.13E-4
64	8	3.27E+0	1.59E-2	1.21E-2	1.75E-4	2.38E-4	1.78E-4
128	8	4.08E+0	7.95E-3	6.06E-3	4.36E-5	7.99E-5	4.45E-5
256	8	5.02E+0	3.98E-3	3.03E-3	1.09E-5	2.74E-5	1.11E-5
rate			$\mathcal{O}(h^{1.01})$	$\mathcal{O}(h^{1.01})$	$\mathcal{O}(h^{2.01})$	$\mathcal{O}(h^{1.63})$	$\mathcal{O}(h^{2.00})$
theory			$\mathcal{O}(h)$	$\mathcal{O}(h)$	$\mathcal{O}(h^{2})$	$\mathcal{O}(h^{1.5})$	$\mathcal{O}(h^{1.5})$

mortars outperform discontinuous linear mortars.

The computed pressure and velocity with discontinuous quadratic and linear mortars on the same non-matching subdomain grids (first/second level of refinement for quadratic/linear mortars) are shown in Figure 6.3. Although the two solutions look the same, the velocity error along the interfaces is somewhat larger for the case of linear mortars, as can be seen

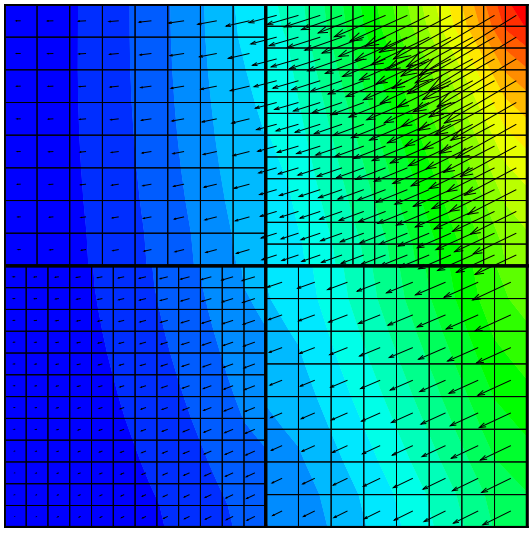

A. Discontinuous quadratic mortars

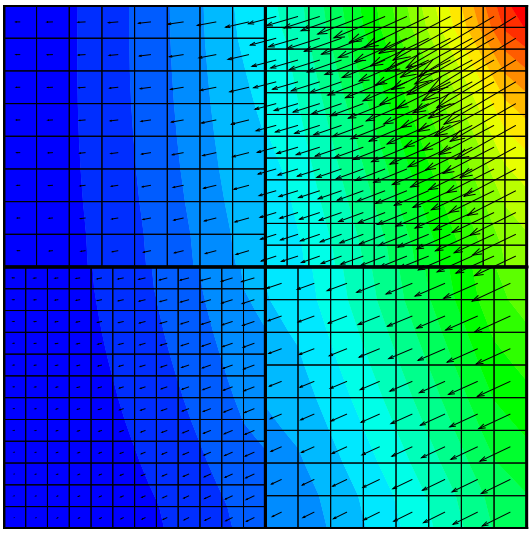

B. Discontinuous linear mortars

Figure 6.3: Computed pressure (shade) and velocity (arrows) for Example 6.1 on non-matching grids.

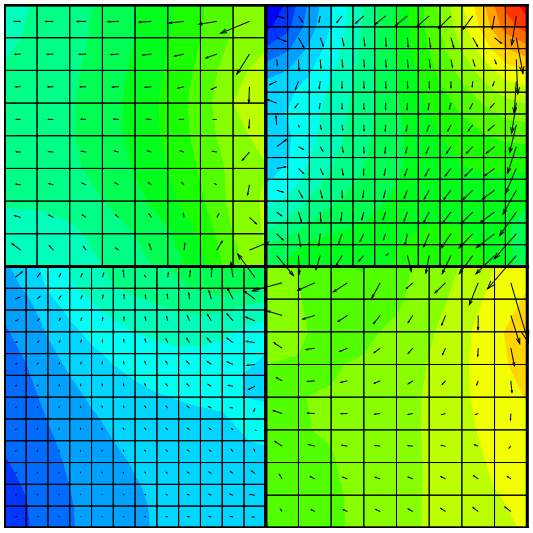

A. Discontinuous quadratic mortars

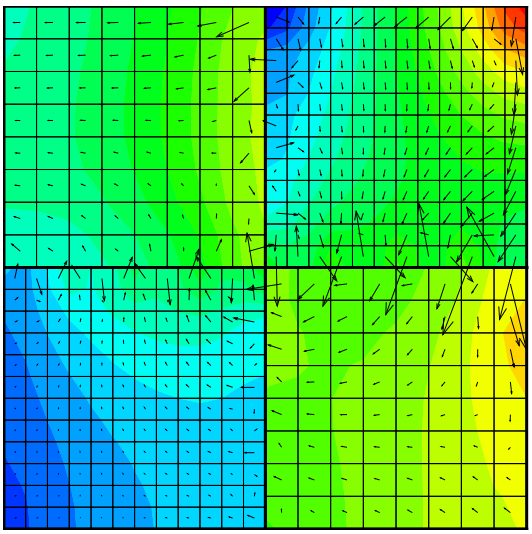

B. Discontinuous linear mortars

Figure 6.4: Error in pressure (shade) and velocity (arrows) for Example 6.1 on non-matching grids.

in Figure 6.4 where the magnified numerical error is shown.

Example 6.2.

In the second example we test a problem with a discontinuous coefficient. We choose $K = I$ for $0 \leq x < 1/2$ and $K = 10I$ for $1/2 < x \leq 1$. The solution

$$p(x,y) = \begin{cases} x^2y^3 + \cos(xy), & 0 \leq x \leq 1/2, \\ \left(\frac{2x+9}{20}\right)^2 y^3 + \cos\left(\frac{2x+9}{20}y\right), & 1/2 \leq x \leq 1, \end{cases}$$

is chosen to be continuous and have continuous normal flux at $x = 1/2$. Convergence rates are given in Tables 6.6–6.9. Again they agree with the theory, even though K is mildly discontinuous.

Table 6.6: Number of iterations, condition number, discrete norm errors and convergence rates for Example 6.2: discontinuous quadratic mortars and matching grids.

$1/h$	*iter.*	*cond.*	$\|\|p - p_h\|\|$	$\|\|\mathbf{u} - \mathbf{u}_h\|\|$	$\|\|\|p - p_h\|\|\|$	$\|\|\|\mathbf{u} - \mathbf{u}_h\|\|\|$	$\|\|\|p - \lambda_H\|\|\|$
4	5	1.83E+0	2.35E-2	8.17E-2	1.51E-3	6.77E-2	4.58E-3
16	8	3.91E+0	5.69E-3	1.95E-2	1.06E-4	4.46E-3	2.98E-4
64	6	3.74E+0	1.42E-3	4.87E-3	6.76E-6	4.53E-4	2.20E-5
256	7	4.88E+0	3.55E-4	1.22E-3	4.34E-7	8.70E-5	2.14E-6
rate			$\mathcal{O}(h^{1.01})$	$\mathcal{O}(h^{1.01})$	$\mathcal{O}(h^{1.96})$	$\mathcal{O}(h^{1.61})$	$\mathcal{O}(h^{1.85})$
theory			$\mathcal{O}(h)$	$\mathcal{O}(h)$	$\mathcal{O}(h^{1.5})$	$\mathcal{O}(h^{1.25})$	$\mathcal{O}(h^{1.5})$

Table 6.7: Number of iterations, condition number, discrete norm errors and convergence rates for Example 6.2: discontinuous linear mortars and matching grids.

$1/h$	*iter.*	*cond.*	$\|\|p-p_h\|\|$	$\|\|\mathbf{u}-\mathbf{u}_h\|\|$	$\|\|\|p-p_h\|\|\|$	$\|\|\|\mathbf{u}-\mathbf{u}_h\|\|\|$	$\|\|\|p-\lambda_H\|\|\|$
4	5	1.83E+0	2.35E-2	8.17E-2	1.51E-3	6.77E-2	4.58E-3
8	7	2.62E+0	1.15E-2	3.94E-2	4.15E-4	1.73E-2	1.16E-3
16	7	3.50E+0	5.69E-3	1.95E-2	1.06E-4	4.37E-3	2.92E-4
32	7	4.55E+0	2.84E-3	9.71E-3	2.68E-5	1.10E-3	7.31E-5
64	7	5.75E+0	1.42E-3	4.85E-3	6.71E-6	2.74E-4	1.83E-5
128	7	7.11E+0	7.10E-4	2.42E-3	1.68E-6	6.86E-5	4.58E-6
256	8	8.63E+0	3.55E-4	1.21E-3	4.21E-7	1.72E-5	1.14E-6
rate			$\mathcal{O}(h^{1.01})$	$\mathcal{O}(h^{1.01})$	$\mathcal{O}(h^{1.98})$	$\mathcal{O}(h^{1.99})$	$\mathcal{O}(h^{2.00})$
theory			$\mathcal{O}(h)$	$\mathcal{O}(h)$	$\mathcal{O}(h^2)$	$\mathcal{O}(h^{1.5})$	$\mathcal{O}(h^2)$

Table 6.8: Number of iterations, condition number, discrete norm errors and convergence rates for Example 6.2: continuous quadratic mortars and non-matching grids.

$1/h$	*iter.*	*cond.*	$\|\|p-p_h\|\|$	$\|\|\mathbf{u}-\mathbf{u}_h\|\|$	$\|\|\|p-p_h\|\|\|$	$\|\|\|\mathbf{u}-\mathbf{u}_h\|\|\|$	$\|\|\|p-\lambda_H\|\|\|$
4	9	1.11E+2	1.84E-2	6.20E-2	1.13E-3	4.58E-2	3.27E-3
16	14	2.55E+1	4.37E-3	1.50E-2	8.07E-5	3.67E-3	2.40E-4
64	15	2.41E+1	1.09E-3	3.73E-3	5.37E-6	6.45E-4	2.45E-5
256	16	3.03E+1	2.72E-4	9.26E-4	3.70E-7	1.27E-4	2.97E-6
rate			$\mathcal{O}(h^{1.01})$	$\mathcal{O}(h^{1.01})$	$\mathcal{O}(h^{1.93})$	$\mathcal{O}(h^{1.40})$	$\mathcal{O}(h^{1.68})$
theory			$\mathcal{O}(h)$	$\mathcal{O}(h)$	$\mathcal{O}(h^{1.5})$	$\mathcal{O}(h^{1.25})$	$\mathcal{O}(h^{1.5})$

Table 6.9: Number of iterations, condition number, discrete norm errors and convergence rates for Example 6.2: continuous linear mortars and non-matching grids.

$1/h$	*iter.*	*cond.*	$\|\|p-p_h\|\|$	$\|\|\mathbf{u}-\mathbf{u}_h\|\|$	$\|\|\|p-p_h\|\|\|$	$\|\|\|\mathbf{u}-\mathbf{u}_h\|\|\|$	$\|\|\|p-\lambda_H\|\|\|$
4	5	1.68E+1	1.84E-2	9.57E-2	1.28E-3	7.04E-2	5.23E-3
8	8	1.70E+1	8.83E-3	4.05E-2	3.29E-4	2.38E-2	1.45E-3
16	14	2.55E+1	4.37E-3	1.75E-2	8.20E-5	7.76E-3	3.53E-4
32	22	3.73E+1	2.18E-3	8.06E-3	2.05E-5	2.62E-3	8.75E-5
64	22	4.32E+1	1.09E-3	3.85E-3	5.10E-6	9.06E-4	2.18E-5
128	24	5.26E+1	5.44E-4	1.88E-3	1.27E-6	3.17E-4	5.46E-6
256	23	6.26E+1	2.72E-4	9.28E-4	3.19E-7	1.11E-4	1.36E-6
rate			$\mathcal{O}(h^{1.01})$	$\mathcal{O}(h^{1.11})$	$\mathcal{O}(h^{2.00})$	$\mathcal{O}(h^{1.55})$	$\mathcal{O}(h^{1.99})$
theory			$\mathcal{O}(h)$	$\mathcal{O}(h)$	$\mathcal{O}(h^2)$	$\mathcal{O}(h^{1.5})$	$\mathcal{O}(h^2)$

Example 6.3.

In the third example we test a three dimensional problem with known analytic solution

$$p(x, y, z) = x + y + z - 1.5$$

and full tensor coefficient

$$K = \begin{pmatrix} x^2 + y^2 + 1 & 0 & 0 \\ 0 & z^2 + 1 & \sin(xy) \\ 0 & \sin(xy) & x^2 y^2 + 1 \end{pmatrix}.$$

Convergence rates are given in Tables 6.10 and 6.11, again confirming the theoretical results. Note that even though this is a problem with a full tensor K, the computed rates exceed the predicted ones (e.g., in Table 6.10, for the discrete pressure error we expect rate of 1.25 but observe 2.02). The computed solution and error in pressure and velocity for the case of continuous quadratic mortars on the first level of refinement for matching grids are shown in Figure 6.5.

Table 6.10: Number of iterations, condition number, discrete norm errors and convergence rates for Example 6.3: discontinuous quadratic mortars and matching grids.

$1/h$	*iter.*	*cond.*	$\|\|p - p_h\|\|$	$\|\|\mathbf{u} - \mathbf{u}_h\|\|$	$\|\|\|p - p_h\|\|\|$	$\|\|\|\mathbf{u} - \mathbf{u}_h\|\|\|$	$\|\|\|p - \lambda_H\|\|\|$
4	10	3.38E+0	4.33E-1	1.01E-1	1.87E-2	3.27E-3	1.42E-2
16	15	9.70E+0	1.08E-1	2.52E-2	1.09E-3	4.60E-4	8.38E-4
64	14	5.15E+0	2.71E-2	6.29E-3	6.69E-5	5.58E-5	5.17E-5
rate			$\mathcal{O}(h^{1.00})$	$\mathcal{O}(h^{1.00})$	$\mathcal{O}(h^{2.03})$	$\mathcal{O}(h^{1.47})$	$\mathcal{O}(h^{2.03})$
theory			$\mathcal{O}(h)$	$\mathcal{O}(h)$	$\mathcal{O}(h^{1.5})$	$\mathcal{O}(h^{1.25})$	$\mathcal{O}(h^{1.25})$

Table 6.11: Number of iterations, condition number, discrete norm errors and convergence rates for Example 6.3: discontinuous linear mortars and matching grids.

$1/h$	*iter.*	*cond.*	$\|\|p-p_h\|\|$	$\|\|\mathbf{u}-\mathbf{u}_h\|\|$	$\|\|\|p-p_h\|\|\|$	$\|\|\|\mathbf{u}-\mathbf{u}_h\|\|\|$	$\|\|\|p-\lambda_H\|\|\|$
4	10	3.48E+0	4.33E-1	1.01E-1	1.87E-2	3.27E-3	1.42E-2
8	13	5.30E+0	2.17E-1	5.04E-2	4.47E-3	1.30E-3	3.42E-3
16	15	7.64E+0	1.08E-1	2.52E-2	1.09E-3	4.60E-4	8.38E-4
32	16	1.05E+1	5.41E-2	1.26E-2	2.69E-4	1.60E-4	2.08E-4
64	19	1.40E+1	2.71E-2	6.29E-3	6.69E-5	5.58E-5	5.17E-5
rate			$\mathcal{O}(h^{1.00})$	$\mathcal{O}(h^{1.00})$	$\mathcal{O}(h^{2.03})$	$\mathcal{O}(h^{1.48})$	$\mathcal{O}(h^{2.02})$
theory			$\mathcal{O}(h)$	$\mathcal{O}(h)$	$\mathcal{O}(h^2)$	$\mathcal{O}(h^{1.5})$	$\mathcal{O}(h^{1.5})$

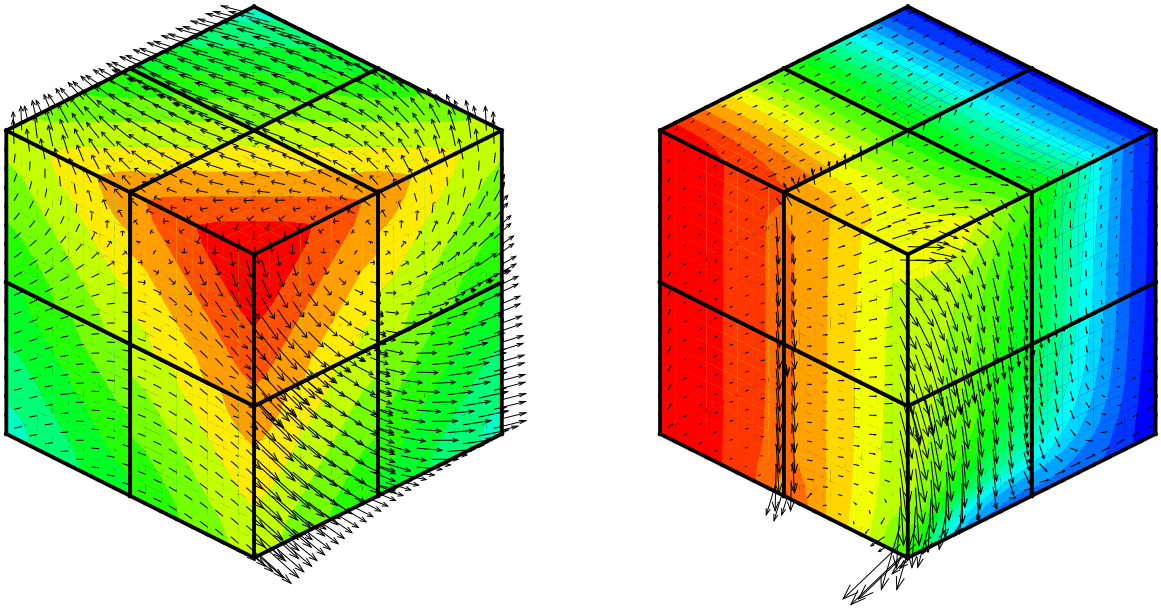

A. Solution B. Error

Figure 6.5: Computed pressure (shade) and velocity (arrows) for Example 6.3: continuous quadratic mortars and matching grids.

Example 6.4.

In the fourth example we study the behavior of the method as we vary the number of subdomains and the degree of the mortar approximating functions. The analytic solution and the tensor coefficient are as in Example 6.1. The fine grid of 256×256 elements was split into three different domain decompositions (coarse grids) of 2×2, 4×4, and 8×8 subdomains. The mortar grids were chosen to be consistent with the optimal choice for velocity superconvergence, i.e., $H = h^{1/2}$ for quadratic mortars and $H = 2h$ for linear mortars.

Convergence rates and number of interface iterations for this test case are given in Tables 6.12 and 6.13. We conclude from the results of this test case that the method scales very well when increasing the number of subdomains. In fact, even though the number of interface iterations increases slightly for more subdomains, the overall cost remains about the same since the subdomain problems become smaller. In addition, for a given domain decomposition, a comparison between linear and quadratic mortars confirms again the better efficiency of the latter.

Table 6.12: Number of iterations and discrete norm errors for Example 6.4: continuous quadratic mortars and multiple domains.

dom.	*iter.*	$\|\|p - p_h\|\|$	$\|\|\mathbf{u} - \mathbf{u}_h\|\|$	$\|\|\|p - p_h\|\|\|$	$\|\|\|\mathbf{u} - \mathbf{u}_h\|\|\|$	$\|\|\|p - \lambda_H\|\|\|$
2×2	16	4.97E-3	4.31E-3	1.61E-5	2.43E-5	1.37E-5
4×4	23	4.97E-3	4.31E-3	1.62E-5	5.20E-5	2.48E-5
8×8	23	4.97E-3	4.31E-3	1.63E-5	9.28E-5	3.83E-5

Example 6.5.

In this example we compare the performance of discontinuous linear and quadratic mortars on a problem with a highly heterogeneous coefficient. The permeability field, shown in Figure 6.6A, is obtained from the SPE Comparative Solution Project (www.spe.org/csp) and varies more than 5 orders of magnitude. We simulate flow from left to right. The computed solution on the finest level is presented in Figure 6.6B. In Table 6.14 we report the number of iterations and condition number. We note that on the finest level the discontinuous

Table 6.13: Number of iterations and discrete norm errors for Example 6.4: continuous linear mortars and multiple domains.

dom.	*iter.*	$\|\|p - p_h\|\|$	$\|\|\mathbf{u} - \mathbf{u}_h\|\|$	$\|\|\|p - p_h\|\|\|$	$\|\|\|\mathbf{u} - \mathbf{u}_h\|\|\|$	$\|\|\|p - \lambda_H\|\|\|$
2×2	23	4.97E-3	4.31E-3	1.61E-5	2.27E-5	1.35E-5
4×4	36	4.97E-3	4.31E-3	1.61E-5	2.78E-5	2.27E-5
8×8	39	4.97E-3	4.31E-3	1.61E-5	3.74E-5	3.41E-5

quadratic mortars are about 30% more efficient than the discontinuous linear mortars. This is similar to what was observed for continuous mortars in the previous smooth examples.

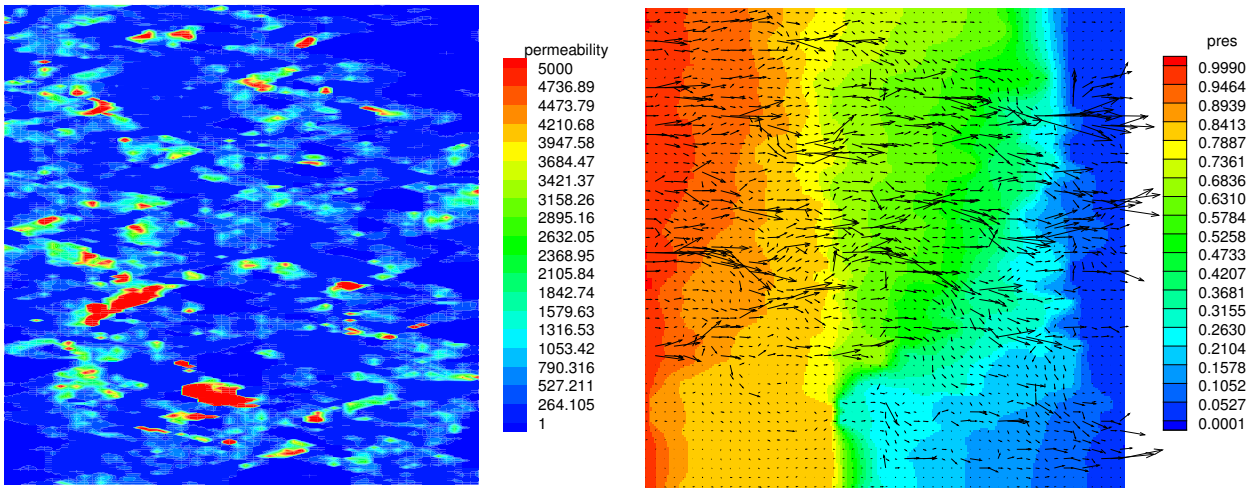

A. Permeability

B. Solution

Figure 6.6: Permeability field and computed pressure (shade) and velocity (arrows) for Example 6.5: discontinuous quadratic mortars and matching grids.

In the last two examples, we test the performance of the residual-based error estimator. The estimator is used as a local error indicator that drives an adaptive mesh refinement process. The following algorithm describes the adaptive procedure.

Table 6.14: Number of iterations and condition number for Example 6.5: discontinuous mortars and matching grids.

$1/h$	*iter.*	*cond.*
4	4	8.62E+0
16	17	4.87E+1
64	22	4.51E+1
256	26	3.12E+1

Quadratic mortars

$1/h$	*iter.*	*cond.*
4	4	4.38E+0
8	11	2.18E+1
16	19	9.35E+1
32	25	1.04E+2
64	25	5.00E+1
128	24	4.42E+1
256	35	3.82E+2

Linear mortars

Grid Refinement Algorithm

1. Solve the problem on a coarse subdomain and mortar grid.
2. For each subdomain Ω_i:
   a. Compute $\omega_i = (\sum_{E\in\mathcal{T}_{h,i}} \omega_E^2 + \sum_{\tau\in\mathcal{T}^{\Gamma_i,H}} \omega_\tau^2)^{1/2}$;
   b. If $\omega_i > .5 \max_{1\le j\le n} \omega_j$, refine $\mathcal{T}_{h,i}$.
3. For each interface $\Gamma_{i,j}$, if either Ω_i or Ω_j has been refined m times, refine $\mathcal{T}_{H,i,j}$.
4. Solve the problem on the refined grid. If either the desired error tolerance or the maximum refinement level has been reached, exit; otherwise, go to Step 2.

Note that we employ the pressure error estimator based on ω_E and ω_τ, defined in (6.29) and (6.30), since it provides an efficient and reliable estimate of the L^2 pressure error, due to Theorem 6.5 and Theorem 6.7 (see also Remark 6.5). Also, according to Step 3, the mortar grids are refined if either adjacent subdomain grid is refined sufficiently many times (depending on the mortar polynomial degree m).

For these last two examples, the unit square domain is decomposed into 6×6 subdomains. The coarse grid in each subdomain is 2×2 with a single mortar element on each interface.

Both continuous and discontinuous piecewise quadratic mortar spaces on the interfaces were tested.

Example 6.6.

Here we test a problem with a boundary layer. The true pressure is

$$p(x, y) = 1000\, x\, y\, e^{-10(x^2+y^2)},$$

with $K = I$. The computed pressures after three refinements for the cases of discontinuous quadratic and linear mortars are shown in Figure 6.7. Observe that the linear mortars produce finer grids that are appropriately refined along the boundary layer while the quadratic mortars give grids that are coarser and more uniform in that region.

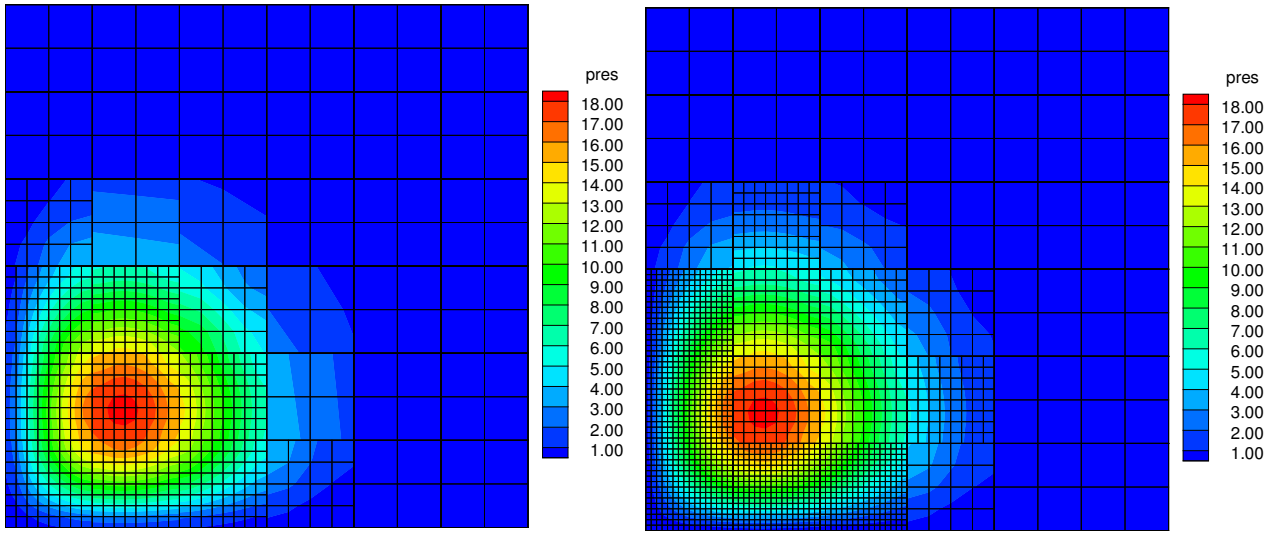

A. Discontinuous quadratic mortars

B. Discontinuous linear mortars

Figure 6.7: Computed pressure on the fourth grid level for Example 6.6

Example 6.7.

In the last example we test a problem with a highly oscillating tensor

$$K = \begin{cases} 105 - 100\sin(20\pi x)\sin(20\pi y), & x, y \in [0, 1/2] \text{ or } x, y \in [1/2, 1], \\ 105 - 100\sin(2\pi x)\sin(2\pi y), & \text{otherwise.} \end{cases}$$

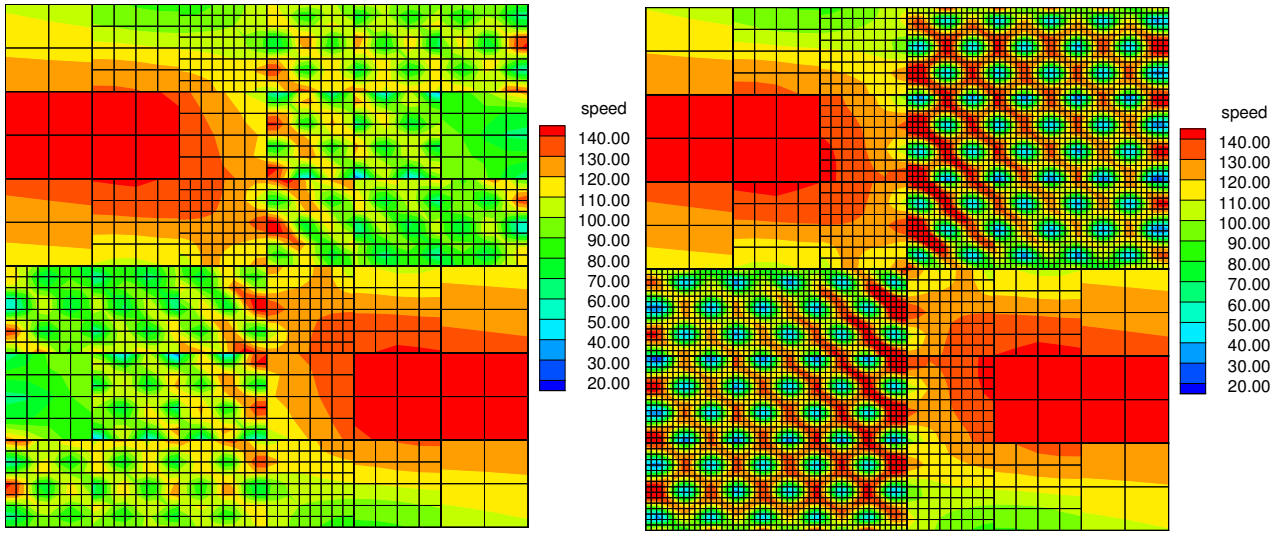

A. Continuous quadratic mortars

B. Continuous linear mortars

Figure 6.8: Computed magnitude of the velocity on the fifth grid level for Example 6.7

The computed magnitude of the velocity after four refinements for the cases of continuous quadratic and linear mortars are shown in Figure 6.8.

Note that the highly oscillating velocity is well resolved by the fine computational grid in the lower-left and the upper-right regions. Some refinement is also observed along the line $x = 1/2$ due to the large jump-flux term ω_τ. As in the previous example, linear mortars produce finer grids, especially in the two regions of high oscillation.

6.6 TWO-PHASE FLOW IN POROUS MEDIA

In this section we extend the multiscale mortar mixed finite element method to two-phase flow in porous media. We will use n_b to denote the number of blocks and n will be related to the discretized time.

Let $0 = t_0 < t_1 < t_2 < ...$, let $\Delta t^n = t_n - t_{n-1}$, and let $f^n = f(t_n)$. In the backward Euler multiblock expanded mixed finite element approximation of (2.41)-(2.45) we seek, for $1 \le i < j \le n_b$ and $n = 1, 2, 3...$, $\mathbf{U}^n_{h,\alpha}|_{\Omega_i} \in \mathbf{V}_{h,i}$, $\tilde{\mathbf{U}}^n_{h,\alpha}|_{\Omega_i} \in \tilde{\mathbf{V}}_{h,i}$, $P^n_h|_{\Omega_i} \in W_{h,i}$, $S^n_h|_{\Omega_i} \in W_{h,i}$, $P^{M,n}_H|_{\Gamma_{i,j}} \in M_{H,i,j}$, and $S^{M,n}_H|_{\Gamma_{i,j}} \in M_{H,i,j}$ such that, for $\alpha = w$ and n,

$$\int_{\Omega_i} \frac{S^n_{h,\alpha} - S^{n-1}_{h,\alpha}}{\Delta t^n} w \, dx + \int_{\Omega_i} \nabla \cdot \mathbf{U}^n_{h,\alpha} \, w \, dx = \int_{\Omega_i} q_\alpha \, w \, dx, \;\; w \in W_{h,i}, \tag{6.80}$$

$$\int_{\Omega_i} \tilde{\mathbf{U}}^n_{h,\alpha} \cdot \mathbf{v} \, dx = \int_{\Omega_i} P^n_{h,\alpha} \nabla \cdot \mathbf{v} \, dx - \int_{\partial\Omega_i \setminus \partial\Omega} P^{M,n}_{H,\alpha} \mathbf{v} \cdot \nu_i \, d\sigma, \;\; \mathbf{v} \in \mathbf{V}_{h,i}, \tag{6.81}$$

$$\int_{\Omega_i} \mathbf{U}^n_{h,\alpha} \cdot \tilde{\mathbf{v}} \, dx = \int_{\Omega_i} \frac{k^n_{h,\alpha} K}{\mu_{h,\alpha}} \rho^n_{h,\alpha} (\tilde{\mathbf{U}}^n_{h,\alpha} + \rho^n_{h,\alpha} g \nabla D) \cdot \tilde{\mathbf{v}} \, dx, \;\; \tilde{\mathbf{v}} \in \tilde{\mathbf{V}}_{h,i}, \tag{6.82}$$

$$\int_{\Gamma_{i,j}} [\mathbf{U}^n_{h,\alpha} \cdot \nu]_{ij} \, \mu \, d\sigma = 0, \;\; \mu \in M_{H,i,j}. \tag{6.83}$$

Here $k^n_{h,\alpha}$ and $\rho^n_{h,\alpha} \in W_{h,i}$ are given functions of the subdomain primary variables P^n_h and S^n_h. The mortar functions $P^{M,n}_{H,\alpha}$ can be computed using (2.45), given the mortar primary variables $P^{M,n}_H$ and $S^{M,n}_H$.

6.6.1 Domain decomposition

To solve the discrete system (6.80)–(6.83) on each time step, we reduce it to an interface problem in the coarse mortar space, see also [68].

Let $\mathcal{M}_H = M_H \times M_H$ be the space of mortar primary variables. We define a non-linear interface bivariate form $b^n : \mathcal{M}_H \times \mathcal{M}_H \to \mathbf{R}$ as follows. For $\psi = (P^{M,n}_H, S^{M,n}_H)^T \in \mathcal{M}_H$ and $\mu = (\mu_w, \mu_n) \in \mathcal{M}_H$, let

$$b^n(\psi, \mu) = \sum_{1 \le i < j \le n_b} \int_{\Gamma_{i,j}} ([\mathbf{U}^n_{h,w}(\psi) \cdot \nu]_{ij} \, \mu_w + [\mathbf{U}^n_{h,n}(\psi) \cdot \nu]_{ij} \, \mu_n) d\sigma,$$

where $(S^n_h(\psi), \mathbf{U}^n_{h,\alpha}(\psi))$ are solutions to the series of subdomain problems (6.80)–(6.82) with Dirichlet boundary data $P^{M,n}_{H,\alpha}(\psi)$.

Define a non-linear interface operator $\mathcal{B}^n : \mathcal{M}_H \to \mathcal{M}_H$ by

$$\langle \mathcal{B}^n \psi, \mu \rangle = b^n(\psi, \mu), \quad \forall \mu \in \mathcal{M}_H,$$

where $\langle \cdot, \cdot \rangle$ is the L^2-inner product in $\mathcal{M}_H$. It is easy to see that $(\psi, S_h^n(\psi), \mathbf{U}_{h,\alpha}^n(\psi))$ is the solution to (6.80)–(6.83), where $\psi \in \mathcal{M}_H$ solves

$$\mathcal{B}^n(\psi) = 0. \tag{6.84}$$

We solve the system of nonlinear equations on the interface (6.84) by an inexact Newton method. Each Newton step s is computed by a forward difference GMRES iteration for solving $(\mathcal{B}^n)'(\psi)s = -\mathcal{B}^n(\psi)$. On each GMRES iteration the action of the Jacobian $(\mathcal{B}^n)'(\psi)$ on a vector μ is approximated by a forward difference which requires only one evaluation of the nonlinear operator $\mathcal{B}^n$. The evaluation of $\mathcal{B}^n$ involves solving subdomain problems (6.80)–(6.82) in parallel and two inexpensive projection steps - from the mortar grid onto the local subdomain grids and from the local grids onto the mortar grid. Since each block can be distributed among a number of processors, the subdomain solvers are parallel themselves. The subdomain problems are also nonlinear and are solved by a preconditioned Newton-Krylov solver [35, 51].

6.6.2 Numerical simulations

In this section we present numerical results illustrating the behavior of the method described above when applied to modeling two-phase subsurface flow. In particular, we compare the multiscale mortar method with the single-scale mortar approach.

The multiblock multiscale methodology has been implemented in the simulator IPARS (Integrated Parallel Accurate Reservoir Simulator) [2] for modeling multiphase flow, developed at the University of Texas at Austin Center for Subsurface Modeling. Here we present the simulation of oil-water immiscible displacement in a horizontal cross-section of a highly heterogeneous reservoir. Data from SPE Comparative Solution Project [31] was used. The simulation domain has dimensions 6144 ft $\times$ 6144 ft. The permeability field is shown in Figure 6.9. Initial oil pressure is 500 psi and initial water saturation is .22, which is close to

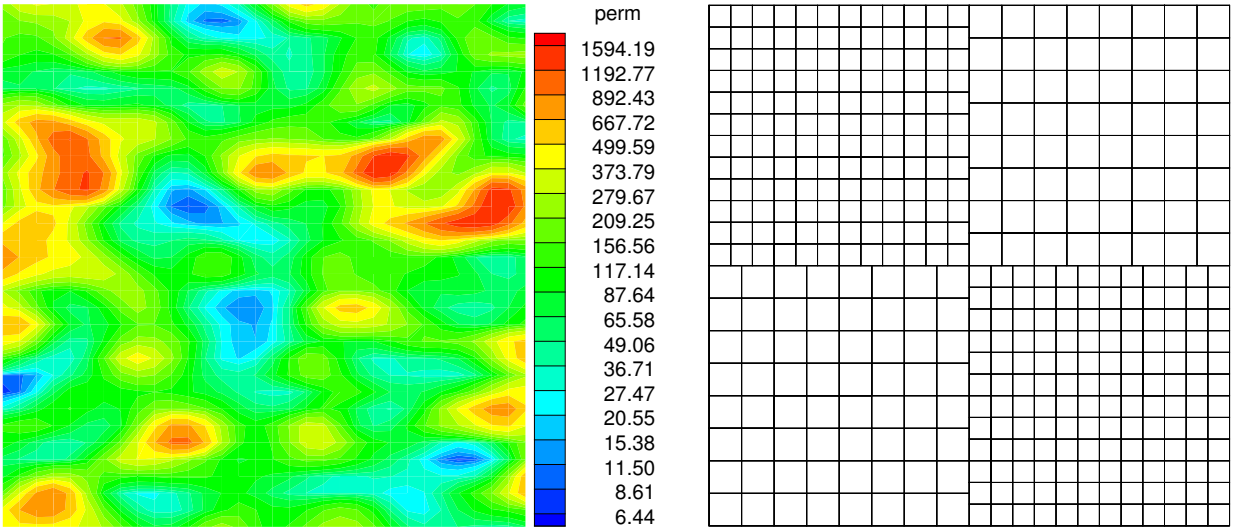

Figure 6.9: Permeability field (left) and grids on the coarsest level (right).

its residual value. Water is injected at the upper left corner at pressure that increases from 505 psi to 5000 psi in the first 100 days. Oil is produced in the lower right corner at pressure 495 psi. The domain is decomposed into four subdomains. We run the simulation on four levels of grid refinement. The subdomain grids on the coarsest level are shown in Figure 6.9. We compare the cases of continuous piecewise linear and quadratic mortars. The grids for linear mortars are chosen to be proportional to the subdomain grids. More precisely, the grid on each mortar is taken to be a coarsening by two of one of the neighboring subdomain grids. This choice satisfies assumption (2.30), see [74]. The choice of grids for the piecewise quadratic mortars is motivated by the theoretical results for single-phase flow, Theorems 6.1, 6.2, and 6.3. We take $N_H = \sqrt{N_h}$, where N_h and N_H are the number of mortar elements for linear and quadratic mortars, respectively. This choice provides optimal convergence $O(h)$ for the multiscale method for single-phase flow.

The two types of simulations produced almost the same solutions. The computed oil pressure and water saturation at 801 days with quadratic mortars on the third grid level are shown in Figure 6.10. The solution computed with linear mortars looks the same and is not shown. The comparison of recovery curves in Figure 6.11 also confirms the match of the two solutions. However, the multiscale method using quadratic mortars on a coarse grid

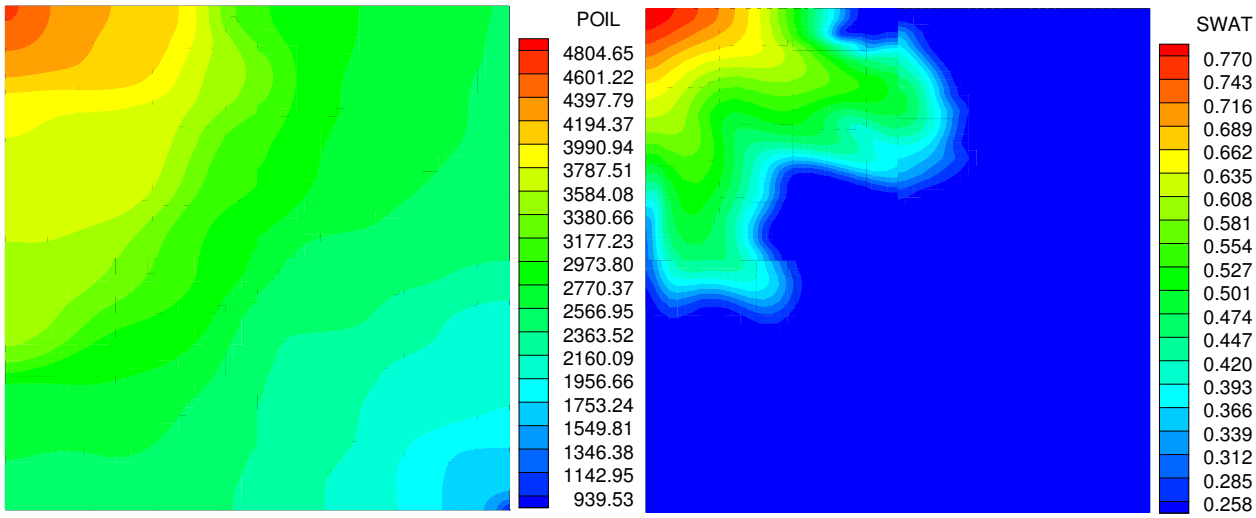

A. *Oil pressure*

B. *Water saturation*

Figure 6.10: Computed solution at 801 days with piecewise quadratic mortars on the third grid level.

is more efficient, as indicated by the results from Table 6.15. There, we report the average number of interface GMRES iterations per time step, which corresponds to the number of subdomain solves per time step. We note that for coarse grids the number of iterations is comparable while for finer grids it is smaller for the quadratic mortars and increases at a slower rate as the grids are refined. For example, on the fourth grid level there is more than a 40 % reduction in the number of iterations; the savings would be even bigger on finer grids.

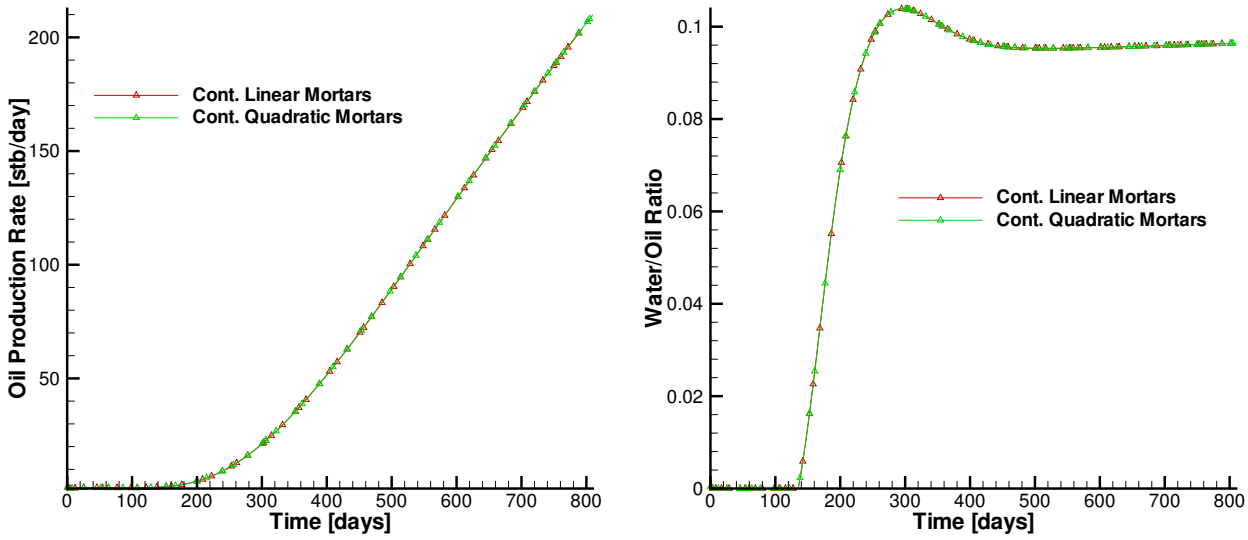

Figure 6.11: Comparison of recovery curves for linear and quadratic mortars.

Table 6.15: Average number of interface GMRES iterations per time step for linear and quadratic mortars.

level	subdomain grids	quadratic mortars		linear mortars	
		mortar grids	GMRES iter	mortar grids	GMRES iter
1	8× 8, 12×12	2	43	4	42
2	16×16, 24×24	3	56	8	55
3	32×32, 48×48	4	61	16	78
4	64×64, 96×96	6	69	32	117

7.0 PARALLEL UNSTRUCTURED MULTIBLOCK SIMULATOR

We have developed a multiblock unstructured flow simulator. It is based on UTPROJ [67], the University of Texas PROJection code which constructs locally mass conservative velocity fields by solving scalar linear second order elliptic equations. It uses hybrid mixed finite element method on general unstructured meshes in two and three space dimensions. The code implements the non-overlapping domain decomposition algorithm of Chapter 5 that reduces the global system to an interface problem which is solved iteratively via a preconditioned conjugate gradient method. The subdomain problems are also solved iteratively via a conjugate gradient method. The code is parallel and uses KELP library [16] for MPI communications between the processors.

We implemented an efficient preconditioner (see Chapter 5) that speeds up the domain decomposition solver. In addition, variable permeability tensor, source term and boundary conditions given by analytical functions were allowed. The solution is postprocessed to generate output visualized with TECPLOT [1].

To generate input for the simulator, a preprocessor was implemented that takes the unstructured block grids generated by GMSH [41] (automatic 3D finite element mesh generator) and some general information about the block geometry. Each block can have the shape of a vertical "cylinder" whose "base" could be any general $2d$ domain. After the "base" is triangulated, its mesh is extruded vertically and then split into layers, thus forming the prismatic elements UTPROJ works with. The preprocessor uses METIS [50] (graph partition library) to partition the grid into subdomains. To do that, we first form the dual graph for the "base", pass it to one of the partitioning routines in METIS to break it into a given number of parts, create smaller "sub-cylinders" related to this partition, and finally, subdivide these cylinders into specified number of layers. Note that, in general, the vertical

interfaces between subdomains within one block will not be planar. As a special case we also allow for the possibility of generating a structured mesh (not necessarily uniform) which could either be partitioned with METIS or divided into rectangular $3d$ boxes, in which case we have to specify the number of subdomains in each of the three directions.

In the case of multiblock, each of the blocks is generated and partitioned in a similar fashion. In addition, we require that two neighboring blocks have a planar, vertical intersection. In the future, if mortars for triangular elements are implemented, the restriction for vertical intersection could be lifted.

Several examples illustrating the capabilities of our parallel multiblock unstructured simulator will be presented next.

Example 7.1.

First, we simulated an oil field with 4 injection and 9 production wells modeled with Dirichlet boundary conditions on the pressure (high for the injection and low for the production wells). On the rest of the boundary zero Neumann boundary conditions are imposed. The 3D domain (single block) is embedded in the cube $[-1/2, 1/2]^3$ and is covered with unstructured prismatic grid. The mesh is then subdivided using METIS into 27 subdomains with matching grids on the interfaces. The permeability tensor is full and is given by

$$K = \begin{pmatrix} 2 & 1 & 1 \\ 1 & 2 & 1 \\ 1 & 1 & 2 \end{pmatrix}$$

The mesh on the second level is shown in Figure 7.1 and the computed pressure and velocity field are given in Figure 7.2. The number of CG iterations with and without preconditioning are reported for several levels of grid refinements and are shown to grow very slowly as h gets smaller (see Table 7.1).

Example 7.2.

Next, we illustrate the multiblock feature of our simulator. To simulate a geological fault, we consider a 2-block domain with curved boundary. The two blocks are covered with unstructured prismatic meshes. The left and right blocks have their grids subdivided using

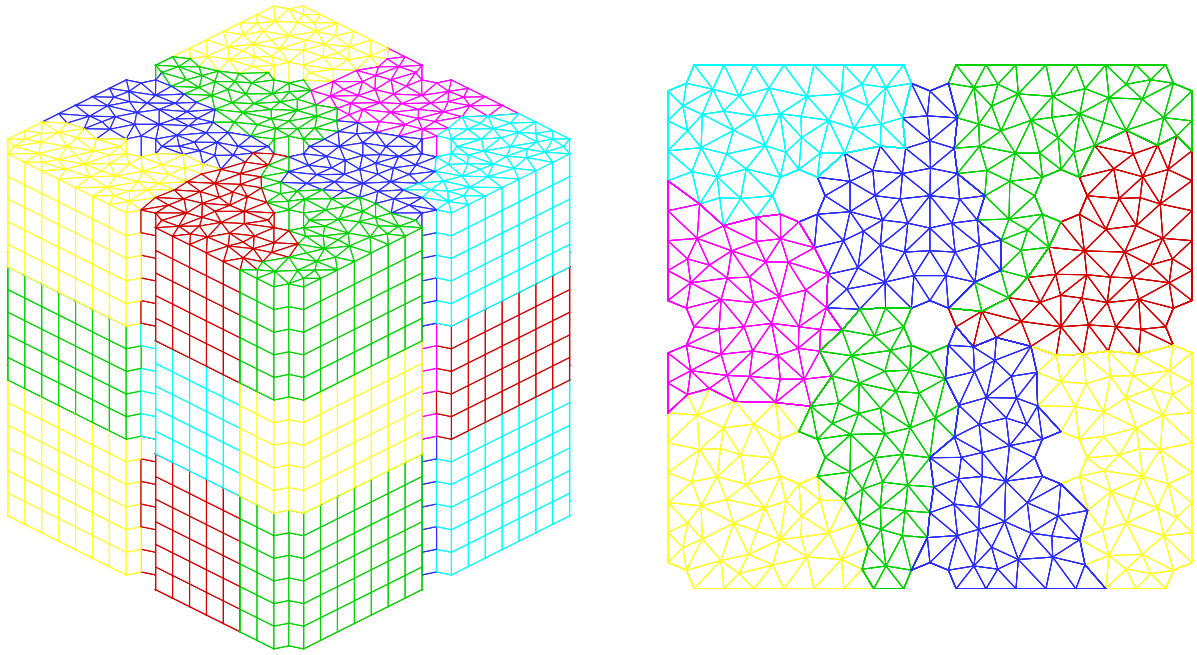

Figure 7.1: Coarse mesh in Example 7.1

METIS into four and six subdomains, respectively. The meshes are shown in Figure 7.3. Note that the two block grids do not match on the block interface. The continuity of flux is imposed via a mortar mixed finite element space on a coarse uniform grid of 8×11. The traces of the block grids on the interface are 9×15 and 8×13, respectively (see Figure 7.4). The boundary conditions are Dirichlet on the left and right face and no-flow on the rest of the boundary. We use identity permeability tensor. Left-to-right flow is imposed through boundary conditions. The solution for discontinuous linear mortar space is shown though

Table 7.1: Number of iterations for Example 7.1

$1/h$	*BalCG*	*CG*
8	14	28
16	14	35
32	15	40
64	16	66

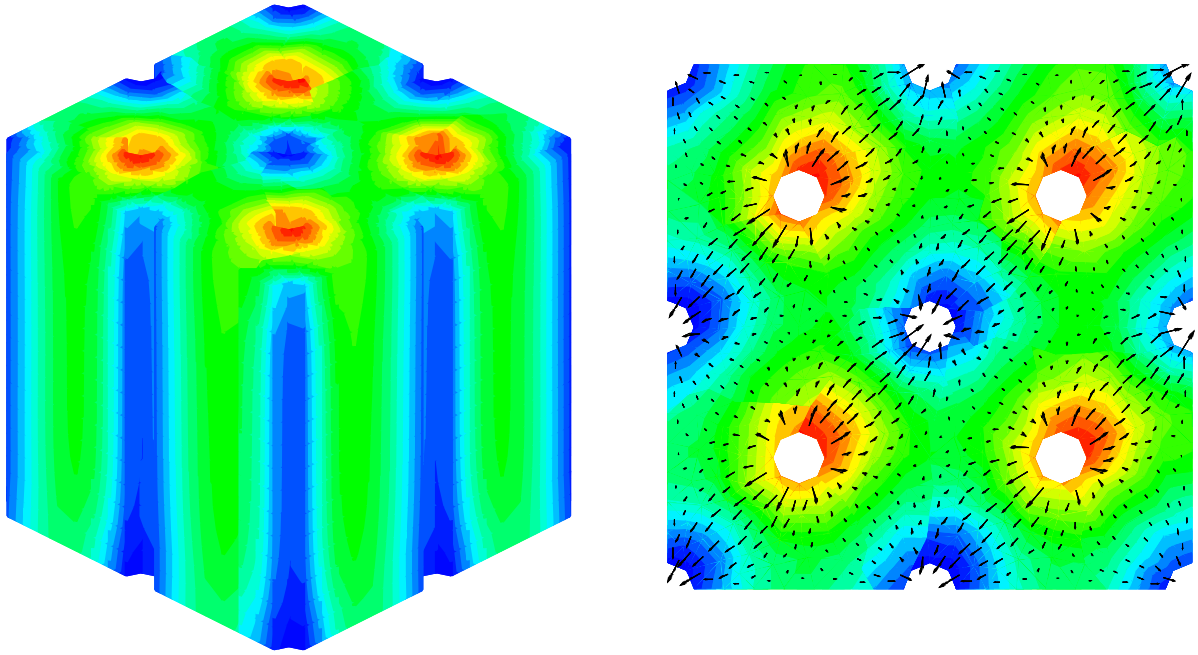

Figure 7.2: Computed pressure (shade) and velocity (arrows) in Example 7.1

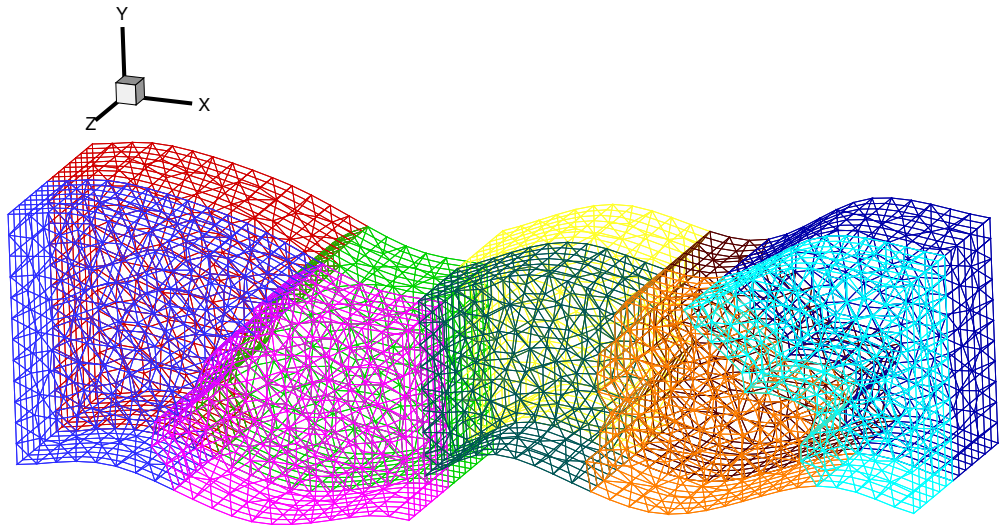

Figure 7.3: Block meshes partitioned between 10 subdomains (color) in Example 7.2

similar results were obtained for the other mortar types. The computed pressure and velocity are given in Figures 7.5 and 7.6. Note the continuity of the flux across the block interface.

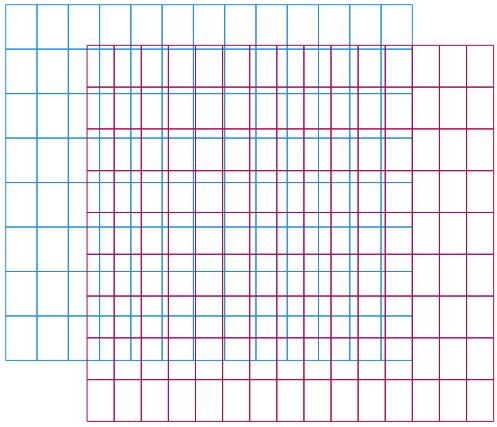

Figure 7.4: Meshes on the block interface in Example 7.2

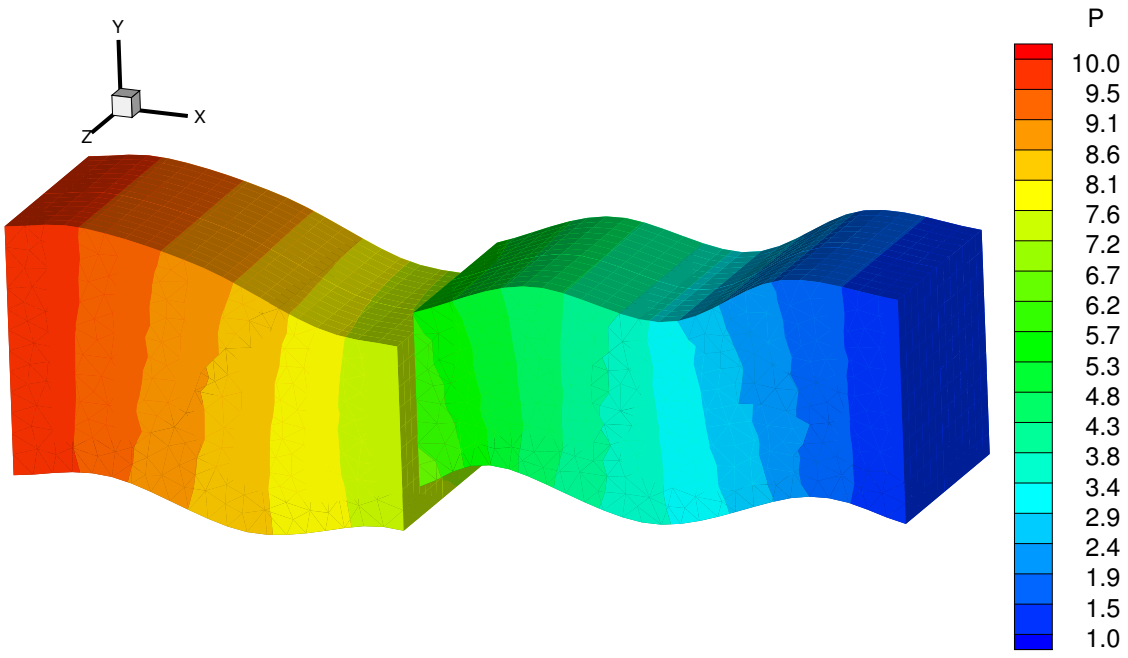

Figure 7.5: Computed pressure for Example 7.2

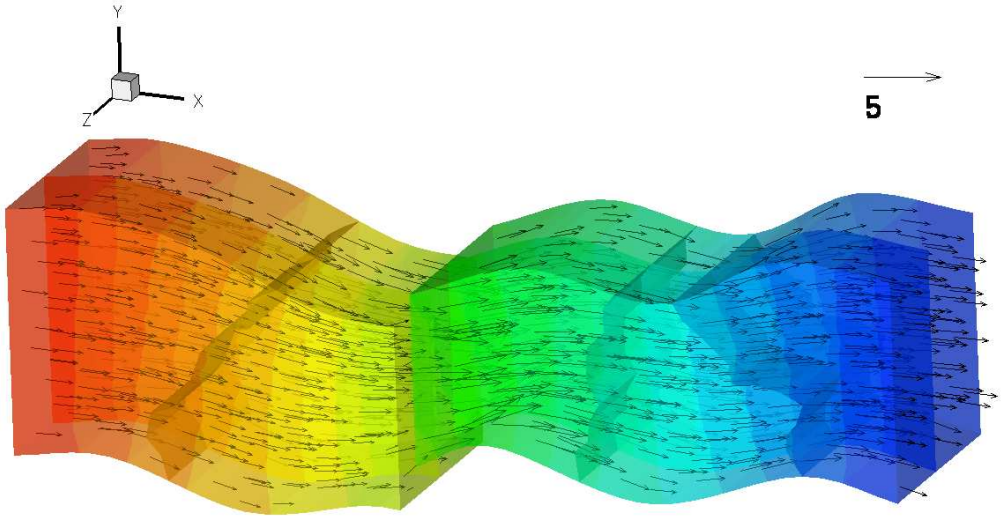

Figure 7.6: Computed velocity (arrows) and pressure (shade) for Example 7.2

APPENDIX

MATHEMATICA NOTEBOOKS

This appendix contains two Mathematica notebooks. They were used to verify some calculations in the proof of equivalence of norms in the mulstiscale case in Section 6.4.

```
In[1]:= f1[x_] := (1 - x);

        a1[k_] := Simplify[n * Integrate[f1[x], {x, (k - 1)/n, k/n}]];

        a1[k]
Out[1]= (1 - 2 k + 2 n)/(2 n)

In[2]:= f2[x_] := x;

        a2[k_] := Simplify[n * Integrate[f2[x], {x, (k - 1)/n, k/n}]];

        a2[k]
Out[2]= (-1 + 2 k)/(2 n)

In[3]:= b11 := Sum[(a1[k])^2, {k, 1, n}];

        b22 := Sum[(a2[k])^2, {k, 1, n}];

        b12 := Sum[a1[k] * a2[k], {k, 1, n}];

In[4]:= B := {{b11, b12}, {b12, b22}}; B
Out[4]= {{(-1 + 2 n) (1 + 2 n)/(12 n), (1 + 2 n^2)/(12 n)}, {(1 + 2 n^2)/(12 n), (-1 + 2 n) (1 + 2 n)/(12 n)}}

In[5]:= c := {c1, c2};

In[6]:= ϕ := Simplify[Inverse[B].c]; ϕ1 := ϕ[[1]]; ϕ2 := ϕ[[2]];

        d1[k_] :=
          Simplify[Coefficient[ϕ1, c1] * a1[k] + Coefficient[ϕ1, c2] * a2[k]];

        d2[k_] :=
          Simplify[Coefficient[ϕ2, c1] * a1[k] + Coefficient[ϕ2, c2] * a2[k]];

In[7]:= Factor[d1[k]]

        Factor[d2[k]]
Out[7]= (-1 + 3 n - 6 k n + 4 n^2)/((-1 + n) n (1 + n))
Out[7]= -(1 + 3 n - 6 k n + 2 n^2)/((-1 + n) n (1 + n))
```

Figure A.1: Linears.nb, page 1

```
In[8]:= a := 2; b := 10;

In[9]:= e1 = Simplify[Sum[(d1[k])^2, {k, 1, n}]]
Out[9]= (1 - 4 n^2)/(n - n^3)

In[10]:= g1[m_] := n * e1/. n → m;

         Plot[g1[n], {n, a, b}];

         N[g1[a]]
```

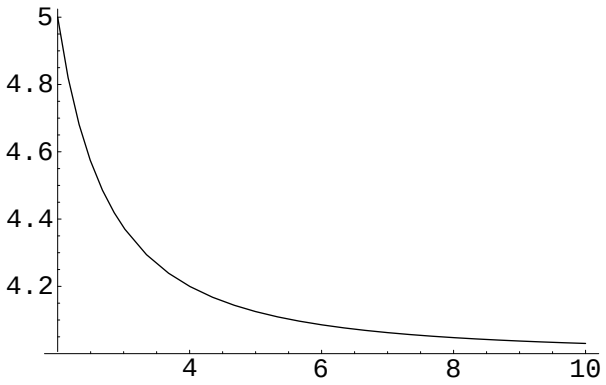


```
Out[10]= 5.

In[11]:= e2 = Simplify[Sum[(d2[k])^2, {k, 1, n}]]
Out[11]= (1 - 4 n^2)/(n - n^3)

In[12]:= g2[m_] := n * e2/. n → m;

         Plot[g2[n], {n, a, b}];

         N[g2[a]]
```

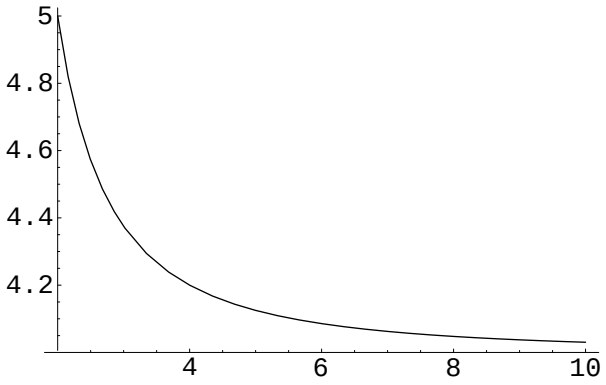


```
Out[12]= 5.
```

Figure A.2: Linears.nb, page 2

```
In[1]:= f1[x_] := (1 - 2x)(1 - x);

        a1[k_] := Simplify[n * Integrate[f1[x], {x, (k - 1)/n, k/n}]];

        a1[k]
Out[1]= (4 + 12 k^2 + 9 n + 6 n^2 - 6 k (2 + 3 n)) / (6 n^2)

In[2]:= f2[x_] := 4 * x(1 - x);

        a2[k_] := Simplify[n * Integrate[f2[x], {x, (k - 1)/n, k/n}]];

        a2[k]
Out[2]= -(2 (2 + 6 k^2 + 3 n - 6 k (1 + n))) / (3 n^2)

In[3]:= f3[x_] := x * (2 * x - 1);

        a3[k_] := Simplify[n * Integrate[f3[x], {x, (k - 1)/n, k/n}]];

        a3[k]
Out[3]= (4 + 12 k^2 + 3 n - 6 k (2 + n)) / (6 n^2)

In[4]:= b11 := Sum[(a1[k])^2, {k, 1, n}];

        b22 := Sum[(a2[k])^2, {k, 1, n}];

        b33 := Sum[(a3[k])^2, {k, 1, n}];

        b12 := Sum[a1[k] * a2[k], {k, 1, n}];

        b13 := Sum[a1[k] * a3[k], {k, 1, n}];

        b23 := Sum[a2[k] * a3[k], {k, 1, n}];

In[5]:= B := {{b11, b12, b13}, {b12, b22, b23}, {b13, b23, b33}}; B
Out[5]= {{(16 - 35 n^2 + 24 n^4)/(180 n^3), ((4 + n^2) (-2 + 3 n^2))/(45 n^3), -(-16 + 5 n^2 + 6 n^4)/(180 n^3)},
         {((4 + n^2) (-2 + 3 n^2))/(45 n^3), (4 (4 - 5 n^2 + 6 n^4))/(45 n^3), ((4 + n^2) (-2 + 3 n^2))/(45 n^3)},
         {-(-16 + 5 n^2 + 6 n^4)/(180 n^3), ((4 + n^2) (-2 + 3 n^2))/(45 n^3), (16 - 35 n^2 + 24 n^4)/(180 n^3)}}

In[6]:= c := {c1, c2, c3};
```

Figure A.3: Quadratics.nb, page 1

```
In[7]:= ϕ := Simplify[Inverse[B].c]; ϕ1 := ϕ[[1]]; ϕ2 := ϕ[[2]]; ϕ3 := ϕ[[3]];

        d1[k_] := Simplify[Coefficient[ϕ1, c1] * a1[k] +
             Coefficient[ϕ1, c2] * a2[k] + Coefficient[ϕ1, c3] * a3[k]];

        d2[k_] := Simplify[Coefficient[ϕ2, c1] * a1[k] +
             Coefficient[ϕ2, c2] * a2[k] + Coefficient[ϕ2, c3] * a3[k]];

        d3[k_] := Simplify[Coefficient[ϕ3, c1] * a1[k] +
             Coefficient[ϕ3, c2] * a2[k] + Coefficient[ϕ3, c3] * a3[k]];

In[8]:= Factor[d1[k]]

        Factor[d2[k]]

        Factor[d3[k]]
```

$$\text{Out[8]}= \frac{4 - 12\,n + 24\,k\,n - 7\,n^2 - 30\,k\,n^2 + 30\,k^2\,n^2 + 18\,n^3 - 36\,k\,n^3 + 9\,n^4}{(-2+n)\,(-1+n)\,n\,(1+n)\,(2+n)}$$

$$\text{Out[8]}= -\frac{-8 + 20\,n^2 - 30\,k\,n^2 + 30\,k^2\,n^2 + 15\,n^3 - 30\,k\,n^3 + 3\,n^4}{2\,(-2+n)\,(-1+n)\,n\,(1+n)\,(2+n)}$$

$$\text{Out[8]}= \frac{4 + 12\,n - 24\,k\,n + 17\,n^2 - 30\,k\,n^2 + 30\,k^2\,n^2 + 12\,n^3 - 24\,k\,n^3 + 3\,n^4}{(-2+n)\,(-1+n)\,n\,(1+n)\,(2+n)}$$

```
In[9]:= a := 3; b := 10;

In[10]:= e1 = Simplify[Sum[(d1[k])^2, {k, 1, n}]]
```

$$\text{Out[10]}= \frac{4 - 17\,n^2 + 9\,n^4}{4\,n - 5\,n^3 + n^5}$$

```
In[11]:= g1[m_] := n * e1/.n → m;

         Plot[g1[n], {n, a, b}];

         N[g1[a]]
```

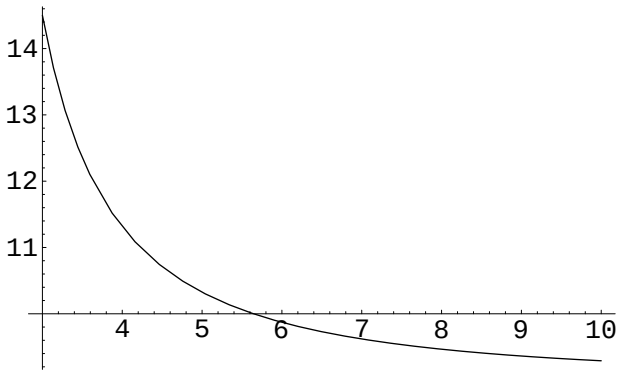


```
Out[11]= 14.5

In[12]:= e2 = Simplify[Sum[(d2[k])^2, {k, 1, n}]]
```

$$\text{Out[12]}= \frac{16 - 20\,n^2 + 9\,n^4}{16\,n - 20\,n^3 + 4\,n^5}$$

Figure A.4: Quadratics.nb, page 2

```
In[13]:= g2[m_] := n * e2/.n → m;

         Plot[g2[n], {n, a, b}];

         N[g2[a]]
```

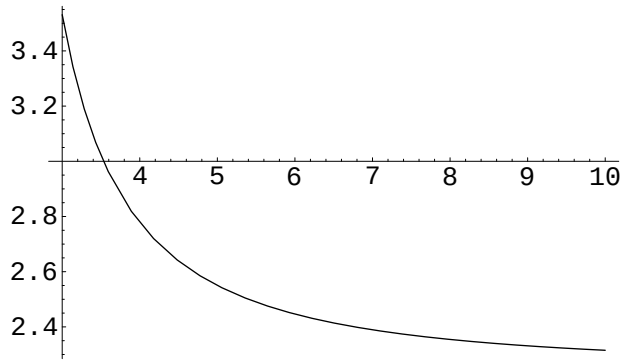


```
Out[13]= 3.53125

In[14]:= e3 = Simplify[Sum[(d3[k])^2, {k, 1, n}]]
Out[14]= (4 - 17 n^2 + 9 n^4) / (4 n - 5 n^3 + n^5)

In[15]:= g3[m_] := n * e3/.n → m;

         Plot[g3[n], {n, a, b}];

         N[g3[a]]
```

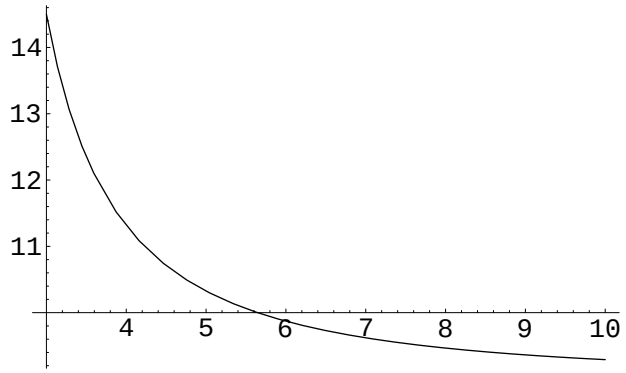


```
Out[15]= 14.5
```

Figure A.5: Quadratics.nb, page 3

```
In[16]:= Simplify[a1[k] - a1[k + 1]]

         Simplify[a2[k] - a2[k + 1]]

         Simplify[a3[k] - a3[k + 1]]
Out[16]= (-4 k + 3 n)/n^2
Out[16]= (8 k - 4 n)/n^2
Out[16]= (-4 k + n)/n^2

In[17]:= r1[k_] := Simplify[a1[k] - a1[k + 1]];

         r1[k]
Out[17]= (-4 k + 3 n)/n^2

In[18]:= r2[k_] := Simplify[a3[k + 1] - a3[k]];

         r2[k]
Out[18]= (4 k - n)/n^2

In[19]:= s11 := Sum[(r1[k])^2, {k, 1, n - 1}];

         s22 := Sum[(r2[k])^2, {k, 1, n - 1}];

         s12 := Sum[r1[k] * r2[k], {k, 1, n - 1}];

In[20]:= S := {{s11, s12}, {s12, s22}}; S
Out[20]= {{(-1 + n) (-8 + 7 n)/(3 n^3), -((-8 + n) (-1 + n))/(3 n^3)},
           {-((-8 + n) (-1 + n))/(3 n^3), (-1 + n) (-8 + 7 n)/(3 n^3)}}

In[21]:= q := {q1, q2};

In[22]:= δ := Simplify[Inverse[S].q]; δ1 := δ[[1]]; δ2 := δ[[2]];

         t1[k_] :=
           Simplify[Coefficient[δ1, q1] * r1[k] + Coefficient[δ1, q2] * r2[k]];

         t2[k_] :=
           Simplify[Coefficient[δ2, q1] * r1[k] + Coefficient[δ2, q2] * r2[k]];

In[23]:= Factor[t1[k]]

         Factor[t2[k]]
Out[23]= n (-4 - 6 k + 5 n)/(4 (-2 + n) (-1 + n))
Out[23]= (-4 + 6 k - n) n/(4 (-2 + n) (-1 + n))
```

Figure A.6: Quadratics.nb, page 4

```
In[24]:= e1 = Simplify[Sum[(t1[k])^2, {k, 1, n - 1}]]
Out[24]= n^2 (-8 + 7 n) / (16 (-2 + n) (-1 + n))

In[25]:= g1[m_] := e1/n/. n → m;

         Plot[g1[n], {n, a, b}];

         N[g1[a]]
```

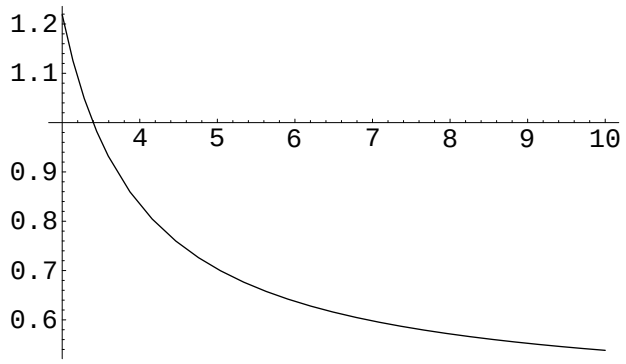


```
Out[25]= 1.21875

In[26]:= e2 = Simplify[Sum[(t2[k])^2, {k, 1, n - 1}]]
Out[26]= n^2 (-8 + 7 n) / (16 (-2 + n) (-1 + n))

In[27]:= g2[m_] := e2/n/. n → m;

         Plot[g2[n], {n, a, b}];

         N[g2[a]]
```

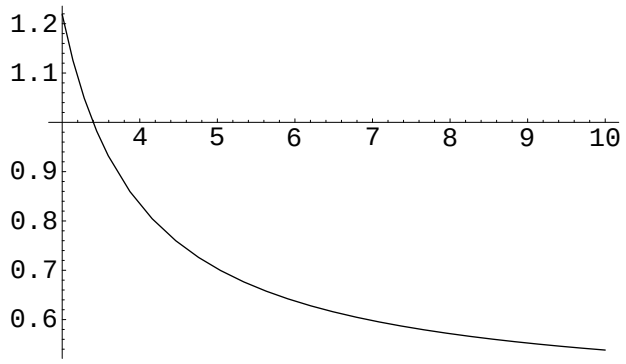


```
Out[27]= 1.21875
```

Figure A.7: Quadratics.nb, page 5

BIBLIOGRAPHY

[1] http://www.tecplot.com.

[2] *IPARS: Integrated Parallel Accurate Reservoir Simulator*, http://www.ices.utexas.edu/CSM/software_csm-ipars.php.

[3] J. E. Aarnes, *On the use of a mixed multiscale finite element method for greater flexibility and increased speed or improved accuracy in reservoir simulation*, Multiscale Model. Simul., 2 (2004), pp. 421–439 (electronic).

[4] J. E. Aarnes, S. Krogstad, and K.-A. Lie, *A hierarchical multiscale method for two-phase flow based upon mixed finite elements and nonuniform coarse grids*, Multiscale Model. Simul., 5 (2006), pp. 337–363 (electronic).

[5] V. I. Agoshkov, *Poincaré-Steklov operators and domain decomposition methods in finite dimensional spaces*, in First International Symposium on Domain Decomposition Methods for Partial Differential Equations, R. Glowinski, G. H. Golub, G. A. Meurant, and J. Periaux, eds., SIAM, Philadelphia, 1988, pp. 73–112.

[6] M. Ainsworth and J. T. Oden, *A posteriori error estimation in finite element analysis*, Comput. Meth. Appl. Mech. Eng., 142 (1997), pp. 1–88.

[7] T. Arbogast, *Analysis of a two-scale, locally conservative subgrid upscaling for elliptic problems*, SIAM J. Numer. Anal., 42 (2004), pp. 576–598.

[8] T. Arbogast and K. J. Boyd, *Subgrid upscaling and mixed multiscale finite elements*, SIAM J. Numer. Anal., 44 (2006), pp. 1150–1171 (electronic).

[9] T. Arbogast, L. C. Cowsar, M. F. Wheeler, and I. Yotov, *Mixed finite element methods on non-matching multiblock grids*, SIAM J. Numer. Anal., 37 (2000), pp. 1295–1315.

[10] T. Arbogast, S. E. Minkoff, and P. T. Keenan, *An operator-based approach to upscaling the pressure equation*, in Computational Methods in Water Resources XII, V. N. B. et al., ed., vol. 1: Computational Methods in Contamination and Remediation of Water Resources, Computational Mechanics Publications, Southampton, U.K., 1998, pp. 405–412.

[11] T. Arbogast, G. Pencheva, M. F. Wheeler, and I. Yotov, *A multiscale mortar mixed finite element method*, Tech. Rep. TR-MATH 06-15, Department of Mathematics, University of Pittsburgh, 2006. Submitted to Multiscale Model. Simul.

[12] T. Arbogast, M. F. Wheeler, and I. Yotov, *Mixed finite elements for elliptic problems with tensor coefficients as cell-centered finite differences*, SIAM J. Numer. Anal., 34 (1997), pp. 828–852.

[13] T. Arbogast and I. Yotov, *A non-mortar mixed finite element method for elliptic problems on non-matching multiblock grids*, Comput. Meth. Appl. Mech. Eng., 149 (1997), pp. 255–265.

[14] D. N. Arnold and F. Brezzi, *Mixed and nonconforming finite element methods: implementation, postprocessing and error estimates*, RAIRO Modèl. Math. Anal. Numèr., 19 (1985), pp. 7–32.

[15] I. Babuska and W. C. Rheinboldt, *Error estimates for adaptive finite element computations*, SIAM J. Numer. Anal., 15 (1978), pp. 736–754.

[16] S. B. Baden, S. J. Fink, and S. R. Kohn, *The KeLP Programming System*. http://www-cse.ucsd.edu/groups/hpcl/scg/kelp.html.

[17] R. E. Bank and A. Weiser, *Some a posteriori error estimators for elliptic partial differential equations*, Math. Comp., 44 (1985), pp. 283–301.

[18] J.-F. Bourgat, R. Glowinski, P. Le Tallec, and M. Vidrascu, *Variational formulation and algorithm for trace operator in domain decomposition calculations*, in Domain decomposition methods (Los Angeles, CA, 1988), SIAM, Philadelphia, PA, 1989, pp. 3–16.

[19] D. Braess and R. Verfürth, *A posteriori error estimators for the Raviart-Thomas element*, SIAM J. Numer. Anal., 33 (1996), pp. 2431–2444.

[20] J. H. Bramble, J. E. Pasciak, and A. H. Schatz, *The construction of preconditioners for elliptic problems by subsructuring. IV*, Mathematics of Computation, 53 (1989), pp. 1–24.

[21] J. H. Brandts, *Superconvergence and a posteriori error estimation for triangular mixed finite elements*, Numer. Math., 68 (1994), pp. 311–324.

[22] F. Brezzi, *Interacting with the subgrid world*, in Numerical analysis 1999 (Dundee), vol. 420 of Chapman & Hall/CRC Res. Notes Math., Chapman & Hall/CRC, Boca Raton, FL, 2000, pp. 69–82.

[23] F. Brezzi, J. Douglas, Jr., R. Duràn, and M. Fortin, *Mixed finite elements for second order elliptic problems in three variables*, Numer. Math., 51 (1987), pp. 237–250.

[24] F. Brezzi, J. Douglas, Jr., M. Fortin, and L. D. Marini, *Efficient rectangular mixed finite elements in two and three space variables*, RAIRO Modèl. Math. Anal. Numèr., 21 (1987), pp. 581–604.

[25] F. Brezzi, J. Douglas, Jr., and L. D. Marini, *Two families of mixed elements for second order elliptic problems*, Numer. Math., 88 (1985), pp. 217–235.

[26] F. Brezzi and M. Fortin, *Mixed and hybrid finite element methods*, Springer-Verlag, New York, 1991.

[27] C. Carstensen, *A posteriori error estimate for the mixed finite element method*, Math. Comp., 66 (1997), pp. 465–476.

[28] G. Chavent and J. Jaffre, *Mathematical models and finite elements for reservoir simulation*, North-Holland, Amsterdam, 1986.

[29] Z. Chen and J. Douglas, Jr., *Prismatic mixed finite elements for second order elliptic problems*, Calcolo, 26 (1989), pp. 135–148.

[30] Z. Chen and T. Y. Hou, *A mixed multiscale finite element method for elliptic problems with oscillating coefficients*, Math. Comp., 72 (2003), pp. 541–576 (electronic).

[31] M. A. Christie and M. J. Blunt, *Tenth SPE comparative solution project: A comparison of upscaling techniques*, SPE Reservoir Eval. Eng., 4 (2001), pp. 308–317.

[32] P. G. Ciarlet, *The finite element method for elliptic problems*, North-Holland, Amsterdam, 1978. Studies in Mathematics and its Applications, Vol. 4.

[33] L. C. Cowsar, J. Mandel, and M. F. Wheeler, *Balancing domain decomposition for mixed finite elements*, Math. Comp., 64 (1995), pp. 989–1015.

[34] L. C. Cowsar and M. F. Wheeler, *Parallel domain decomposition method for mixed finite elements for elliptic partial differential equations*, in Fourth International Symposium on Domain Decomposition Methods for Partial Differential Equations, R. Glowinski, Y. Kuznetsov, G. Meurant, J. Periaux, and O. Widlund, eds., SIAM, Philadelphia, 1991.

[35] C. N. Dawson, H. Klíe, M. F. Wheeler, and C. S. Woodward, *A parallel, implicit, cell-centered method for two-phase flow with a preconditioned Newton-Krylov solver*, Comput. Geosci., 1 (1997), pp. 215–249 (1998).

[36] Y.-H. De Roeck and P. Le Tallec, *Analysis and test of a local domain-decomposition preconditioner*, in Fourth International Symposium on Domain Decomposition Methods for Partial Differential Equations (Moscow, 1990), SIAM, Philadelphia, PA, 1991, pp. 112–128.

[37] J. Douglas, Jr. and F. A. Milner, *Interior and superconvergence estimates for mixed methods for second order elliptic problems*, RAIRO Modèl. Math. Anal. Numèr., 19 (1985), pp. 397–428.

[38] R. Durán, *Superconvergence for rectangular mixed finite elements*, Numer. Math., 58 (1990), pp. 287–298.

[39] R. E. Ewing, R. D. Lazarov, and J. Wang, *Superconvergence of the velocity along the Gauss lines in mixed finite element methods*, SIAM J. Numer. Anal., 28 (1991), pp. 1015–1029.

[40] R. E. Ewing, M. Liu, and J. Wang, *Superconvergence of mixed finite element approximations over quadrilaterals*, SINUM, 36 (1999), pp. 772–787.

[41] C. Geuzaine and J.-F. Remacle, *Gmsh: a three-dimensional finite element mesh generator with built-in pre- and post-processing facilities.* www.geuz.org/gmsh.

[42] D. Gilbarg and N. S. Trudinger, *Elliptic partial differential equations of second order*, Springer-Verlag, Berlin, 1983.

[43] R. Glowinski and M. F. Wheeler, *Domain decomposition and mixed finite element methods for elliptic problems*, in First International Symposium on Domain Decomposition Methods for Partial Differential Equations, R. Glowinski, G. H. Golub, G. A. Meurant, and J. Periaux, eds., SIAM, Philadelphia, 1988, pp. 144–172.

[44] P. Grisvard, *Elliptic problems in nonsmooth domains*, vol. 24 of Monographs and Studies in Mathematics, Pitman (Advanced Publishing Program), Boston, MA, 1985.

[45] R. H. W. Hoppe and B. I. Wohlmuth, *Adaptive multilevel techniques for mixed finite element discretizations of elliptic boundary value problems*, SIAM J. Numer. Anal., 34 (1997), pp. 1658–1681.

[46] T. Y. Hou and X.-H. Wu, *A multiscale finite element method for elliptic problems in composite materials and porous media*, J. Comput. Phys., 134 (1997), pp. 169–189.

[47] T. Y. Hou, X.-H. Wu, and Z. Cai, *Convergence of a multiscale finite element method for elliptic problems with rapidly oscillating coefficients*, Math. Comp., 68 (1999), pp. 913–943.

[48] T. J. R. Hughes, *Multiscale phenomena: Green's functions, the Dirichlet-to-Neumann formulation, subgrid scale models, bubbles and the origins of stabilized methods*, Comput. Methods Appl. Mech. Engrg., 127 (1995), pp. 387–401.

[49] T. J. R. Hughes, G. R. Feijóo, L. Mazzei, and J.-B. Quincy, *The variational multiscale method—a paradigm for computational mechanics*, Comput. Methods Appl. Mech. Engrg., 166 (1998), pp. 3–24.

[50] G. Karypis, *METIS: Family of Multilevel Partitioning Algorithms.* www-users.cs.umn.edu/~karypis/metis.

[51] S. Lacroix, Y. Vassilevski, J. Wheeler, and M. Wheeler, *Iterative solution methods for modeling multiphase flow in porous media fully implicitly*, SIAM J. Sci. Comput., 25 (2003), pp. 905–926 (electronic).

[52] P. Le Tallec, *Neumann-Neumann domain decomposition algorithms for solving 2D elliptic problems with nonmatching grids*, East-West J. Numer. Math., 1 (1993), pp. 129–146.

[53] J. L. Lions and E. Magenes, *Non-homogeneous boundary value problems and applications*, vol. 1, Springer-Verlag, 1972.

[54] J. Mandel, *Balancing domain decomposition*, Comm. Numer. Methods Engrg, 9 (1993), pp. 233–241.

[55] J. Mandel and M. Brezina, *Balancing domain decomposition for problems with large jumps in coefficients*, Math. Comp., 65 (1996), pp. 1387–1401.

[56] M. Nakata, A. Weiser, and M. F. Wheeler, *Some superconvergence results for mixed finite element methods for elliptic problems on rectangular domains*, in The mathematics of finite elements and applications, V (Uxbridge, 1984), Academic Press, London, 1985, pp. 367–389.

[57] J. C. Nedelec, *Mixed finite elements in* $\mathbf{R}^3$, Numer. Math., 35 (1980), pp. 315–341.

[58] J. A. Nitsche and A. H. Schatz, *Interior estimates for Ritz-Galerkin methods*, Math. Comp., 28 (1974), pp. 937–958.

[59] G. Pencheva and I. Yotov, *Balancing domain decomposition for mortar mixed finite element methods on non-matching grids*, Numer. Linear Algebra Appl., 10 (2003), pp. 159–180.

[60] R. A. Raviart and J. M. Thomas, *A mixed finite element method for 2nd order elliptic problems*, in Mathematical Aspects of the Finite Element Method, Lecture Notes in Mathematics, vol. 606, Springer-Verlag, New York, 1977, pp. 292–315.

[61] J. E. Roberts and J.-M. Thomas, *Mixed and hybrid methods*, in Handbook of Numerical Analysis, Vol. II, P. G. Ciarlet and J. Lions, eds., Elsevier Science Publishers B.V., 1991, pp. 523–639.

[62] A. H. Schatz and L. B. Wahlbin, *Interior maximum norm estimates for finite element methods*, Math. Comp., 31 (1977), pp. 414–442.

[63] ——, *Interior maximum-norm estimates for finite element methods. II*, Math. Comp., 64 (1995), pp. 907–928.

[64] J. M. Thomas, *Sur l'analyse numerique des methodes d'elements finis hybrides et mixtes*, PhD thesis, Sciences Mathematiques, à l'Universite Pierre et Marie Curie, 1977.

[65] R. Verfürth, *A posteriori error estimation and adaptive mesh-refinement techniques*, J. Comput. Appl. Math., 50 (1994), pp. 67–83.

[66] J. A. Wheeler, M. F. Wheeler, and I. Yotov, *Enhanced velocity mixed finite element methods for flow in multiblock domains*, Comput. Geosci., 6 (2002), pp. 315–332.

[67] M. F. Wheeler, C. N. Dawson, V. J. Parr, E. W. Jenkins, and J. Li, *Development of Parallel 3-D Locally Conservative Projection Codes for Reduction of Local Mass Errors in Hydrodynamic Velocity Field Data*, Tech. Rep. 01-10, ERDC MSRC, May 2001.

[68] M. F. Wheeler and I. Yotov, *Physical and computational domain decompositions for modeling subsurface flows*, in Domain decomposition methods, 10 (Boulder, CO, 1997), vol. 218 of Contemp. Math., Amer. Math. Soc., Providence, RI, 1998, pp. 217–228.

[69] M. F. Wheeler and I. Yotov, *Multigrid on the interface for mortar mixed finite element methods for elliptic problems*, Comput. Methods Appl. Mech. Engrg., 184 (2000), pp. 287–302.

[70] ——, *A posteriori error estimates for the mortar mixed finite element method*, SIAM J. Numer. Anal., 43 (2005), pp. 1021–1042 (electronic).

[71] B. I. Wohlmuth, *Hierarchical a posteriori error estimators for mortar finite element methods with Lagrange multipliers*, SIAM J. Numer. Anal., 36 (1999), pp. 1636–1658.

[72] ——, *A residual based error estimator for mortar finite element discretizations*, Numer. Math., 84 (1999), pp. 143–171.

[73] B. I. Wohlmuth and R. H. W. Hoppe, *A comparison of a posteriori error estimators for mixed finite element discretizations by Raviart-Thomas elements*, Math. Comp., 68 (1999), pp. 1347–1378.

[74] I. Yotov, *Mixed finite element methods for flow in porous media*, PhD thesis, Rice University, Houston, Texas, 1996. TR96-09, Dept. Comp. Appl. Math., Rice University and TICAM report 96-23, University of Texas at Austin.